1-31-2005

Sensitivity Analysis Of Design Parameters For Trunnion-Hub Assemblies Of Bascule Bridges Using Finite Element Methods

Jai P. Paul
University of South Florida

Sensitivity Analysis Of Design Parameters For Trunnion-Hub Assemblies Of Bascule Bridges Using Finite Element Methods

by

Jai P. Paul

A thesis submitted in partial fulfillment
of the requirements for the degree of
Master of Science in Mechanical Engineering
Department of Mechanical Engineering
College of Engineering
University of South Florida

Major Professor: Autar K. Kaw, Ph.D.
Glen Besterfield, Ph.D.
Muhammad M. Rahman, Ph.D.

Date of Approval:
January 31, 2005

Keywords: Thermal Stresses, Design of Experiments,
Non-Linear Material Properties, Interferences, ANSYS

DEDICATION

To my mother, who has supported me and has believed in me, and to my wife, Beena, who encouraged and motivated me at all times. They helped me, mentally and emotionally, to achieve my goals during my entire Masters program and especially during my thesis.

ACKNOWLEDGMENT

It gives me immense pleasure and great pride to present my thesis report titled, "Sensitivity Analysis of Design Parameters for Trunnion-Hub Assemblies of Bascule Bridges using Finite Element Methods".

I express my sincere thanks and gratitude to Dr. Autar K. Kaw, whose guidance and direction helped me tremendously to complete this work. It is my privilege that I had the chance to work with the Florida Professor of the Year, 2004. His expertise in the field of Solid Mechanics including thermal stresses is the best I have ever witnessed and is definitely admirable. I am deeply indebted to him for the financial support, and for the academic and computer resources he provided. I am also thankful for his patience and for his generosity.

I wish to thank Dr. Glen Besterfield, for helping me perform the sensitivity analysis according to the design of experiments standard and for his help with ANSYS.

I also thank Dr. Muhammad M. Rahman, for his contributions in helping me understand the thermal processes and for being on my committee.

I am deeply indebted to Dr. Niranjan Pai, for his suggestions and his timely hints which helped me every time I faced problems when working with ANSYS. I also thank the ANSYS users' group who helped me with prompt responses to my questions.

I want to thank my fellow graduate student, Nathan Collier, for helping me in analyzing the data obtained. My interactions with him have always served as a check of my work and helped me verify it.

Above all, I want to thank God in Jesus Christ, whose presence in my life has always encouraged and comforted me. Because He lives, I can face tomorrow.

TABLE OF CONTENTS

LIST OF TABLES

.

LIST OF FIGURES

SENSITIVITY ANALYSIS OF DESIGN PARAMETERS FOR TRUNNION-HUB ASSEMBLIES OF BASCULE BRIDGES USING FINITE ELEMENT METHODS

Jai P. Paul

ABSTRACT

Hundreds of thousands of dollars could be lost due to failures during the fabrication of Trunnion-Hub-Girder (THG) assemblies of bascule bridges. Two different procedures are currently utilized for the THG assembly. Crack formations in the hubs of various bridges during assembly led the Florida Department of Transportation (FDOT) to commission a project to investigate why the assemblies failed.

Consequently, a research contract was granted to the Mechanical Engineering department at USF in 1998 to conduct theoretical, numerical and experimental studies. It was found that the steady state stresses were well below the yield strength of the material and could not have caused failure. A parametric finite element model was designed in ANSYS to analyze the transient stresses, temperatures and critical crack lengths in the THG assembly during the two assembly procedures. The critical points and the critical stages in the assembly were identified based on the critical crack length. Furthermore, experiments with cryogenic strain gauges and thermocouples were developed to determine the stresses and temperatures at critical points of the THG assembly during the two assembly procedures.

One result revealed by the studies was that large tensile hoop stresses develop in the hub at the trunnion-hub interface in *AP1* when the trunnion-hub assembly is cooled for insertion into the girder. These stresses occurred at low temperatures, and resulted in low values of critical crack length. A suggestion to solve this was to study the effect of thickness of the hub and to understand its influence on critical stresses and crack lengths.

In addition, American Association of State Highway and Transportation Officials (AASHTO) standards call for a hub radial thickness of 0.4 times the inner diameter, while currently a thickness of 0.1 to 0.2 times the inner diameter is used.

In this thesis, the geometrical dimensions are changed according to design of experiments standards to find the sensitivity of these parameters on critical stresses and critical crack lengths during the assembly. Parameters changed are hub radial thickness to trunnion outer diameter ratio, trunnion outer diameter to trunnion bore diameter ratio and variations in the interference. The radial thickness of the hub was found to be the most influential parameter on critical stresses and critical crack lengths.

CHAPTER 1
INTRODUCTION

1.1 Bascule Bridges

A bascule bridge is a type of movable bridge that can be opened or closed to facilitate the movement of water-borne traffic such as ships and yachts. *Bascule* is the French word for *seesaw*. It belongs to the first class of levers, where the fulcrum is located between the effort and the resistance. However, the bascule bridge belongs to the second or third class of levers depending on how the load is designated.

The bascule bridge opens like a lever on a fulcrum (see Figure 1.1). The fulcrum that is fit into the girder of the bridge is made of a trunnion shaft attached to the leaf girder via a hub, as shown in Figure 1.2, and supported on bearings to permit rotation of the leaf. The trunnion, hub and girder when fitted together are referred to as a trunnion-hub-girder (THG) assembly. The THG assembly forms the pivotal element of the bascule mechanism. To open and close the girder (that is, the leaf) of the bascule bridge, power is supplied to the THG assembly by means of a curved rack and pinion gear at the bottom of the girder.

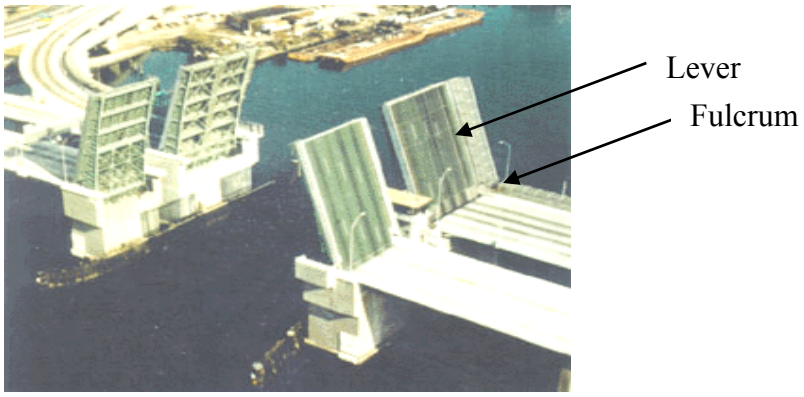

Figure 1.1 Bascule Bridge.

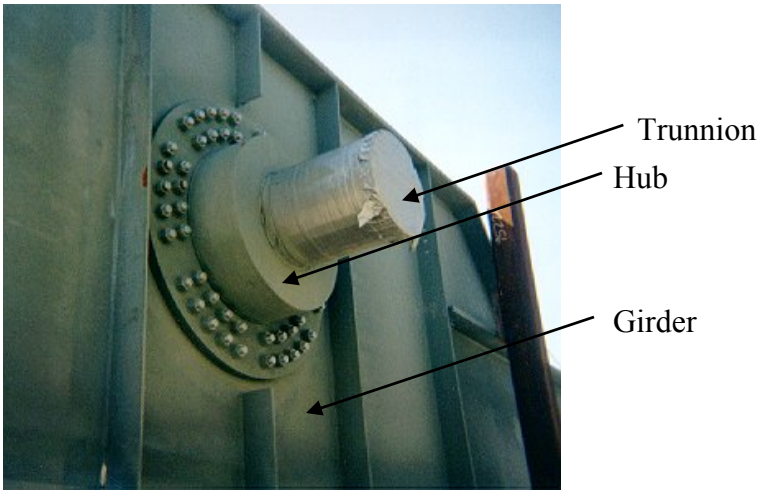

Figure 1.2 Trunnion-Hub-Girder (THG) Assembly

Assemblies of this type are generally constructed with interference fits between the trunnion and the hub, and between the hub and the girder. The interference fits allow the trunnion to form a rigid assembly with the leaf and permits the rotation of leaf through bearings. The two interference fits are supplemented by keys or dowel pins at the trunnion, and by structural bolts at the girder in some cases. Typical interference fits used in the THG assemblies for Florida bascule bridges are *FN2* and *FN3* fits (Shigley and Mishke, 1986).

FN2 and *FN3* fits are *US Standard Fits*. According to Shigley and Mishke (1986), *FN2* designation is, "Medium-drive fits that are suitable for ordinary steel parts or for shrink fits on light sections. They are about the tightest fits that can be used with high-grade cast-iron external members". *FN3* designation is, "Heavy drive fits that are suitable for heavier steel parts or for shrink fits in medium sections".

1.2 Assembly Procedures

The Trunnion-Hub-Girder assembly can be manufactured in two different ways; called Assembly Procedure 1 (*AP1*) and Assembly Procedure 2 (*AP2*), as shown in Figure 1.3.

Assembly Procedure 1

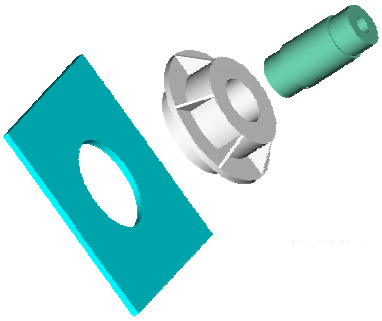

Trunnion, Hub and Girder

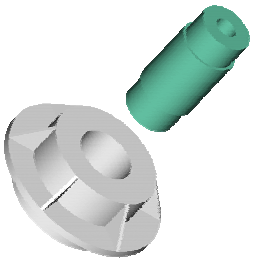

Trunnion fitted into Hub

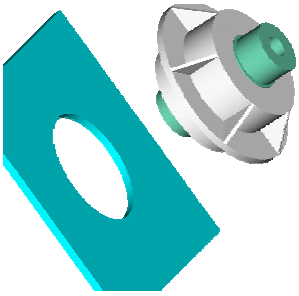

Trunnion-Hub fitted into Girder

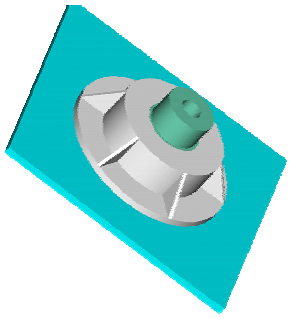

Completed THG assembly

Assembly Procedure 2

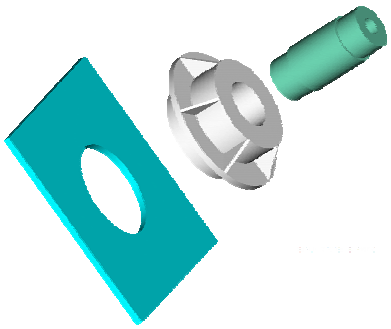

Trunnion, Hub and Girder

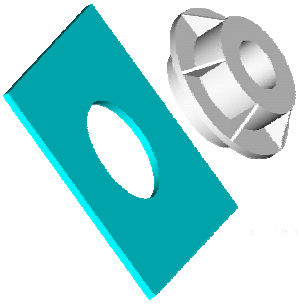

Hub fitted into Girder

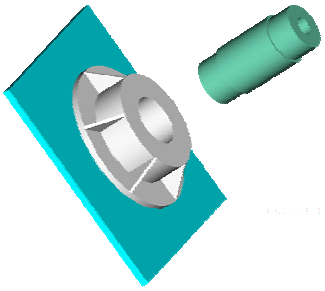

Trunnion fitted into Hub-Girder

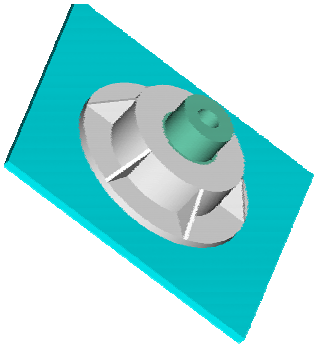

Completed THG assembly

Figure 1.3 Two Different Assembly Procedures

AP1 involves the following four steps:

- The trunnion is first shrunk by cooling in liquid nitrogen.
- This shrunk trunnion is then inserted into the hub and allowed to warm up to ambient temperature to develop an interference fit on the trunnion-hub interface.
- The resulting trunnion-hub assembly is then shrunk by cooling in liquid nitrogen.
- The shrunk trunnion-hub assembly is then inserted into the girder and allowed to warm up to ambient temperature to develop an interference fit on the hub-girder interface.

AP2 consists of the following four steps:

- The hub is first shrunk by cooling in liquid nitrogen.
- This shrunk hub is then inserted into the girder and allowed to warm up to ambient temperature to develop an interference fit on the hub-girder interface.
- The trunnion is then shrunk by cooling in liquid nitrogen.
- The shrunk trunnion is then inserted into the hub-girder assembly and allowed to warm up to ambient temperature to develop an interference fit on the trunnion-hub interface.

During either of these assembly procedures, the trunnion, hub and girder develop both structural stresses and thermal stresses. The structural stresses arise due to interference fits between the trunnion-hub and the hub-girder. The thermal stresses are a result of temperature gradients within the component. These temperature gradients come into play when either the trunnion or the hub is immersed in liquid nitrogen or when a cold trunnion is inserted into the hub, which is at room temperature. The term *Transient Stress* will be used to mean stresses during the assembly procedure. The term *Steady State Stress* will be used to mean the stresses in the trunnion, hub and girder at the end of the assembly procedure.

1.3 Overview

Chapter One, *Introduction*, describes what a bascule bridge is, how it works, the construction and the assembly procedures involved in the manufacture of bascule bridges.

Chapter Two, *Background*, describes the history, previous work done at USF, which involves the literatures reviewed, FEA and experimental analyses and their results and conclusions along with recommendations suggested. The objective of this thesis is also explained.

Chapter Three, *Technical Details*, describes the geometry of the THG assembly, the analytical background, and the non-linear material properties of the metal and liquid nitrogen.

Chapter Four, *Finite Element Modeling*, describes the modeling approach, the elements used, and assumptions used. Particular emphasis is given to the selection of elements and their proper orientations for the thermal and structural analyses.

Chapter Five, *Design of Experiments*, explains the guidelines for experiments, and simultaneously presents the systematic approach to this thesis in accordance with the guidelines established. It also describes the statistical data analysis procedure used along with the calculations involved.

Chapter Six, *Results,* presents the observations and the results obtained for the sensitivity of the trunnion inner diameter, hub outer diameter, and the interference at the trunnion-hub interface on the critical crack length and the critical stresses developed during the assembly. It also explains the results obtained.

Chapter Seven, *Conclusions and Recommendations*, presents the conclusions of this thesis based on the results obtained. Recommendations for future work are also suggested.

Appendix A gives the flowchart of the programs used for this thesis. It also gives the procedures to be followed to start and run the different programs.

Appendix B explains the various test analyses carried out to verify the different simulations. It uses various processes, whose results or behavior are already established, and simulates the same using ANSYS to obtain similar results.

CHAPTER 2
BACKGROUND

2.1 Where It All Started

On May 3rd, 1995, during the Step 3 of *AP1*, described in chapter 1, a cracking sound was heard in the trunnion-hub assembly immediately after immersion in liquid nitrogen for the Christa McAuliffe Bridge in Brevard County, FL. When the trunnion-hub assembly was taken out of liquid nitrogen, the hub was found to be cracked near the inner radius of the hub (see Figure 2.1). In another case in February 1998, while inserting the trunnion into the hub during Step 2 of *AP1*, the trunnion began to stick to the hub in the Venetian Causeway Bascule Bridge. In this case, the trunnion had been cooled down in a dry ice/alcohol medium and the resulting contraction in the trunnion was probably not sufficient to slide into the hub.

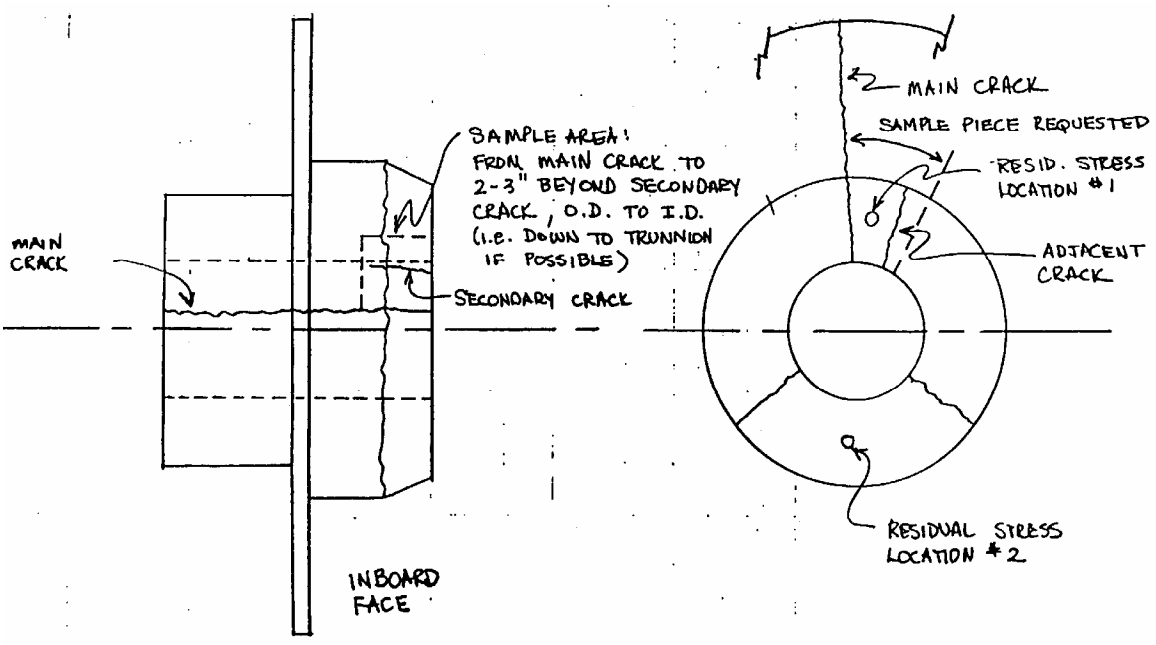

Figure 2.1 Locations of Cracks on Hub[1]

[1] Figure 2.1 is reprinted from an independent consultant's report.

These failures during the assembly procedure became a concern for the Florida Department of Transportation and they wanted to find the reason. Why were these failures taking place and only on a few of the many THG assemblies carried out in Florida? Why were they not happening on the same THG assemblies again? How can we avoid losses of hundreds of thousands of dollars in material, labor and delay in replacing failed assemblies? Preliminary investigations done by independent consulting firms and the assembly manufacturers gave various reasons for the possible failure including high cooling rate, use of liquid nitrogen for cooling, residual stresses in the castings and the assembly procedure itself. FDOT officials wanted to carry out a complete numerical and experimental study to find out the reason for these failures, how they could be avoided in the future and develop clear specifications for the assembly procedure.

2.2 Previous Work Done at USF

In 1998, the FDOT gave a two-year grant (www.eng.usf.edu/~besterfi/bascule/) to the USF Mechanical Engineering Department to investigate the problem.

2.2.1 Literature Reviewed

The study (www.eng.usf.edu/~besterfi/bascule/) primarily focused on analyzing transient stresses and failures caused due to them. This broad scope encompassed topics such as temperature-dependent material properties, thermoelastic contact, thermal shock and fracture toughness.

Pourmohamadian and Sabbaghian (1985) modeled the transient stresses with temperature dependent material properties under an axisymmetric load in a solid cylinder. However, their model did not incorporate non-symmetric loading, complex geometries and thermoelastic contact, all of which are present in the THG assembly.

The trunnion-hub interface and the hub-girder interface are in thermoelastic contact. Attempts were made to model thermoelastic contact between two cylinders by Noda (1985). However, the models were only applicable for cylinders and not for non-standard geometries. In addition, the issue of temperature-dependent material properties was not addressed in this study.

Transient stresses in a cylinder under non-axisymmetric temperature distribution were studied by Takeuti and Noda (1980). Due to the complex geometry, temperature-dependent material properties of the THG assembly and non-axisymmetric temperature distribution, this study was relevant to the research efforts. However, the issues of thermoelastic contact and complex geometries were not addressed in this study. Noda also modeled a transient thermoelastic contact problem with a position dependent heat transfer coefficient (1987) and transient thermoelastic stresses in a short length cylinder (1985). These efforts, although useful to understanding the thermoelastic modeling, did not address the issues of temperature dependent material properties and complex geometries.

The following studies aided in understanding the role of fracture toughness in the study. Thomas, et al. (1985) found the thermal stresses due to the sudden cooling of cylinder after heating due to convection. The results indicated the magnitude of stresses attained during the cooling phase increases with increasing duration of heating. Consequently, the duration of application of the convective load can be a factor influencing the maximum stresses attained in the assembly.

Parts of the THG assembly are subjected to thermal shock when they are cooled down before shrink fitting. Oliveira and Wu (1987) determined the fracture toughness for hollow cylinders subjected to stress gradients arising due to thermal shock. The results covered a wide range of cylinder geometries.

It is clear that the drawback of all previous studies of transient thermal stresses is their inability to deal with non-standard geometries. Further, previous research efforts address some of the issues (that is, temperature dependent material properties, thermoelastic contact, non-axisymmetric loading, thermal shock) but never all of them.

At the outset, it became apparent that isolating and pinpointing the causes of failure intuitively is difficult for three reasons. First, it was observed that cracks were formed in some bridge assemblies but not in others. Secondly, the cracks occurred in different parts of the hub for different bridges and at different loading times. Finally, the problem involves the interplay of several issues, that is,

- Complex geometries, such as, gussets on the hub, make it a 3-D elasticity and heat transfer problem.
- Thermal-structural interaction, due to the cooling and warming of the THG components and the shrink fitting of these components, results in both thermal and mechanical stresses. In addition, conduction takes place along contact surfaces.
- Temperature-dependent material properties, such as, coefficient of thermal expansion, specific heat, thermal conductivity, yield strength and fracture toughness, can be highly nonlinear functions of temperature.

Hence, an intuitive analysis is not merely difficult but intractable. To research more into the problem, three studies were conducted.

2.2.2 Design Tools for THG Assemblies

The first study for the grant was conducted by Denninger (2000) to find the steady state stresses in the THG assembly by developing several design tools.

Due to the shrink fitting done to the system, and based on the type of standard fits at the interfaces of the trunnion-hub and hub-girder, interferences are created at the two interfaces. These interferences cause pressures at the interfaces and, correspondingly, develop hoop (also called circumferential and tangential), radial, and Von-Mises stresses in the THG assembly. Tool 3, the relevant tool for this thesis, requires the user to specify the industry standard interference fit (*FN2* or *FN3*) at each of the two interfaces. The critical stresses as well as the radial displacements in each member (trunnion, hub, and girder) are calculated using the given information (see Figure 2.2). This program allows the user to check what the approximate steady state stresses would be after assembly. In this program, the user can see if the hoop stresses (both compressive and tensile, if applicable) are more than the yield stresses, which may cause hoop cracks in that respective cylinder. The Von-Mises stress is also given to show how these stresses directly compare with the yield strength of the material.

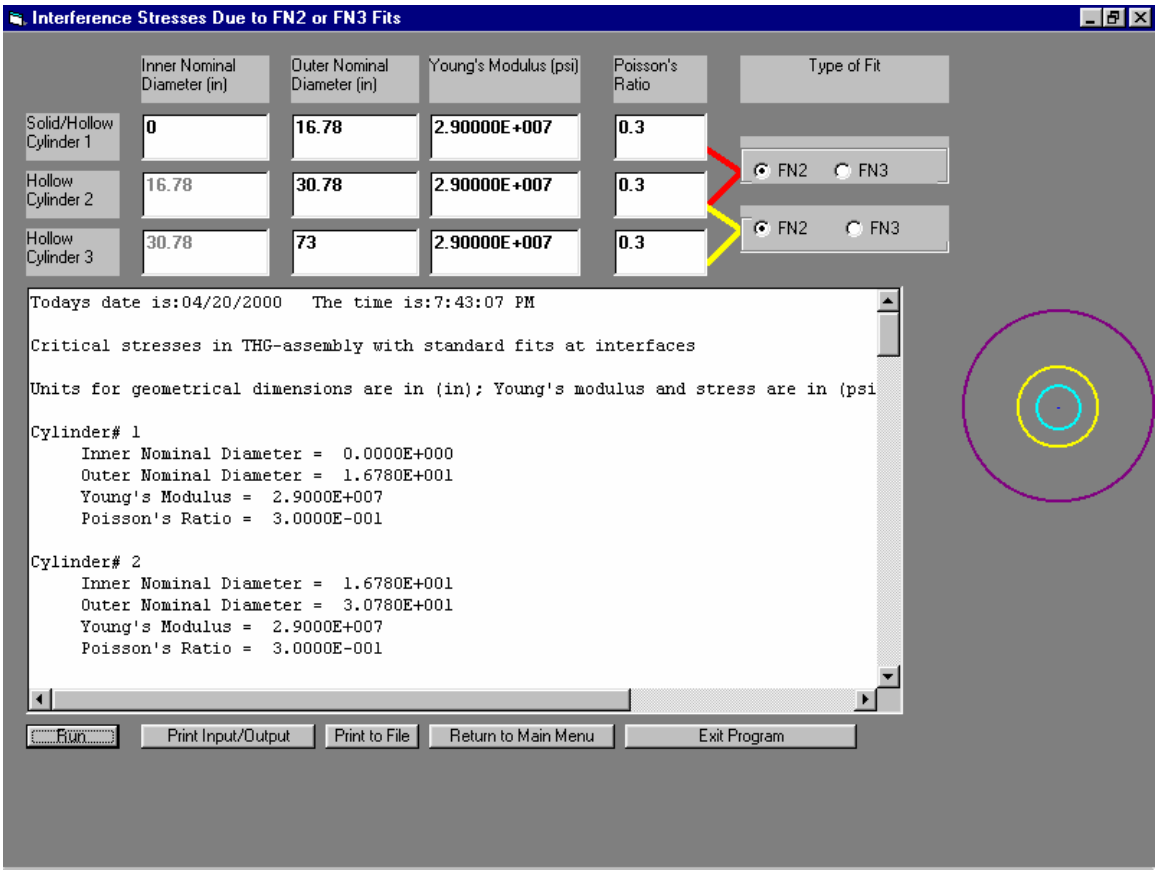

Figure 2.2 Introductory Screen for the Interference Stresses Due to *FN2* and *FN3* Fits (Denninger 2000)

This study showed that the steady state stresses are well below the ultimate tensile strength and yield strength of the materials used in the assembly. Hence, these stresses could not have caused the failure. The first study concluded that the transient stresses needed to be investigated since they could be more than the allowable stresses. The stresses during the assembly process come from two sources – thermal stresses due to temperature gradients, and mechanical stresses due to interference at the trunnion-hub and hub-girder interfaces.

Are these transient stresses more than the allowable stresses? Since fracture toughness decreases with a decrease in temperature, do these transient stresses make the assembly prone to fracture? These are some of the questions to be answered.

2.2.3 Parametric Finite Element Analysis

The second study for the grant was conducted by Ratnam (2000). A parametric finite element model was designed in ANSYS called the Trunnion-Hub-Girder Testing Model (THGTM) to analyze the stresses, temperatures and critical crack lengths in the THG assembly during the two assembly procedures. The finite element approach was most suitable because it could handle the interplay of complex geometries, coupled thermal and structural fields, and temperature dependent properties.

This study used critical crack length and hoop stress, for comparing the two assembly procedures. The relevant theory for crack formation in the Trunnion-Hub-Girder (THG) was formulated based on several observations. First, the steady state stresses after assembly were well below the yield point and could not have caused failure. Second, experimental observations indicate the presence of small cracks in the assembly. Third, the brittle nature of the material (ASTM A203-A) ruled out failure due to Von Mises stresses. Finally, cracks were formed during the immersion of the trunnion-hub assembly in liquid nitrogen. This observation is important as fracture toughness decreases with a decrease in temperature while yield strength increases with a decrease in temperature.

The results obtained are important from two perspectives, one of which is explicitly presented in the results and the other, is implicitly suggested. The explicit result is the comparison between the two assembly procedures. Implicitly presented in the results is a comparison of different bridges explaining why some THG assemblies are more prone to cracking than others.

The geometric parameters for the three bridges, namely, Christa McAuliffe Bridge, Hillsborough Avenue Bridge and 17th Street Causeway Bridge, are presented in Table 2.1. Interference values for *FN2* fits were obtained from the Bascule Bridge Design Tools (Denninger, 2000). In this study the worst case, that is, maximum interference between the trunnion and hub, and minimum interference between the hub and the girder, is analyzed. These values of interference will cause the largest tensile hoop stress in the hub. The interference values, based on *FN2* fits, used in this analysis are presented in Table 2.2. These parameters are shown in Figures 3.1 through 3.3.

Geometric Parameters	Bridge		
	Christa McAuliffe	Hillsborough Avenue	17th Street Causeway
height of the girder flange(in)	1.5	1	0.75
height of the girder web(in)	82	90	60
Extension of the trunnion on the gusset side (in)	18.5	20	6
distance to hub flange(in)	4.25	8.5	4.25
total length of the girder(in)	82	90	60
total length of the hub(in)	16	22	11
total length of the trunnion, (in)	53.5	62	23
outer radius of the hub (minus flange) (in)	16	15.39	8.88
outer radius of the hub flange(in)	27	24.5	13.1825
inner radius of the trunnion(in)	1	1.125	1.1875
outer radius of the trunnion (inner radius of the hub) (in)	9	8.39	6.472
gusset thickness(in)	1.5	1.5	1.25
backing ring width(in)	1.75	1.75	0.78125
width of the girder flange(in)	17	14	1.25
width of the girder (web) (in)	1.5	1	0.75
width of hub flange(in)	1.75	1.75	1.25

Table 2.1 Geometric Parameters

Diametrical Interference	Bridge		
	Christa McAuliffe	Hillsborough Avenue	17th Street Causeway
Trunnion-Hub (in)	0.008616	0.008572	0.007720
Hub-Girder (in)	0.005746	0.005672	0.004272

Table 2.2 Interference Values

The THGTM is used to analyze the stresses and critical crack length at possible locations of failure. The point with the greatest probability of failure was chosen and the critical crack lengths, hoop stress and temperature against time for that point were plotted. A comparison of the highest hoop stress and critical crack length is presented in Table 2.3 for all of the bridges.

Bridge	*AP1*		*AP2*	
	Critical Crack Length (in)	**Maximum Hoop Stress (ksi)**	**Critical Crack Length (in)**	**Maximum Hoop Stress (ksi)**
Christa McAuliffe	0.2101	28.750	0.2672	33.424
Hillsborough Avenue	0.2651	29.129	0.2528	32.576
17th Street Causeway	0.6420	15.515	1.0550	17.124

Table 2.3 Critical Crack Length and Maximum Hoop Stress for Different Assembly Procedures and Different Bridges

Examinations of the results revealed significant differences in the behavior of each bridge. In some bridges, a lower critical crack length was found to occur during *AP1* (that is, Christa McAuliffe and 17th Street Causeway) while in others (that is, Hillsborough Avenue) the opposite was true, however, only slightly. In addition, a slightly lower value of critical crack length during *AP1* versus *AP2* of Christa McAuliffe Bridge was observed. A phenomenon called crack arrest that prevents these cracks from growing catastrophically was studied to explain how in some cases crack formation could be arrested in spite of low values of critical crack length during the assembly process. It was concluded that crack arrest is more likely to occur during *AP2* than during *AP1* because the possibility of crack arrest is greater when thermal stresses alone are present, as they are transient and change rapidly, as compared to procedures when a combination of both thermal and interference stresses are present.

The maximum hoop stress was found to be less than the yield strength in all the bridge assemblies indicating that they will not fail due to large stresses.

2.2.4 Experimental Analysis

The earlier two studies (Denninger (2000) and Ratnam (2000)) had provided theoretical estimates of steady state and transient stresses. Also, the latter study had presented a comparison of the stresses in the two assembly procedures. The theoretical values of stresses, from these two studies needed to be validated against experimental values of stresses obtained from full-scale models. This formed the basis of the third study, Nichani (2001), which was to experimentally determine transient and steady state stresses and temperatures during both assembly procedures.

Trunnion-hub-girders were instrumented with cryogenic strain gauges and thermocouples to determine stresses and temperatures at critical points. These sensors monitor strains and temperatures during all steps (cool down in liquid nitrogen and warm up in ambient air) as explained in Chapter 1.

Two identical sets of trunnion, hub and girder were assembled, one using assembly procedure 1 (*AP1*) and the other using assembly procedure 2 (*AP2*). The stresses developed during these two procedures were compared against each other. The aim of these studies was to determine which of the assembly procedures was safer in terms of lower stresses and/or larger critical crack lengths. Nominal dimensions of the trunnion, hub and girder are shown in Table 2.4.

Component	Inner Diameter (in)	Outer Diameter (in)	Length or Thickness[2] (in)	Interference (in)
Trunnion	2.375	12.944	23	0.0077
Hub	12.944	17.760	11	
Girder	17.760	60.00[3]	0.75	0.0047

Table 2.4 Nominal Dimensions of Full-Scale Trunnion and Hub

[2] The trunnion and hub are expressed in terms of length and the girder is expressed in terms of thickness.
[3] The girder was approximated by a flat plate (60" ×60" × 0.75") with a hole of diameter 17.76".

The details of the positions of the gauges on the trunnion and the hub are shown in Figure 2.3 and in Figure 2.4 for *AP1* and for *AP2*, respectively.

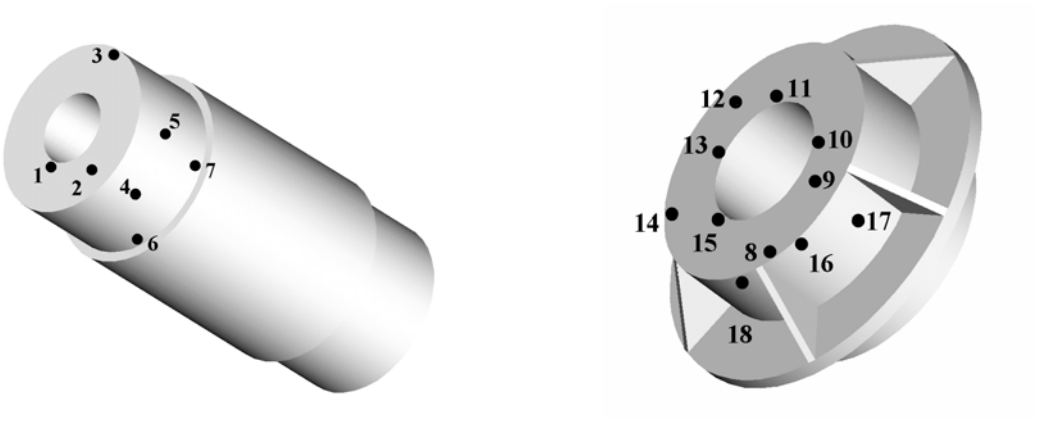

Figure 2.3 Positions of Gauges on Trunnion and Hub for *AP1*

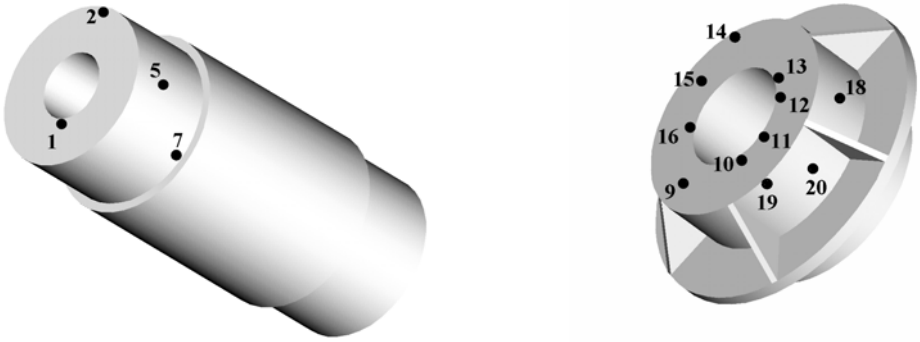

Figure 2.4 Positions of the Gauges on Trunnion and Hub for *AP2*

The thermocouples were mounted about half an inch from each strain gauge. Therefore, each mark in Figure 2.3 represents a set of one strain gauge and one thermocouple. One strain gauge and one thermocouple were placed on the diameter of the hole in the girder. This gauge would find the stress in the girder at the hub-girder interface.

Table 2.5 summarizes the comparisons of the results of *AP1* and *AP2* obtained from the experimental analysis based on all three criterions, hoop stress, *CCL* and Von Mises stress. The critical crack length (*CCL*) and factor of safety (FOS) in Table 2.6 are based upon the fracture toughness and yield strength. The maximum hoop and Von-

Mises stresses are calculated by finding these stresses at the strain gauge locations throughout the assembly procedure. The factor of safety is calculated from finding the minimum of the ratio between the yield strength and hoop stress at the strain gauge locations.

Procedure	Hoop Stress (ksi)	Critical Crack Length (*CCL*) (in)	Von Mises Stress (ksi)	Factor of safety (FOS)
AP1	25.7	0.3737	49.2	2.95
AP2	19.5	0.7610	30.9	3.29

Table 2.5 Summary of Comparison of Results of AP1 and AP2

	Assembly Procedure	*CCL* (in)	Yield Strength (ksi)	Hoop Stress (ksi)	Temp (^{0}F)	Time
Expt'l Analysis	*AP1*	0.3737	96	25.7	-278	8th minute into trunnion-hub cool down (step 3 of *AP1*)
	AP2	0.7610	65	19.5	-171	3rd minute into hub cool down (step 1 of *AP2*)
FEA Analysis	*AP1*	0.2037	53	37.0	-92	3rd minute into trunnion-hub cool down (step 3 of *AP1*)
	AP2	0.6196	53	21.5	-92	1st minute of trunnion warm up into hub (step 3 of *AP2*)

Table 2.6 Comparison of Results of the Two Assembly Procedures Obtained from Experimental and FEA Analyses

Table 2.6 gives the comparison of results obtained from the experimental analysis and the FEA analysis. It can be seen that the results are similar and largely agree.

2.2.5 Conclusions

The hypothesis at the beginning of the study that *AP2* resolves the problems associated with *AP1* was validated largely by the results obtained from the experimental and the FEA analyses. It was found that large tensile hoop stresses develop in the hub at the trunnion-hub interface in *AP1* when the trunnion-hub assembly is cooled for insertion into the girder. These stresses occur at low temperatures, and result in low values of critical crack length. Peak stresses during *AP2* occur when the hub is cooled for insertion into the girder. Note that the critical crack length allowed under *AP1* is less than half that could be allowed under *AP2*. In other words, the critical crack length for *AP2* could be more than double that could be allowed under *AP1*.

The conclusions of this report were that for the given full-scale geometry and interference values, *AP2* was safer than *AP1* in terms of lower hoop stresses, lower Von-Mises stresses and larger critical crack lengths. However, since each bridge is different, there can be possible situations where *AP1* may turn out to be a better process. One common problem associated with both assembly processes studied was thermal shock. In *AP2*, the sharp thermal gradient sometimes led to very low values of critical crack length (*CCL*). In *AP1*, a combination of high thermal and interference stresses results in possibility of crack formation. A lower thermal gradient can improve both the assembly processes.

Based on the results, the following were some recommendations:

- Consider heating the outer component as an alternative to cooling the inner component.
- Consider staged cooling wherein the trunnion or hub is first cooled from room temperature to 0^0F, then dry-ice/alcohol is used to cool it down further to -109^0F, before being cooled to -321^0F (liquid nitrogen).
- Study the effect of warming one component while cooling the other component in a medium other than liquid nitrogen, such as dry ice/alcohol.
- Studying the effect of thickness of hub on the hoop stress developed. Conduct sensitivity analysis of geometry of the bridge to understand their influence on stress distribution.

2.3 Objectives for Present Work

In an effort to continue with the studies on the THG assemblies, this thesis focuses on one of the results revealed by the studies that large tensile hoop stresses develop in the hub at the trunnion-hub interface in *AP1* when the trunnion-hub assembly is cooled for insertion into the girder. As a suggestion to solve this, it was proposed to develop a sensitivity study of the geometrical parameters of the THG assembly. These mainly include developing specifications for

- the hub radial thickness – currently 0.1 to 0.2 times the inner diameter is used in Florida, while American Association of State Highway and Transportation Officials (AASHTO) standards call for a hub thickness of 0.4 times the inner diameter,
- the inner diameter of the trunnion – the trunnions are presently made hollow and the inner diameter is made to be about $1/5^{th}$ the outer diameter.
- the variations in the interference fits.

It would be imperative to find the effect of these three parameters as they have a significant effect on the transient stresses and transient fracture resistance of the assembly.

CHAPTER 3
TECHNICAL DETAILS

3.1 Introduction

This chapter deals with the geometrical details of the trunnion, the hub and the girder. The thermal and structural boundary conditions on the trunnion-hub-girder assembly during the assembly procedure *AP1* are discussed. The material properties of the metal and liquid nitrogen are also discussed.

3.2 Geometric Details

The geometric specifications of the trunnion, hub and girder are shown in Figures 3.1, 3.2 and 3.3, respectively.

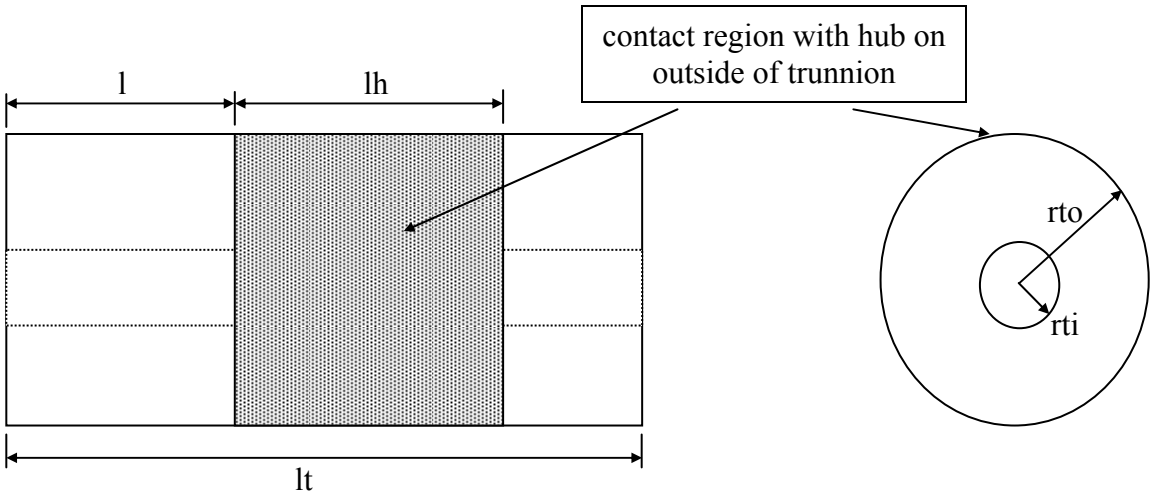

Figure 3.1 Trunnion Dimensions

The dimensional parameters of the trunnion are

lt = total length of the trunnion,

l = Extension of the trunnion on the gusset side (length to hub on the trunnion on the gusset side),

lh = total length of the hub,

rti = inner radius of the trunnion, and

rto = outer radius of the trunnion (inner radius of the hub)

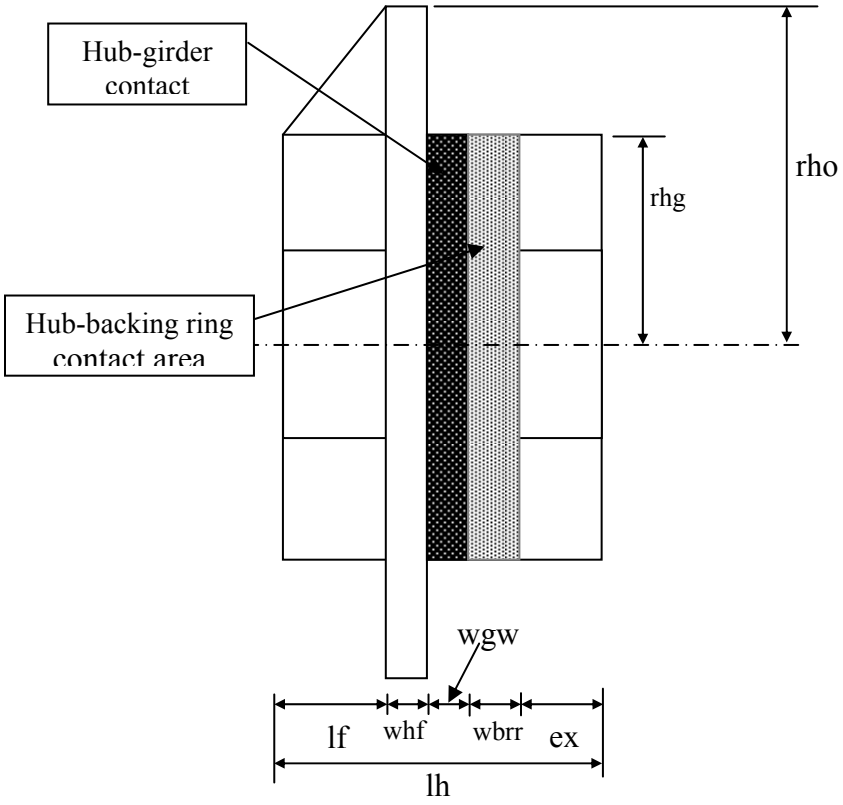

Figure 3.2 Hub Dimensions.

The dimensional parameters of the hub are

rhg = outer radius of the hub (minus flange),

rho = outer radius of the hub flange,

wbr = backing ring width,

wgw = width of the girder (web),

whf = width of hub flange,

lf = distance to hub flange,

lh = total length of the hub,

tg = gusset thickness, and

ex = distance from the end of the backing ring to the end of the hub.

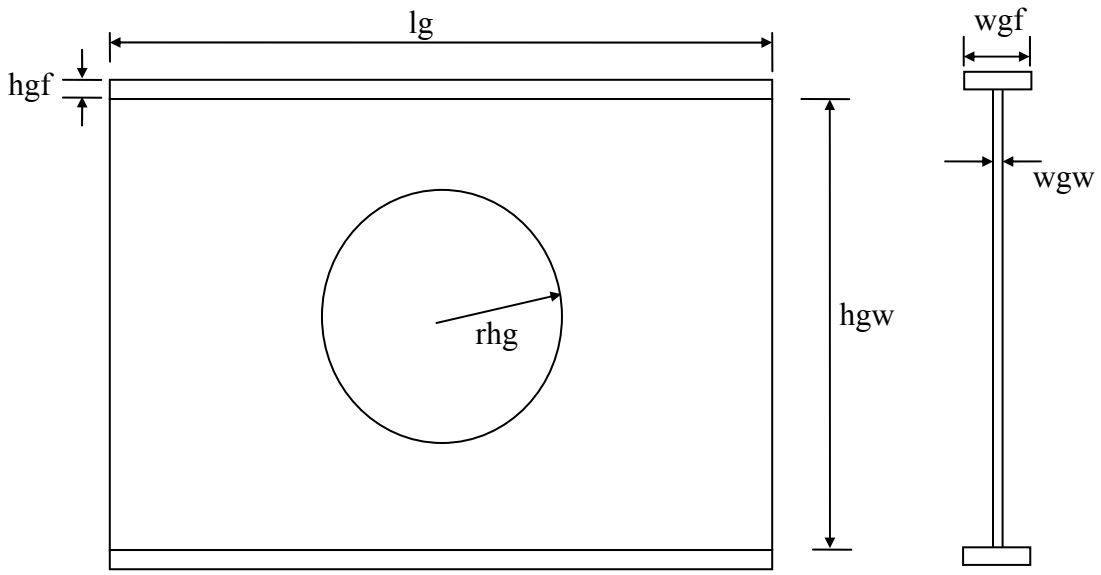

Figure 3.3 Girder Dimensions.

The dimensional parameters of the girder are

wgf = width of the girder flange,

hgw = height of the girder web,

lg = width of the girder,

hgf = height of the girder flange, and

wgw = width of the girder web.

3.3 Analytical Details

The equations of equilibrium, the strain-displacement equations and the stress-strain equations for the trunnion-hub-girder assembly are discussed in this section. To develop these equations, the following symbols are used, where i = 1, 2 and 3 represents the trunnion, hub, and girder, respectively.

σ_r^i = radial stress

σ_θ^i = hoop stress

σ_z^i = axial stress

$\tau_{r\theta}^i$ = shear stress in $r\theta$ plane

ε_r^i = radial strain

ε_θ^i = hoop strain

ε_z^i = axial strain

u_r^i = radial displacement

u_θ^i = hoop displacement

u_z^i = axial displacement

$\gamma_{r\theta}^i$ = shear strain in the $r\theta$ plane

$\gamma_{\theta z}^i$ = shear strain in the θz plane

γ_{rz}^i = shear strain in the $r z$ plane

$\nu_i(T)$ = temperature dependent Poisson's ratio

$K_i(T)$ = temperature dependent thermal conductivity

$G_i(T)$ = temperature dependent shear modulus

$h_c(T)$ = temperature dependent heat transfer coefficient of cooling medium

$h_w(T)$ = temperature dependent heat transfer coefficient of warming medium

3.3.1 Equilibrium Equations

The equations of equilibrium are given by:

$$\frac{\partial \sigma_r^i}{\partial r} + \frac{1}{r}\frac{\partial \tau_{r\theta}^i}{\partial \theta} + \frac{\sigma_r^i - \sigma_\theta^i}{r} + \frac{\partial \tau_{rz}^i}{\partial z} = 0, \tag{3.1}$$

$$\frac{\partial \tau_{r\theta}^i}{\partial r} + \frac{1}{r}\frac{\partial \sigma_\theta^i}{\partial \theta} + \frac{\partial \tau_{\theta z}^i}{\partial z} + \frac{2\tau_{r\theta}^i}{r} = 0, \tag{3.2}$$

$$\frac{\partial \sigma_z^i}{\partial z} + \frac{\partial \tau_{rz}^i}{\partial r} + \frac{1}{r}\frac{\partial \tau_{\theta z}^i}{\partial \theta} + \frac{\tau_{rz}^i}{r} = 0, \tag{3.3}$$

3.3.2 Stress-Strain Equations

The stress-strain equations are given by:

$$\varepsilon_r^i = \frac{1}{E_i(T)}\left(\sigma_r^i - \nu_i(T)\left(\sigma_\theta^i + \sigma_z^i\right)\right) - \int_{T_o}^{T} \alpha(T)dT \tag{3.4}$$

$$\varepsilon_\theta^i = \frac{1}{E_i(T)}\left(\sigma_\theta^i - \nu_i(T)\left(\sigma_r^i + \sigma_z^i\right)\right) - \int_{T_0}^{T} \alpha(T)dT \tag{3.5}$$

$$\varepsilon_z^i = \frac{1}{E_i(T)}\left(\sigma_z^i - \nu_i(T)\left(\sigma_\theta^i + \sigma_r^i\right)\right) - \int_{T_0}^{T} \alpha(T)dT \tag{3.6}$$

$$\gamma_{r\theta}^i = \frac{\tau_{r\theta}^i}{G_i(T)} \tag{3.7}$$

$$\gamma_{rz}^i = \frac{\tau_{rz}^i}{G_i(T)} \tag{3.8}$$

$$\gamma_{z\theta}^i = \frac{\tau_{z\theta}^i}{G_i(T)} \tag{3.9}$$

3.3.3 Strain-Displacement Equations

The strain-displacement equations are given by:

$$\varepsilon_r^i = \frac{\partial u_r^i}{\partial r} \tag{3.10}$$

$$\varepsilon_\theta^i = \frac{1}{r}\frac{\partial u_\theta^i}{\partial r} + \frac{u_r^i}{r} \tag{3.11}$$

$$\varepsilon_z^i = \frac{\partial u_z^i}{\partial z} \tag{3.12}$$

$$\gamma_{r\theta} = \frac{1}{r}\frac{\partial u_r^i}{\partial \theta} + \frac{\partial u_\theta^i}{\partial r} - \frac{u_\theta^i}{r} \tag{3.13}$$

$$\gamma_{rz} = \frac{\partial u_r^i}{\partial z} + \frac{\partial u_z^i}{\partial r} \tag{3.14}$$

$$\gamma_{z\theta} = \frac{1}{r}\frac{\partial u_z^i}{\partial \theta} + \frac{\partial u_\theta^i}{\partial z} \tag{3.15}$$

3.4 Boundary Conditions for the Trunnion-Hub Assembly

The boundary conditions for the THG assembly during each step of *AP1* are discussed in this section. To study the boundary conditions, the end co-ordinates are established as shown in Figures 3.4, 3.5 and 3.6. Because of the complexity of the geometry, the boundary conditions given are only at the surfaces of contact (before and after contact) and those imposed for limiting rigid body motions in the finite element analysis. Areas for which the boundary conditions are not specified are stress free.

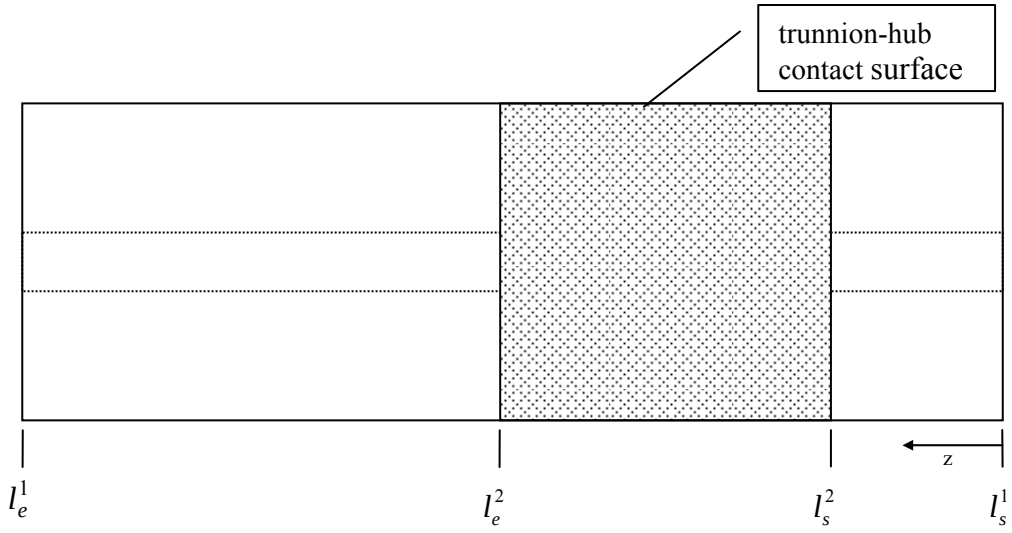

Figure 3.4a Trunnion Coordinates (side view)

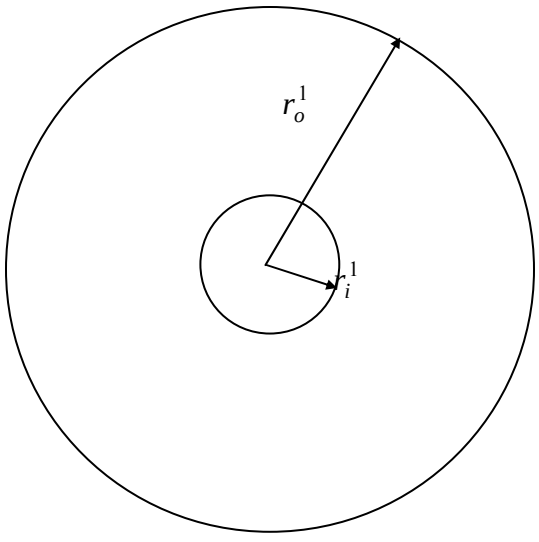

Figure 3.4b Trunnion Coordinates (front view).

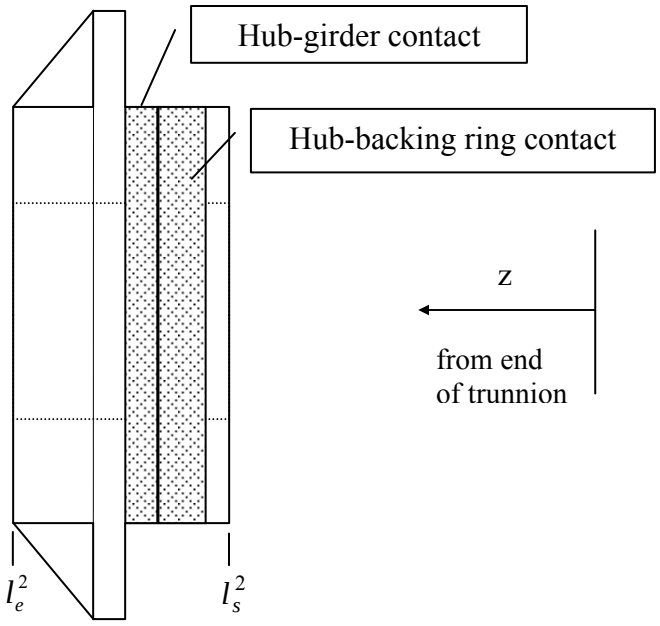

Figure 3.5a Hub Coordinates (side view)

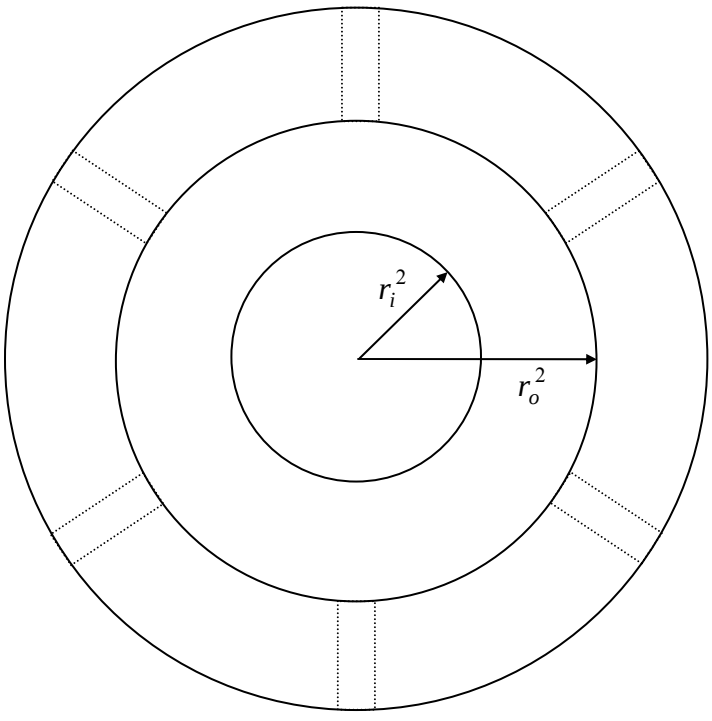

Figure 3.5b Hub Coordinates (front view)

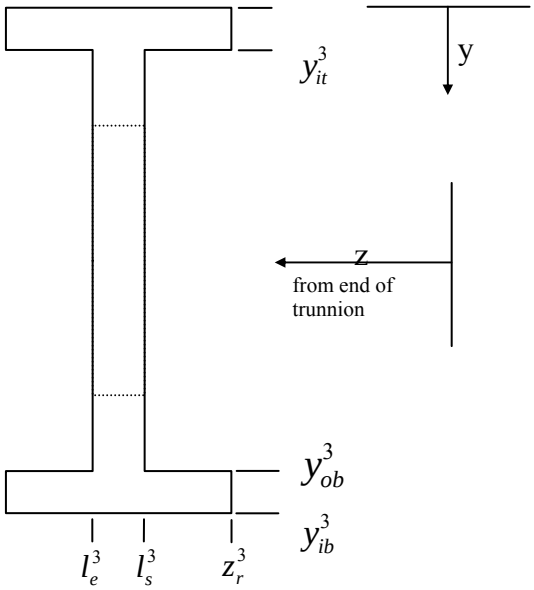

Figure 3.6a Girder Coordinates (side view)

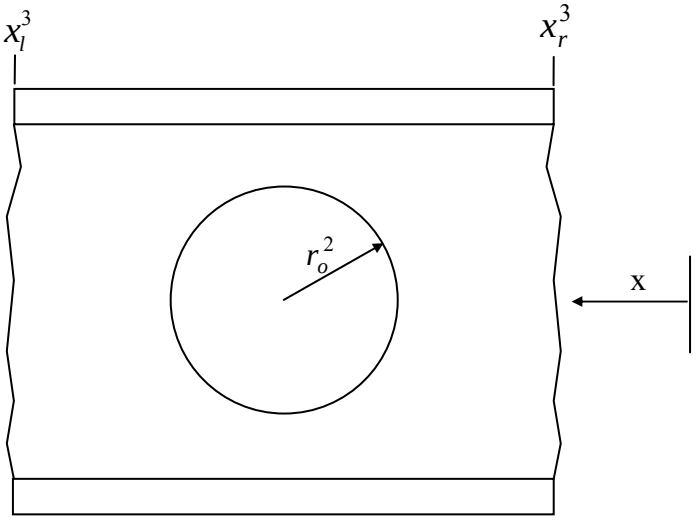

Figure 3.6b Girder Coordinates (front view)

3.4.1 Cooling the Trunnion-Hub Assembly

The main goal of this thesis is to change the geometrical parameters of the trunnion and the hub, and to find the sensitivity of these parameters on critical stresses and critical crack lengths during the whole assembly. The most critical part of the assembly, from previous studies, was identified as the trunnion-hub interface immediately after it is immersed in liquid nitrogen for cooling, and before sliding into the girder. Hence, the main interests of this thesis are the structural conditions after the trunnion-hub contact, the thermal conditions during cooling of the trunnion-hub and the structural conditions immediately after the cooling, and before sliding it into the girder.

The trunnion-hub assembly is immersed in a cooling medium at temperature T_c until it approaches steady state at time t_c.

The thermal boundary conditions at the inside radius of the trunnion, $r = r_i^1$ are:

$$-K_1(T)\frac{\partial T}{\partial r} = h_c(T)(T - T_c) \qquad r = r_i^1,\ l_s^1 \le z \le l_e^1,\ 0 \le t \le t_c \tag{3.16}$$

At the outer radius of the trunnion, $r = r_o^1$, there are non-contact and contact surfaces.

At the non-contact surface,

$$-K_1(T)\frac{\partial T}{\partial r} = h_c(T)(T - T_c) \qquad r = r_i^1, l_s^1 \le z \le l_s^2, l_e^2 \le z \le l_e^1, 0 \le t \le t_c \tag{3.17}$$

At the contact surface,

$$K_1(T)\frac{\partial T}{\partial r} = K_2(T)\frac{\partial T}{\partial r} \qquad r = r_o^1,\ l_s^2 \le z \le l_e^2,\ 0 \le t \le t_c \tag{3.18}$$

At the outer radius of the hub, $r = r_o^2$

$$-K_2(T)\frac{\partial T}{\partial r} = h_c(T)(T - T_c) \qquad r = r_o^2, l_s^2 \le z \le l_e^2, 0 \le t \le t_c \tag{3.19}$$

The structural boundary conditions on the inside radius of the trunnion, $r = r_i^1$ are

$$u_\theta^1(r_i^1, \theta, z, t) = 0; \qquad 0 \le \theta \le 2\pi,\ l_s^1 \le z \le l_e^1,\ 0 \le t \le t_c \tag{3.20}$$

$$\sigma_r^1(r_i^1, \theta, z, t) = 0 \qquad 0 \le \theta \le 2\pi,\ l_s^1 \le z \le l_e^1,\ 0 \le t \le t_c \tag{3.21}$$

At the outer radius of the trunnion, $r = r_o^1$ where there is no contact

$$\tau_{r\theta}^1(r_o^1,\theta,z,t) = 0; \qquad 0 \le \theta \le 2\pi,\ l_s^1 \le z \le l_s^2,\ l_e^2 \le z \le l_e^1,\ 0 \le t \le t_c \tag{3.22}$$

$$\sigma_r^1\left(r_o^1,\theta,z,t\right) = 0 \qquad 0 \le \theta \le 2\pi,\ l_e^2 \le z \le l_e^1,\ l_e^2 \le z \le l_e^1,\ 0 \le t \le t_c \tag{3.23}$$

At the surface in contact at the trunnion outer radius, $r = r_o^1$

$$\sigma_r^1\left(r_o^1,\theta,z,t\right) = \sigma_r^2\left(r_i^2,\theta,z,t\right) \qquad 0 \le \theta \le 2\pi, l_s^2 \le z \le l_e^2, 0 \le t \le t_c \tag{3.24}$$

$$\tau_{r\theta}^1\left(r_o^1,\theta,z,t\right) = \tau_{r\theta}^2\left(r_i^2,\theta,z,t\right) \qquad 0 \le \theta \le 2\pi, l_s^2 \le z \le l_e^2, 0 \le t \le t_c \tag{3.25}$$

$$u_r^1\left(r_o^1,\theta,z,t\right) = u_r^2\left(r_i^2,\theta,z,t\right) \qquad 0 \le \theta \le 2\pi, l_s^2 \le z \le l_e^2, 0 \le t \le t_c \tag{3.26}$$

$$u_\theta^1\left(r_o^1,\theta,z,t\right) = u_\theta^2\left(r_i^2,\theta,z,t\right) \qquad 0 \le \theta \le 2\pi, l_s^2 \le z \le l_e^2, 0 \le t \le t_c \tag{3.27}$$

At the outer radius of the hub, $r = r_o^2$

$$\tau_{r\theta}^2 = \left(r_o^2,\theta,z,t\right) = 0 \qquad 0 \le \theta \le 2\pi, l_s^2 \le z \le l_e^2, 0 \le t \le t_c \tag{3.28}$$

$$\sigma_r^2 = \left(r_o^2,\theta,z,t\right) = 0 \qquad 0 \le \theta \le 2\pi, l_s^2 \le z \le l_e^2, 0 \le t \le t_c \tag{3.29}$$

At the right edge of the hub at $z = l_s^2$, the hub is constrained to avoid rigid body motion by the following conditions:

$$u_z^2\left(r,\theta,l_s^2,t\right) = 0 \qquad r_i^2 \le r \le r_o^2, 0 \le \theta \le 2\pi, 0 \le t \le t_c \tag{3.30}$$

$$\tau_{rz}^2\left(r,\theta,l_s^2,t\right) = 0 \qquad r_i^2 \le r \le r_o^2, 0 \le \theta \le 2\pi, 0 \le t \le t_c \tag{3.31}$$

$$\tau_{z\theta}^2\left(r,\theta,l_s^2,t\right) = 0 \qquad r_i^2 \le r \le r_o^2, 0 \le \theta \le 2\pi, 0 \le t \le t_c \tag{3.32}$$

3.5 Nonlinear Material Properties of Metal

The nonlinear material properties for a typical steel, Fe-2.25 Ni (ASTM A203-A) are plotted in the next several pages. Though nonlinear material properties in general are explored, particular emphasis is given to properties at low temperatures.

3.5.1 Young's Modulus

The elastic modulus of all metals increases monotonically with increase in temperature. The elastic modulus E_T can be fitted into a semi-empirical relationship:

$$E_T = E_0 - \frac{S}{e^{\frac{T_e}{T}} - 1} \tag{3.33}$$

where

E_0 = elastic constant at absolute zero,

S = constant, and

T_e = Einstein characteristic temperature.

The Young's modulus remains stable with change in temperature, i.e., the variation is not very large (see Figure 3.7), and hence is assumed to remain constant throughout this analysis.

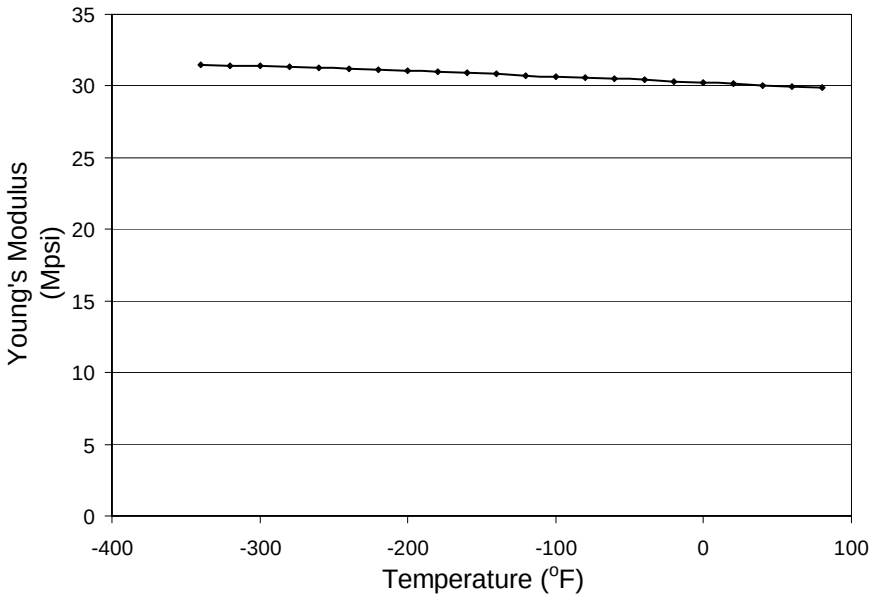

Figure 3.7 Young's Modulus of Steel as a Function of Temperature

3.5.2 Coefficient of Thermal Expansion

The coefficient of thermal expansion at different temperatures is determined principally by thermodynamic relationships with refinements accounting for lattice

vibration and electronic factors. The electronic component of coefficient of thermal expansion becomes significant at low temperatures in cubic transition metals like iron (Reed, 1983). The coefficient of thermal expansion increases with increase in temperature by a factor of three from -321^0F to 80^0F as shown in the Figure 3.8.

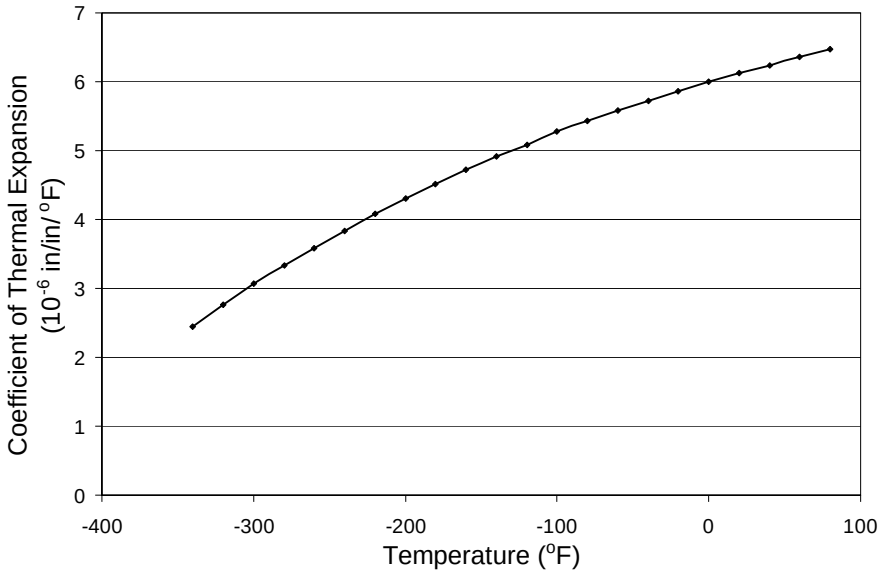

Figure 3.8 Coefficient of Thermal Expansion of Steel as a Function of Temperature

3.5.3 Thermal Conductivity

The coefficient of thermal conductivity (see Figure 3.9) increases with an increase in temperature by a factor of two from -321^0F to 80^0F. Thermal conduction takes place via electrons, which is limited by lattice imperfections and phonons. In alloys, the defect scattering effect (αT) is more significant than the phonon scattering effect (αT^{-2}) (Reed, 1983).

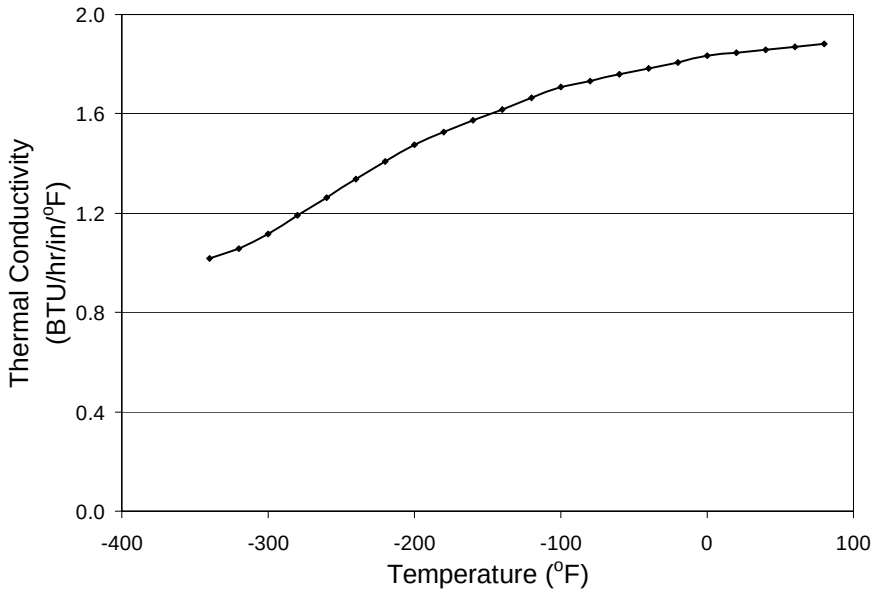

Figure 3.9 Thermal Conductivity of Steel as a Function of Temperature

3.5.4 Density

For the range of temperatures of interest to our study the density remains nearly constant, as shown in Figure 3.10.

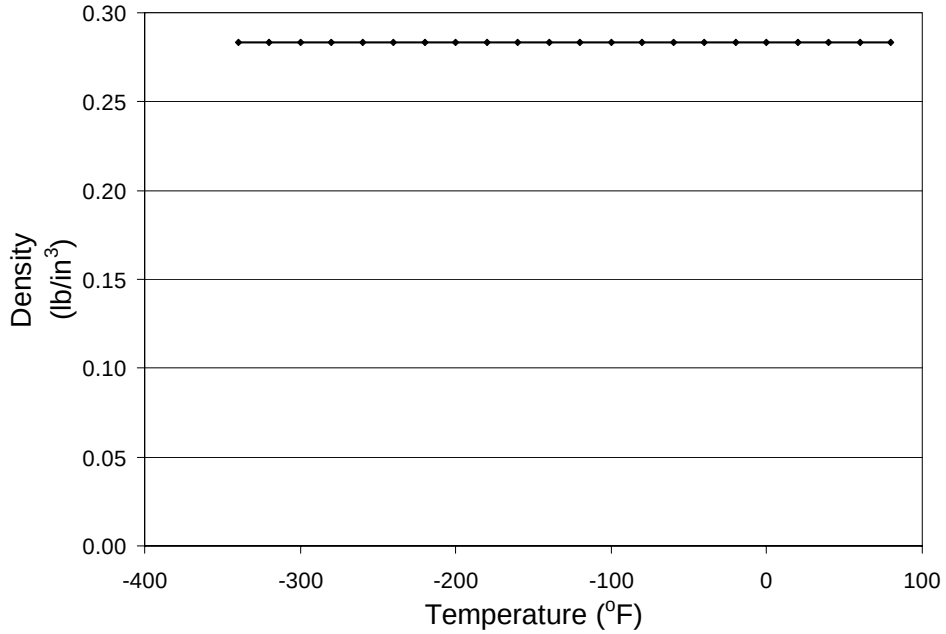

Figure 3.10 Density of Steel as a Function of Temperature

3.5.5 Specific Heat

Lattice vibrations and electronic effects affect the specific heat of a material. The contribution of two effects can be shown by

$$C = \beta T^3 + \gamma T \tag{3.34}$$

where,

β = volume coefficient of thermal expansion,

βT^3 = lattice contribution,

γ = normal electronic specific heat, and

γT = electronic contribution.

Note that specific heat decreases by a factor of five over the temperature range in question, as shown in Figure 3.11.

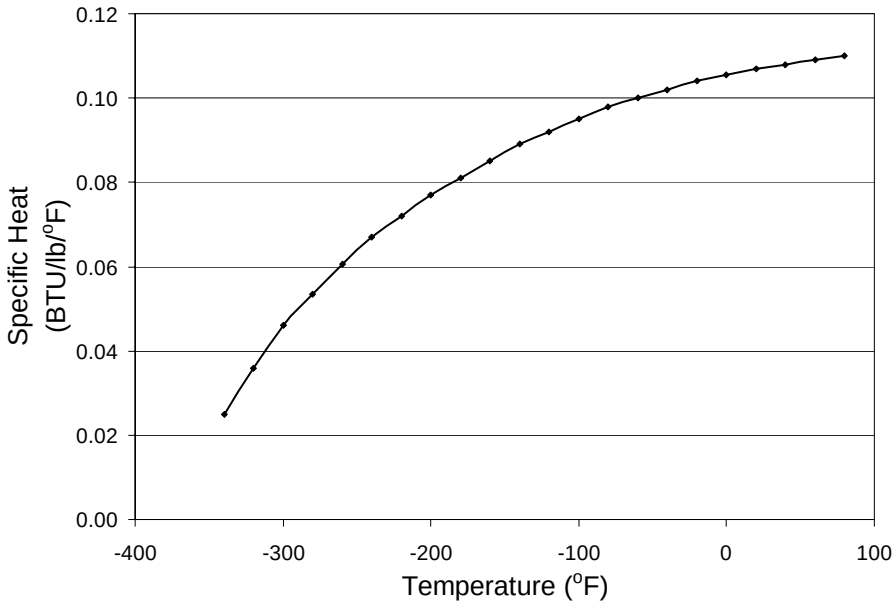

Figure 3.11 Specific Heat of Steel as a Function of Temperature

3.6 Nonlinear Material Properties of Liquid Nitrogen

The temperature dependent convective heat transfer coefficients for liquid nitrogen is plotted next.

3.6.1 Coefficient of Convection of Liquid Nitrogen

The convective heat transfer coefficient of liquid nitrogen is dependent on many factors, such as, surface finish, size of the object and shape of the object, to name a few. Based on the previous discussion, the convective heat transfer coefficient of liquid nitrogen is shown in Figure 3.12 (Brentari and Smith, 1964). This data was chosen because it very closely matches the surface finish, and object sizes and shapes used for trunnions and hubs. Note that the convective heat transfer coefficient of liquid nitrogen is evaluated at the wall temperature.

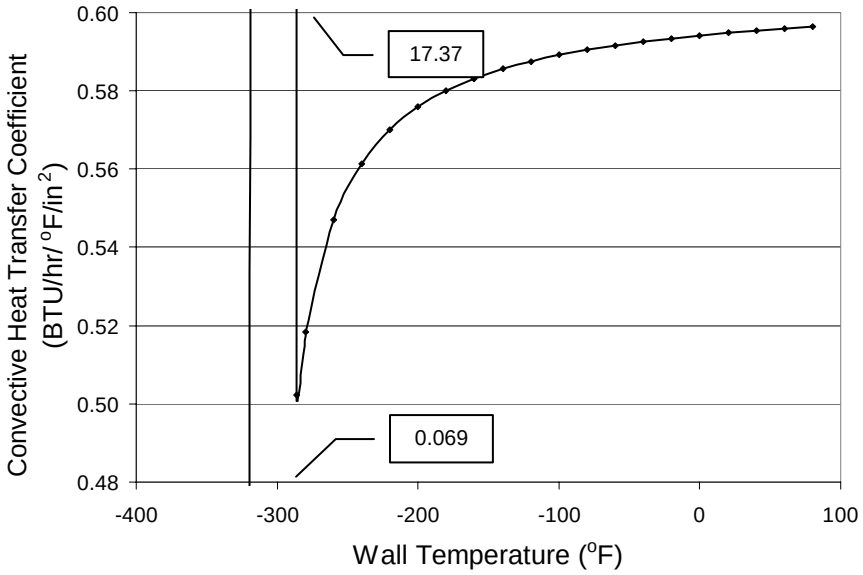

Figure 3.12 Convective Heat Transfer Coefficient of Liquid Nitrogen as a Function of Temperature.

3.6.2 Convection to Liquid Nitrogen at -321^0F

The phenomenon of convection to liquid nitrogen is quite complex and involves multi-phase heat transfer. Whenever an object at ambient temperature (that is, 80^0F) comes into contact with liquid nitrogen, *film boiling* occurs until the temperature of the object reaches approximately -260^0F. This phenomenon of film boiling occurs when there is a large temperature difference between the cooling surface and the boiling fluid. At the point when film boiling stops, the minimum heat flux occurs and the phenomenon

of *transition boiling* occurs until the temperature of the object reaches –290^{0}F. At the point when transition boiling stops, the maximum heat flux occurs and the phenomenon of *nucleate boiling* occurs until the temperature of the object reaches the temperature of liquid nitrogen. Nucleate boiling occurs when small bubbles are formed at various nucleation sites on the cooling surface. When nucleate boiling starts the object cools very rapidly.

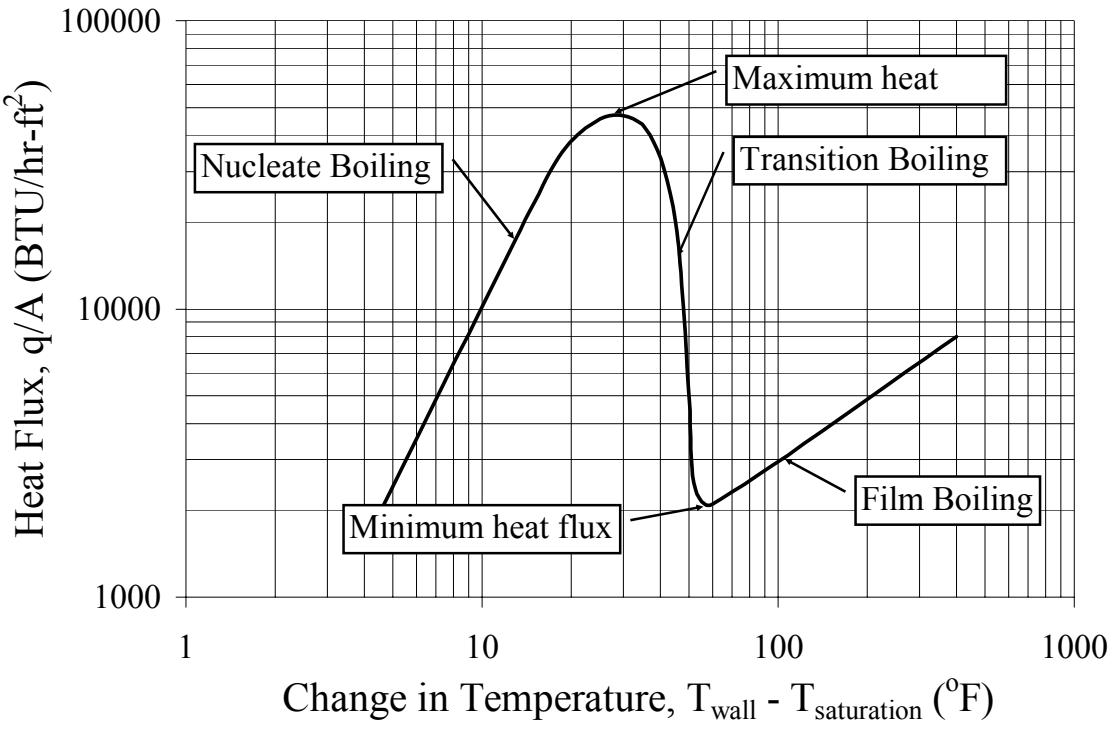

Figure 3.13 Heat Flux versus Temperature Difference for Liquid Nitrogen (Barron 1999)

CHAPTER 4
FINITE ELEMENT MODELING

4.1 Introduction

This chapter explains the modeling approach used in ANSYS to model the trunnion-hub assembly including the loads and the different processes. An understanding of this is necessary to comprehend and appreciate the results obtained. The analysis used is called the Sequential Coupled Field analysis which is one of the types of Coupled Field analysis (ANSYS Coupled Field Analysis Guide, Release 7.0). The inherent assumptions and some problems associated with the Finite Element Modeling of thermo-structural analysis and their resolutions using some non-conventional approaches are described. Assumptions made in the model are justified based on the physics of the problem, computational time versus accuracy trade-off, limitations of finite element method, and the need for simplicity.

4.2 Coupled Field Analysis

A coupled-field analysis is one that consists of the interactions between two or more disciplines or fields of engineering. For example, a piezoelectric analysis, handles the interaction between the structural and electric fields: it solves for the applied displacements due to voltage distribution, or vice versa. Thermal-stress analysis, thermal-electric analysis, fluid-structure analysis, magnetic-thermal analysis, magneto-structural analysis and micro-electromechanical systems (MEMS) are other examples of coupled-field analysis.

This study involves the coupling of the thermal and structural fields. ANSYS features two types of Coupled Field analysis: Direct and Sequential.

4.2.1 Direct Coupled Field Analysis

The direct method often consists of just one analysis that uses a coupled-field element type (for example, SOLID5, PLANE13, or SOLID98) containing all necessary degrees of freedom. Coupling is handled by calculating element matrices or element load vectors that contain all necessary terms, simultaneously. This method is used when the responses of the two phenomena are dependent upon each other, and is computationally more intensive.

4.2.2 Sequential Coupled Field Analysis (Indirect Coupled Field)

The sequential method involves two or more sequential analyses in which, the results of one analysis are used as the loads of the following analysis, each belonging to a different field. This method is used where there is one-way interaction between the two fields. There are two types of sequential analysis: sequentially coupled physics and sequential weak coupling.

In a sequentially coupled physics analysis, the results from the first analysis are applied as loads for the second analysis. The load is transferred external to the analysis, and they must explicitly be transferred using the physics environment. An example of this type of analysis is a sequential thermal-stress analysis where nodal temperatures from the thermal analysis are applied as body force loads in the subsequent stress analysis.

In a sequential weak coupling analysis the solution for the fluid and solid analysis occurs sequentially, and the load transfer between the fluid and the solid region occurs internally across a similar or dissimilar mesh interface. An example of this type of analysis is a fluid-structure interaction analysis requiring transfer of fluid forces and heat flux from the fluid to the structure and displacements and temperature from the structure to the fluid.

4.3 The Finite Element Model

This thesis concentrates on step 3 of *AP1* (see section 1.2) in which the trunnion-hub assembly is cooled in liquid nitrogen. Prior to this step, the assembly has interference stresses from the 2nd step, in which the shrunk trunnion is inserted into the hub to form an

interference fit. Hence, it becomes imperative to have the interference stresses present in the assembly before subjecting it to cooling in liquid nitrogen.

To incorporate this, the interference values are calculated based on the trunnion outer diameter or the hub inner diameter, using *FN2* fit specifications (see section B.2). These values are then added to the diameters and the geometry is constructed in ANSYS. A structural analysis to determine the interference stresses is done by allowing the interference fit to take place. The problem is solved with no additional displacement constraints or external forces. The trunnion is constrained within the hub due to its geometry. Stresses are generated due to the general misfit between the target (hub) and the contact (trunnion) surfaces.

The trunnion-hub assembly is hence obtained with the interference stresses and this assembly is now subjected to cooling in a liquid nitrogen bath. This is done in ANSYS by subjecting the exposed areas of the assembly to convection to a cooling medium whose properties are the same as that of liquid nitrogen. The result of this thermal analysis is the temperature distribution in the trunnion-hub assembly. The temperature distribution thus obtained is applied as the load to the subsequent structural analysis, to obtain the thermal-stresses in the trunnion-hub assembly. It is important to understand that the stresses obtained after this analysis is the combination of the stresses due to the interference between the trunnion and the hub (interference stresses), and the stresses due to the temperature gradient (thermal stresses).

4.4 Elements Used for Finite Element Modeling

The elements for the finite element model are chosen from the ANSYS element library (ANSYS Element Reference Manual, Release 7.0), which consists of various elements to represent the different physical materials used in real life.

4.4.1 ANSYS Element Library and Classification

They are grouped based on the following characteristics to make element type selection easier.

Two-Dimensional versus Three-Dimensional Models: ANSYS models may be either two-dimensional or three-dimensional depending upon the element types used. Axisymmetric models are considered to be two-dimensional.

Element Characteristic Shape: In general, four shapes are possible: point, line, area, or volume.

Degrees of Freedom and Discipline: The degrees of freedom of the element determine the discipline for which the element is applicable: structural, thermal, fluid, electric, magnetic, or coupled-field. The element type should be chosen such that the degrees of freedom are sufficient to characterize the model's response.

4.4.2 Selection of Elements

The elements used in this model are chosen based on all of the characteristics described in the previous section, including the different physical analyses the model undergoes. The method of selection of the elements is briefly described in this section.

The geometry of the trunnion-hub assembly is 3-dimensional and has volume. Therefore, the elements used for the finite element model are chosen only from among the solid elements of the element library.

The first analysis that the trunnion-hub assembly undergoes is a structural analysis which is done to include the interference stresses that develop at the end of Step 2 (section 1.2), caused when the trunnion is shrink fit into the hub. Since it is a structural analysis, a structural solid element (SOLID45) is chosen.

The interference between the trunnion and the hub is simulated with the help of special elements called *Contact Elements*. ANSYS supports both rigid-to-flexible and flexible-to-flexible surface-to-surface contact elements. These contact elements use a *target surface* and a *contact surface* to form a contact pair. The target and associated contact surfaces are identified via a shared real constant set. These surface-to-surface elements are well-suited for applications such as interference fit assembly contact or entry contact, forging, and deep-drawing problems. Since, the trunnion and the hub are expected to undergo deformation; the contact is identified as flexible-to-flexible contact.

In problems involving contact between two boundaries, one of the boundaries is conventionally established as the *target* surface, and the other as the *contact* surface. Contact elements are constrained against penetrating the target surface. However, target elements can penetrate through the contact surface. For flexible-to-flexible contact, the choice of which surface is designated contact or target can cause a different amount of penetration and thus affect the solution accuracy. Many guidelines are presented in the ANSYS Structural Analysis Guide, Release 7.0, which can be followed when designating the surfaces. The most relevant guideline for this model reads,

> "If one surface is markedly larger than the other surface, such as in the instance where one surface surrounds the other surface, the larger surface should be the target surface".

Using the above guideline, the hub is designated as the target surface and the trunnion is designated as the contact surface. TARGE170 is used to model the target surface with CONTA174 as the contact surface, since the contact pair is 3-dimensional. They behave as structural contact having structural degrees of freedom in the first analysis.

The interference fit trunnion-hub assembly, then, undergoes a thermal analysis when it is cooled in liquid nitrogen. A thermal solid element is required for this analysis. However, it is not required to select another element from the ANSYS element library as ANSYS automatically changes the structural element to its corresponding thermal element when the element type is changed from structural to thermal. In this case, ANSYS changes SOLID45 to its corresponding thermal element SOLID70. However, the contact elements cannot be changed as they do not have any other elements associated with them. Hence, their degrees of freedom are changed to make them behave as thermal contact.

The final analysis the trunnion-hub assembly undergoes is a structural analysis where the total stress, that is, the combination of interference stresses and the stresses due to the temperature gradient (thermal stresses), is obtained. Since this is a structural analysis, the elements are changed back to structural elements, as they were in the first analysis. The thermal element SOLID70 is changed back to SOLID45 by ANSYS when

the element is changed from thermal to structural. The contact elements are changed back to structural contact by changing their degrees of freedom.

In summary, four elements are used in this model; SOLID45, SOLID70, TARGE170 and CONTAC174. The following section gives a brief description of each of these elements.

4.4.3 Element Characteristics

The structural solid element used for the structural analyses is SOLID45. It is generally used for the three-dimensional modeling of solid structures. The element is defined by eight nodes having three degrees of freedom at each node: translations in the nodal x, y, and z directions.

The thermal solid element used for the thermal analysis is SOLID70. It has a three-dimensional thermal conduction capability. The element has eight nodes with a single degree of freedom, temperature, at each node. The element is applicable to a three-dimensional, steady-state or transient thermal analysis.

Figure 4.1 shows an 8-node (I,J,K,L,M,N,O,P) hexahedral solid element with 6 surfaces. It represents both, SOLID45 and SOLID70, since they have the same geometry, node locations, and coordinate system.

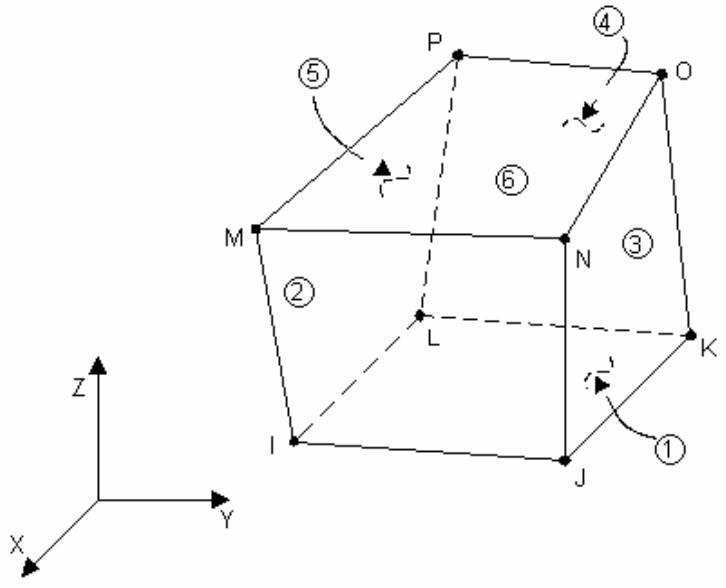

Figure 4.1 SOLID45--3D Structural Solid, and SOLID70--3D Thermal Solid

Figure 4.2 shows the trunnion-hub assembly with the hexahedral solid elements. The element type is SOLID45 for the structural analyses and SOLID70 for the thermal analysis.

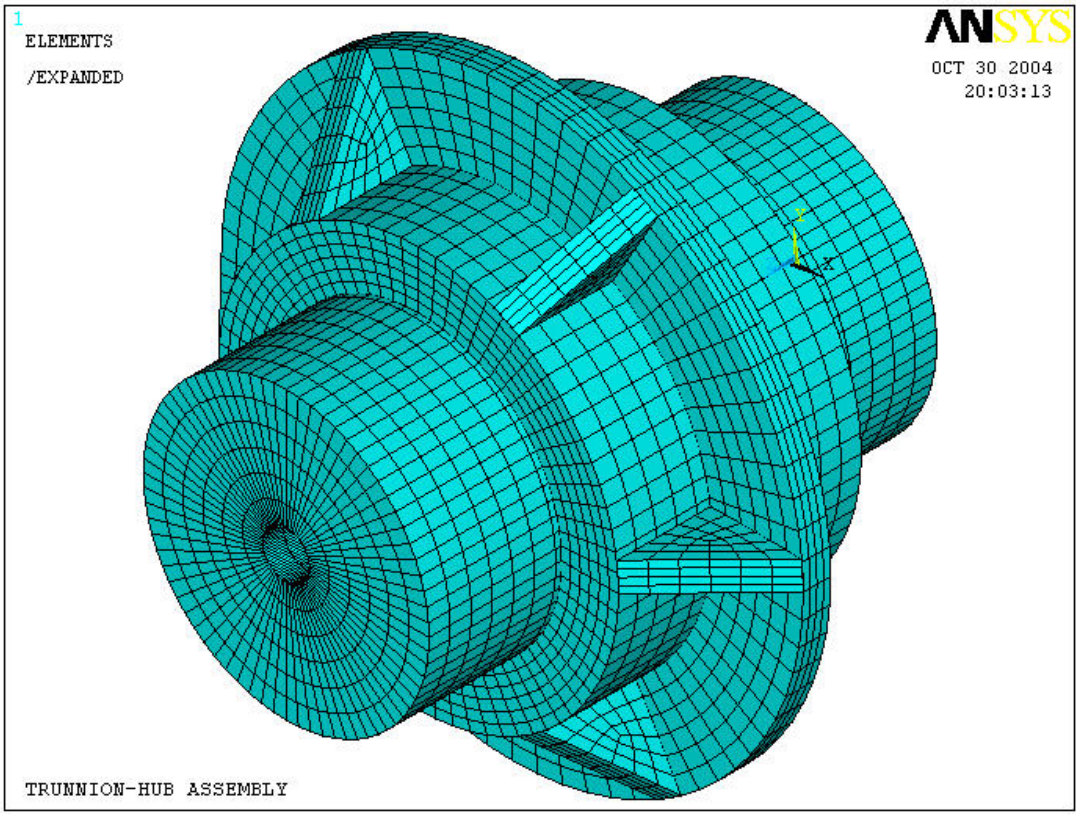

Figure 4.2 Trunnion-Hub Assembly with SOLID45 and Solid70 Elements

The contact surface for the trunnion at the trunnion-hub contact is modeled using CONTA174. CONTA174 is used to represent contact and sliding between 3-D target surfaces and a deformable surface (trunnion), defined by this element. This element is located on the surfaces of 3-D solid or shell surfaces. It has the same geometric characteristics as the solid or shell element face with which it is connected. It can be used in almost every discipline of engineering as it can support any degree of freedom when the corresponding keyopt is changed. Contact occurs when the element surface penetrates one of the target segment elements on a specified target surface. Figure 4.3 shows the

element CONTA174 overlaying the outside diameter surface of the trunnion at the trunnion-hub interface.

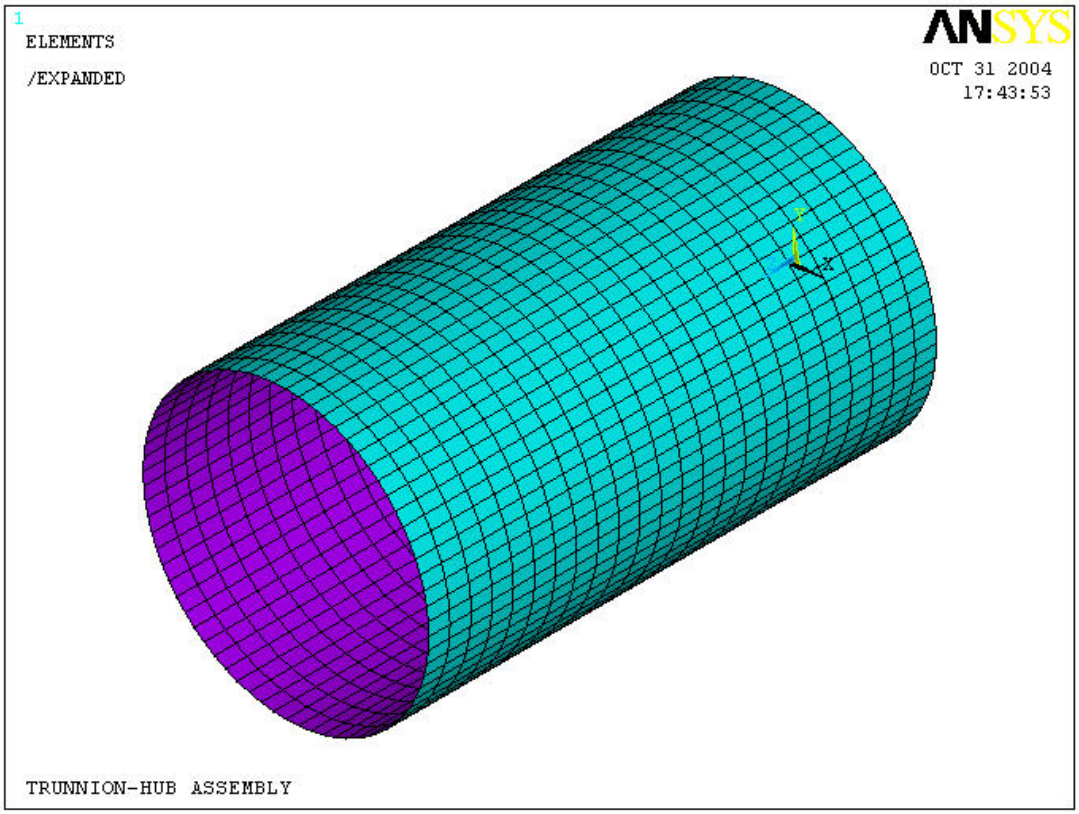

Figure 4.3 CONTA174 Overlaying the Trunnion Outer Diameter Surface

The target surface for the hub at the trunnion-hub contact is modeled using TARGE170. TARGE170 is used to represent various 3-D target surfaces for the associated contact elements. The contact elements themselves overlay the solid elements describing the boundary of a deformable body (trunnion), and are potentially in contact with the target surface (hub), defined by TARGE170. This target surface is discretized by a set of target segment elements (TARGE170) and is paired with its associated contact surface via a shared real constant set. Any translational or rotational displacement, temperature, and voltage can be imposed on the target segment element. Forces and moments can also be imposed on target elements. Figure 4.4 shows the target element

TARGE170 overlaying the inside diameter surface of the hub at the trunnion-hub interface.

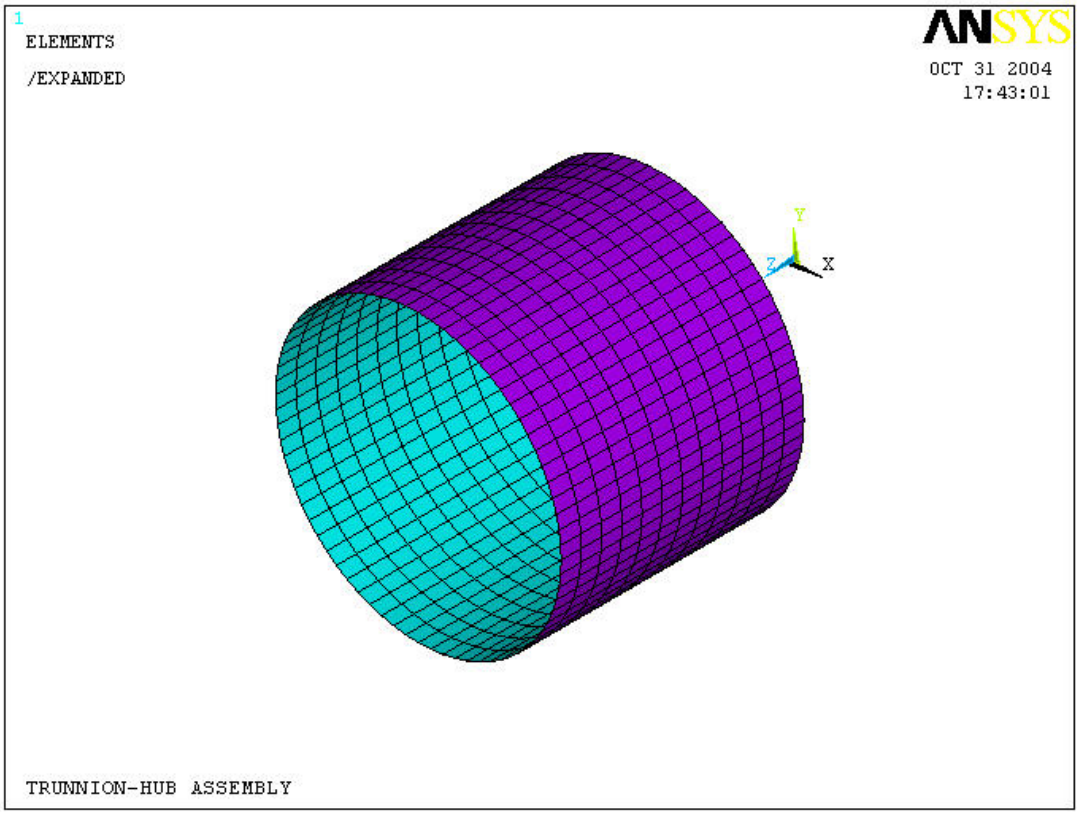

Figure 4.4 TARGE170 Overlaying the Hub Inner Diameter Surface

4.5 Assumptions

4.5.1 Sequential coupled field approach

The assumption in this approach is that the structural results are dependent upon the thermal results but not vice-versa. This is a fair assumption as the effect of strains on the thermal analysis is negligible.

4.5.2 Finite element method assumptions

The standard inaccuracies associated with any finite element model due to mesh density, time increments, number of sub-steps, etc. are present in this model (Logan, 1996).

4.5.3 Material properties

The material properties of the trunnion hub assembly and the cooling medium are temperature dependent and are evaluated at specified temperature increments. The properties in between or outside the extremes of these values are interpolated and extrapolated, respectively.

CHAPTER 5
DESIGN OF EXPERIMENTS

5.1 Introduction

To efficiently perform experiments involving more than one factor that affect the desired result, a scientific approach to planning the experiment must be employed. Design of Experiments (Montgomery, 2001) refers to the process of planning the experiment so that appropriate data that can be analyzed by statistical methods will be collected, resulting in valid and objective conclusions. The statistical approach to experimental design is necessary if we wish to draw meaningful conclusions from the data. Thus, there are two aspects to any experimental problem: the design of the experiment and the statistical analysis of the data. The two subjects are closely related because the method of analysis depends directly on the design employed.

5.2 Guidelines for Designing Experiments

When performing any scientific procedures, it is important and recommended that proper guidelines be laid out that will help in achieving the desired goals without wavering, and in less time. The guidelines for efficiently designing experiments are explained in the following sections.

5.2.1 Recognition of and Statement of the Problem

A clear statement of the problem often contributes substantially to better understanding of the phenomenon being studied and the final solution of the problem. The trunnion-hub assembly presents a clear and well defined problem. In making the trunnion-hub-girder assembly for the fulcrum of bascule bridges, Assembly Procedure 1 (section 1.4) is used in many parts of the country, including Florida. During cooling of the trunnion-hub assembly to shrink fit it into the girder, cracks developed that ultimately

caused failure in the assembly process and hence, loss of thousands of dollars. While AASHTO (American Association of State Highway and Transportation Officials) has its own specifications for the geometry, different standards are made use of in the actual assemblies. Therefore, it is important to study and analyze the effects of important geometric factors on the stresses produced and failure criteria in the trunnion-hub assembly during cooling.

5.2.2 Choice of Factors, Levels and Range

This is often done simultaneously with selection of response variable (see section 5.2.3), or in the reverse order. Many times after performing the first trial, the results give a good idea to determine which factors affect it more and which ones have little effect on the results. After obtaining the results for the first FDOT grant, the principal investigators at the University of South Florida suggested that the outer radius of the hub, the inner bore of the trunnion, and the interference fit were key factors that affected the cracks developed during the cooling of the trunnion-hub assembly. The levels and ranges for these factors are obtained from AASHTO standards (see section 6.5) and the presently used values.

5.2.3 Selection of Response Variables

In selecting the response variables, it should be made certain that the variables really provide useful information about the process under study. As cracks were developed during the assembly processes, the main variable to be studied is the failure criteria. Failure in metals can occur either when the stresses developed exceed the allowable yield stress of the material or when the length of the cracks developed exceed the allowable crack length. To verify the former, the minimum stress ratio is calculated. Stress ratio can be defined as the ratio of the yield strength of the material to the stress induced. To verify the latter, the minimum critical crack length is determined.

5.2.4 Choice of Experimental Design

In selecting the design, it is important to keep the experimental objectives in mind. In many engineering experiments, some of the factor levels will result in different values of the response. Consequently, we are interested in identifying *which* factors cause this difference and in estimating the *magnitude* of the response change. Choice of design involves the consideration of various experimental conditions including the time for cooling, mesh, and the number of runs. The time for cooling was determined by knowing that the most stresses are produced during the initial cooling stages when the temperature gradient is the largest. Therefore, the time for cooling was set to 300 seconds (5 min). The cooling time was justified as the values for the critical crack length and stress ratio increased after sudden decreases. The number of trials was calculated using the 2^k factorial method.

5.2.5 Performing the Experiment

When running the experiment it is vital to monitor the process carefully to ensure that everything is being done according to plan. Prior to conducting the experiment, a few trial runs or pilot runs are often helpful. These runs provide information about the consistency of the experiment, a check on measurement system, a rough idea of experimental error, and a chance to practice the overall experimental technique. This also provides an opportunity to revisit the decisions made in the previous steps. A lot of trial runs were run to check the experiment and to verify the different analyses. Appendix B contains a detailed explanation of each of the different runs and their results.

5.2.6 Statistical Analysis of the Data

Statistical methods should be used to analyze the data so that results and conclusions are objective rather than judgmental in nature. The primary advantage of statistical methods is that they add objectivity to the decision making process. Statistical techniques coupled with good engineering or process knowledge and common sense will usually lead to sound conclusions. The statistical method used to obtain the results is the ANOVA 2^k factorial method.

5.2.7 Conclusions and Recommendations

Once the data have been analyzed, practical conclusions must be drawn about the results and a course of action recommended. The following chapter explains the results and conclusions with recommendations, in detail.

5.3 Factorial Design

Many experiments involve the study of the effects of *2* or more factors. Factorial Designs are most efficient for such type of experiments. Factorial Designs (Montgomery 2001) could be defined as experiments in which each trial or run contains all possible combinations of the levels of the factors that are investigated when it is necessary to study the joint effect of the factors on the response(s). There are several special cases of the general factorial design that are important because they are widely used in research work. The most important of these special cases is that of k factors, each at only two levels. It is called the 2^k factorial design. The levels of the factors are arbitrarily called *low* and *high*. The effect of a factor is defined to be the change in response produced by a change in the level of the factor. When the difference in response between the levels of one factor is not the same at all levels of the other factors, then it can be said that there is an interaction between the factors.

Factorial Designs are advantageous and could be considered as the best method when there are *2* or more factors involved. The number of experiments required to determine the effect of each factor is reduced (2^k, where k is the number of factors), misleading conclusions can be avoided when interaction is present, and the effects of a factor at several levels of the other factors can be estimated yielding conclusions that are valid over a range of experimental conditions.

Three factors are considered in this thesis to be of considerable importance; the variations in the interference fits, the hub radial thickness, and the trunnion bore diameter. Since it involves *3* factors, it is called 2^3 Factorial Design and the total number of experiments required is $2^3 = 8$ experiments. There are three different notations that are widely used for the runs in the 2^k design. The first notation is the + and – notation. The

second is the use of lowercase letter labels and the final notation uses 1 and 0 to denote high and low factor levels, respectively, instead of + and –.

5.4 Calculations Involved in 2^3 Factorial Designs

If the factors involved are *A, B,* and *C*, then the 8 experiments are named as shown in table 5.1.

Run	*A*	*B*	*C*	Labels	*A*	*B*	*C*
1	-	-	-	(1)	0	0	0
2	+	-	-	a	1	0	0
3	-	+	-	b	0	1	0
4	+	+	-	ab	1	1	0
5	-	-	+	c	0	0	1
6	+	-	+	ac	1	0	1
7	-	+	+	bc	0	1	1
8	+	+	+	abc	1	1	1

Table 5.1 Notations for Experiment Combinations

The main effects of the factors *A, B*, and *C*, for n replicates, are found using the following formulae (Montgomery 2001), respectively.

$$A = \frac{1}{4n}[a - (1) + ab - b + ac - c + abc - bc] \tag{5.1}$$

$$B = \frac{1}{4n}[b + ab + bc + abc - (1) - a - c - ac] \tag{5.2}$$

$$C = \frac{1}{4n}[c + ac + bc + abc - (1) - a - b - ab] \tag{5.3}$$

The two factor interaction effects *AB, AC,* and *BC,* for n replicates, are found using the following formulae, respectively.

$$AB = \frac{1}{4n}[ab - a - b + (1) + abc - bc - ac + c] \tag{5.4}$$

$$AC = \frac{1}{4n}[(1) - a + b - ab - c + ac - bc + abc] \tag{5.5}$$

$$BC = \frac{1}{4n}[(1) + a - b - ab - c - ac + bc + abc] \tag{5.6}$$

The overall interaction effect ABC, for n replicates, is found using the following formula.

$$ABC = \frac{1}{4n}[abc - bc - ac + c - ab + b + a - (1)] \tag{5.7}$$

In equations 5.1 through 5.7, the quantities in brackets are called *Contrasts* of the treatment combinations. The sum of squares for the effects are calculated using

$$SS = \frac{(Contrast)^2}{8n}$$

The total sum of squares is calculated by summing the squares of all the data values and subtracting from this number the square of the grand mean times the total number of data values. Mathematically,

$$SS_T = \sum_{i=1}^{a}\sum_{j=1}^{b}\sum_{k=1}^{c}\sum_{l=1}^{n} y_{ijkl}^2 - \frac{y_{....}^2}{abcn} \qquad \begin{cases} i = 1, 2, ...a \ ; & j = 1, 2, ...b \\ k = 1, 2, ...c \ ; & l = 1, 2, ...n \end{cases},$$

where $y_{....} = \sum_{i=1}^{a}\sum_{j=1}^{b}\sum_{k=1}^{c}\sum_{l=1}^{n} y_{ijkl}$, and *i, j, k* are the three factors – factor *A*, factor *B*, and factor *C*, respectively, and *l* is the number of *n* replicates.

The property that the treatment sum of squares plus the error sum of squares equals the total sum of squares is utilized to compute the error sum of squares. Hence, it is usually calculated by subtraction.

$$SS_E = SS_T - (SS_A + SS_B + SS_C + SS_{AB} + SS_{AC} + SS_{BC} + SS_{ABC})$$

The percentage contribution of each effect is then found by calculating the ratio of the respective sum of squares and the total sum of squares and multiplying by 100. Mathematically, the percentage contribution of effect *A* is calculated as $\frac{SS_A}{SS_T} \times 100$. Once, the percentage contribution of each effect is found, the one with the highest value is said to have the most effect on the experiment.

The p-values are then found to confirm the magnitude of these effects. In general, smaller the p-values, more significant are the effects.

CHAPTER 6
RESULTS

6.1 Introduction

The results obtained from the finite element analysis and the statistical analysis of the data are presented in this chapter. As discussed in earlier chapters, the purpose of this thesis is to study the effect of important parameters on the critical stresses and the critical crack length in the trunnion-hub assembly when it is cooled in liquid nitrogen, and also to optimize the geometry of the assembly in accordance with the AASHTO standards. Previous studies done at USF performed analyses on three different bridges; Christa McAuliffe Bridge, Hillsborough Avenue Bridge and 17th Street Causeway Bridge. Since we are studying the trunnion-hub assembly for bascule bridges in general, it will suffice to study the effects on one bridge. For the thesis, the 17th Street Causeway Bridge was chosen as the specimen bridge. The geometric parameters used are as shown in figures 6.1 and 6.2, and Table 6.1. The material properties of the metal used and the thermal properties of liquid nitrogen are presented in Chapter 3.

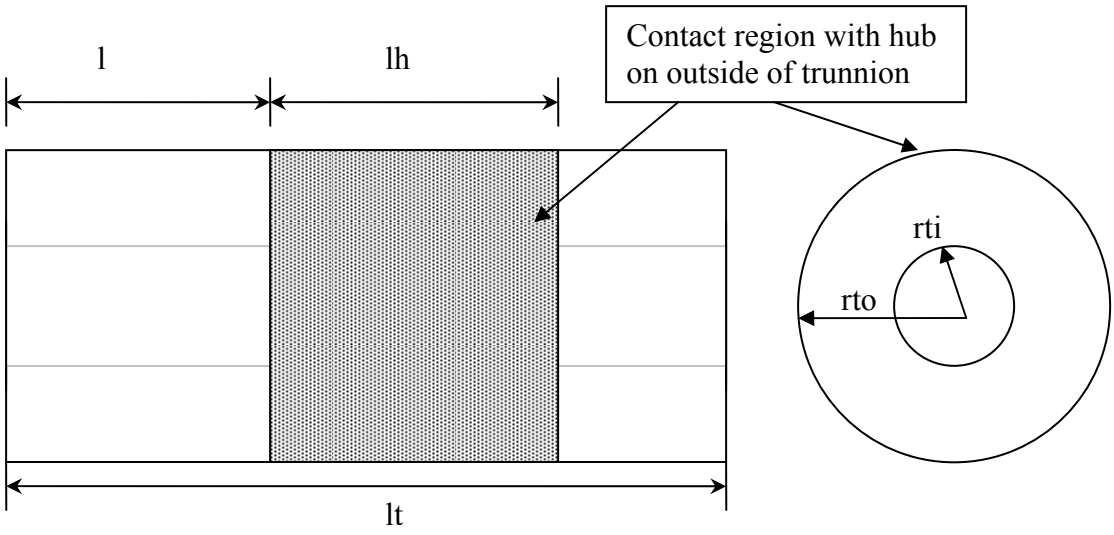

Figure 6.1 Trunnion dimensions

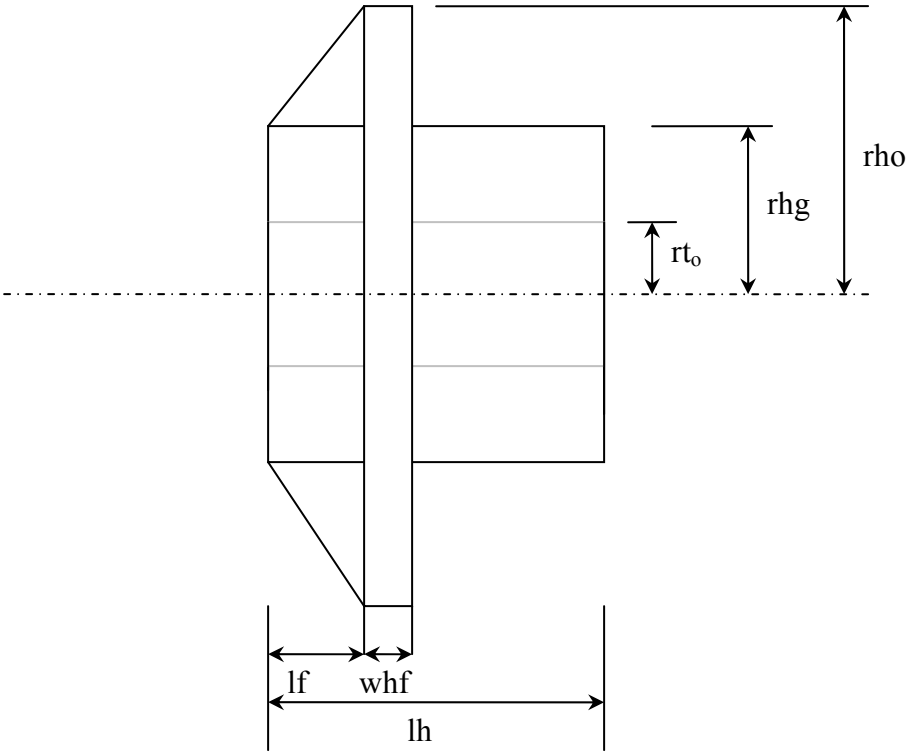

Figure 6.2 Hub dimensions

Geometric Parameters	Bridge
	17th Street Causeway
rto (in) = outer radius of the trunnion (inner radius of the hub)	6.472
rti (in) = inner radius of the trunnion	1.1875
lt (in) = total length of the trunnion,	23
l (in) = Extension of the trunnion on the gusset side	6
lh (in) = total length of the hub	11
lf (in) = distance to hub flange	4.25
whf (in) = width of hub flange	1.25
rhg (in) = outer radius of the hub	8.88
rho (in) = outer radius of the hub flange	13.1825
tg (in) = gusset thickness	1.25
δ(in) = Interference between trunnion-hub (max)	0.00386

Table 6.1 Geometric Dimensions for 17th Street Causeway Bridge

6.2 Fracture Toughness and Yield Strength

The two responses that we are interested in studying are the Critical Crack Length and the Stress Ratio. The critical crack length depends on the hoop stress (σ_θ) developed and the fracture toughness (K_{IC}) of the material. The fracture toughness of the material is temperature dependent and it decreases with a decrease in temperature as shown in Figure 6.3. The stress ratio depends on the total stress induced (Von-Mises Stress) and the yield strength (Y_s) of the material. The yield strength is also temperature dependent and it increases with a decrease in temperature, also shown in Figure 6.3.

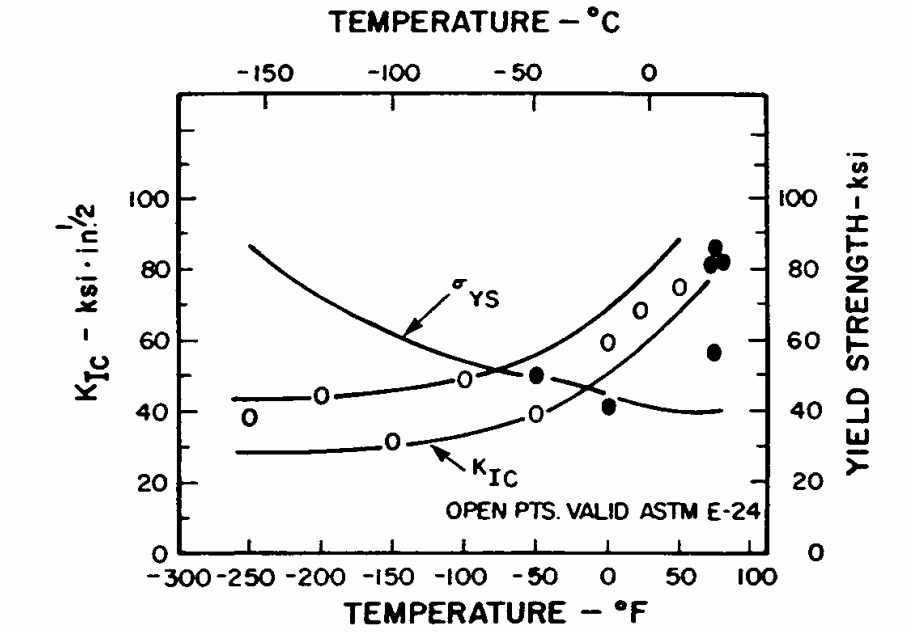

Figure 6.3 Fracture Toughness and Yield Strength of the Material (Greenberg 1969)

For an edge radial crack in a hollow cylinder that is small in comparison to the radial thickness of the cylinder (see Figure 6.4), the stress intensity factor or the fracture toughness at the crack tip is given by

$$K_I = f_e \sigma_\theta \sqrt{\pi a} \tag{6.1}$$

where a = crack length,

f_e = edge effect factor[4],

K_I = stress intensity factor, and

σ_θ = hoop stress; it is obtained straight from the finite element model.

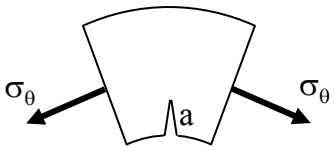

Figure 6.4 Critical Crack Length

If $K_I = K_{IC}(T)$ where $K_{IC}(T)$ is the temperature dependent critical stress intensity factor or fracture toughness of the material, then the critical crack length (that is, the maximum crack length allowable before a crack propagates catastrophically) is determined by equation 6.2 (Kanninen and Popelar, 1985).

$$a_c = \frac{K_{Ic}^2(T)}{f_e^2 \pi \sigma_\theta^2} \tag{6.2}$$

where a_c = critical crack length.

The stress ratio is defined as the ratio of the yield strength of the material to the stress induced in the material. Since the yield strength is temperature dependent and increases with a decrease in temperature, it is calculated using the graph in figure 6.3. The Von-Mises stress is used as the induced stress and it is obtained straight from the finite element model. Mathematically, stress ratio can be expressed as,

$$Stress\ ratio = \frac{Y_s(T)}{\sigma_e}, \text{ where } \sigma_e \text{ is the Von-Mises stress.} \tag{6.3}$$

No exact data is found to calculate the values of yield strength and fracture toughness at different temperatures. The only information available is the graph from figure 6.3. Discrete points were approximated from the curves and used to either interpolate or extrapolate to obtain the required values based on the temperature. The

[4] f_e equals 1.25 for an edge crack which would be the worst case scenario.

lower curve was used for fracture toughness. These points for yield strength and fracture toughness are listed in Table 6.2 and 6.3, respectively.

Temperature °F	Yield Strength ksi	Temperature °F	Yield Strength ksi
-340	102	-120	54
-320	95	-100	52
-300	89	-80	50.5
-280	83	-60	49
-260	78	-40	48
-240	73	-20	47.5
-220	68	0	47
-200	64	20	47
-180	60.5	40	47
-160	58	60	47
-140	56	80	47

Table 6.2 Yield Strength as a Function of Temperature (Greenberg 1969)

Temperature °F	Fracture Toughness ksi √in
-250.0	28
-200.0	29
-150.0	30
-100.0	34
-50.0	39
0.0	51
50.0	68
70.0	77

Table 6.3 Fracture Toughness as a Function of Temperature (Greenberg 1969)

6.3 Post-Processing to get Final Results

The ANSYS program creates excel files with the results for each second of the cooling time in the working directory. The files contain the x, y and z values of the nodes in the polar co-ordinate system, their temperature, total hoop stress and total Von-Mises stress. The temperature of the node is used to find its fracture toughness and yield strength as described in section 6.2. Using the fracture toughness and the hoop stress of the node, the critical crack length (*CCL*) at the location is found using equation 6.2. Similarly, using the yield strength and the Von-Mises stress of the node, the stress ratio (*SR*) at the location is found using equation 6.3. Since the cooling is allowed for 300 seconds (see section 5.2.4), 300 excel files are created – one for each second. Hence, we now have the data for all locations at all times. Using basic functions in excel to find maximum and minimum, the location at which the *CCL* and *SR* are the least, is found for every second of cooling, and a new excel sheet is created with these values. Subsequently, from this data the minimum values of *CCL* and *SR* are found. These values will be the least values for *CCL* and *SR* for the whole run. Once the least values of *CCL* and *SR* for all the cases are found, statistical data analysis is done to find the percentage contributions of each factor.

6.4 Results for 5% Variation Analyses

As discussed earlier, the effects of the trunnion inner diameter, the hub outer diameter and the interference values, on the critical crack length and the stress ratio, are of importance in this thesis. The trunnion inner diameter, and the hub outer diameter are varied by +5% and -5%, and the interference value, is varied from maximum interference to minimum interference. This set of experiments is primarily done for two reasons; first of all, to estimate the percentage contributions of each factor and to study their effects on the critical crack length and the stress ratio. Secondly, they are done to verify the results obtained from the analyses. This is done from the fact that the data obtained from the different levels of one factor for constant values of the other factors, forms a straight line when plotted against the response variable.

The original values for the trunnion inner radius, hub outer radius and the interference value is obtained from Table 6.1. The different levels for the trunnion inner radius and the hub outer radius are obtained by taking -5% and +5% of the original values. The different levels for the interference value are obtained by finding the minimum, the maximum, and the average (mid) value (see Appendix B, section B2). The levels of the factors used are as shown in Table 6.4. Since there are 3 levels for the 3 factors, a total of $3^3 = 27$ experiments are done.

Variable Parameters		**1**	**2**	**3**
		(-5%)	**(nominal)**	**(+5%)**
Inner radius of the trunnion	T_i	1.1281	1.1875	1.2468
Outer radius of the hub (minus flange)	H_i	8.436	8.88	9.324
Radial Interference (in)	IN_i	0.0021249 (min)	0.0029925 (mid)	0.00386 (max)

Table 6.4 Values of the Different Levels of the Factors for the 5% Variations

The experiments were done using the above values and the results obtained were processed as explained in section 6.3. Table 6.5 gives the critical crack length values, its locations and the time it occurs for the 27 cases. Similarly, Table 6.6 gives the stress ratio values, its locations and the time it occurs for the 27 cases. This data is first verified by plotting it against different levels of one factor while keeping the other two constant. The results would be accurate if each of the plots obtained is a straight line. This is shown in figures 6.5 through 6.7. The interference value is made to vary in figures 6.5(a) and 6.5(b) while keeping the trunnion inner radius and hub outer radius constant; trial numbers 1, 2 and 3 are used. Similarly, in figures 6.6(a) and 6.6(b), the hub outer radius is made to vary while keeping the other two constant; trial numbers 3, 6 and 9 are used. And in figures 6.7(a) and 6.7(b), the trunnion inner radius is made to vary while keeping the other two constant; trial numbers 1, 10 and 19 are used.

Trial No	Treatment Combinations	X (in)	Y (Deg)	Z (in)	Time (sec)	CCL (in)
1	*T1-H1-IN1*	1.1281	-150	23	114	0.22998
2	*T1-H1-IN2*	6.472	-145	17	161	0.19648
3	*T1-H1-IN3*	6.472	-150	17	163	0.16011
4	*T1-H2-IN1*	1.1281	-90	23	114	0.23111
5	*T1-H2-IN2*	6.472	-150	17	180	0.21960
6	*T1-H2-IN3*	6.472	-150	17	183	0.17851
7	*T1-H3-IN1*	1.1281	-90	23	113	0.23266
8	*T1-H3-IN2*	9.324	-125	17	95	0.22157
9	*T1-H3-IN3*	6.472	-150	17	194	0.19326
10	*T2-H1-IN1*	1.1875	-90	23	111	0.23501
11	*T2-H1-IN2*	6.472	-145	17	161	0.19866
12	*T2-H1-IN3*	6.472	-150	17	163	0.16176
13	*T2-H2-IN1*	1.1875	-90	23	111	0.23619
14	*T2-H2-IN2*	6.472	-150	17	179	0.22225
15	*T2-H2-IN3*	6.472	-150	17	183	0.18051
16	*T2-H3-IN1*	1.1875	-90	23	111	0.23779
17	*T2-H3-IN2*	9.324	-125	17	95	0.22267
18	*T2-H3-IN3*	6.472	-150	17	193	0.19549
19	*T3-H1-IN1*	1.2468	-150	23	109	0.24031
20	*T3-H1-IN2*	6.472	-145	17	161	0.20093
21	*T3-H1-IN3*	6.472	-150	17	162	0.16345
22	*T3-H2-IN1*	1.2468	-150	23	109	0.24154
23	*T3-H2-IN2*	8.88	-125	17	93	0.22451
24	*T3-H2-IN3*	6.472	-150	17	183	0.18259
25	*T3-H3-IN1*	1.2468	-90	23	108	0.24321
26	*T3-H3-IN2*	9.324	-125	17	95	0.22381
27	*T3-H3-IN3*	9.324	-125	17	95	0.19719

Table 6.5 Critical Crack Length Values for 5% Variations

Trial No	Treatment Combinations	X (in)	Y (Deg)	Z (in)	Time (sec)	SR (in)
1	*T1-H1-IN1*	8.436	-120	12.416	68	1.80818
2	*T1-H1-IN2*	6.472	-150	17	81	1.65213
3	*T1-H1-IN3*	6.472	-150	17	76	1.47924
4	*T1-H2-IN1*	8.88	-120	12.416	71	1.76913
5	*T1-H2-IN2*	8.88	-120	12.416	70	1.65414
6	*T1-H2-IN3*	6.472	-150	17	78	1.52274
7	*T1-H3-IN1*	9.324	-120	12.416	74	1.75506
8	*T1-H3-IN2*	9.324	-120	12.416	73	1.65464
9	*T1-H3-IN3*	6.472	-150	17	80	1.55340
10	*T2-H1-IN1*	8.436	-120	12.416	68	1.81288
11	*T2-H1-IN2*	6.472	-150	17	79	1.65819
12	*T2-H1-IN3*	6.472	-150	17	74	1.48405
13	*T2-H2-IN1*	8.88	-120	12.416	71	1.77317
14	*T2-H2-IN2*	8.88	-120	12.416	70	1.65791
15	*T2-H2-IN3*	6.472	-150	17	78	1.52812
16	*T2-H3-IN1*	9.324	-120	12.416	74	1.75862
17	*T2-H3-IN2*	9.324	-120	12.416	73	1.65802
18	*T2-H3-IN3*	6.472	-150	17	80	1.55915
19	*T3-H1-IN1*	8.436	-120	12.416	67	1.81769
20	*T3-H1-IN2*	6.472	-90	17	78	1.66455
21	*T3-H1-IN3*	6.472	-150	17	73	1.48916
22	*T3-H2-IN1*	8.88	-120	12.416	71	1.77734
23	*T3-H2-IN2*	8.88	-120	12.416	70	1.66179
24	*T3-H2-IN3*	6.472	-150	17	77	1.53357
25	*T3-H3-IN1*	9.324	-120	12.416	74	1.76230
26	*T3-H3-IN2*	9.324	-120	12.416	73	1.66152
27	*T3-H3-IN3*	6.472	-150	17	80	1.56511

Table 6.6 Stress Ratio Values for 5% Variations

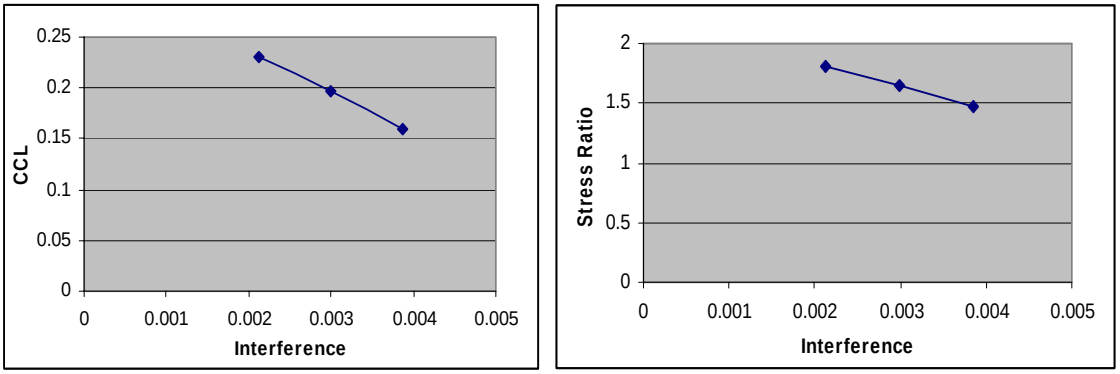

(a) (b)

Figure 6.5 Different Levels of Interference against CCL and SR Values

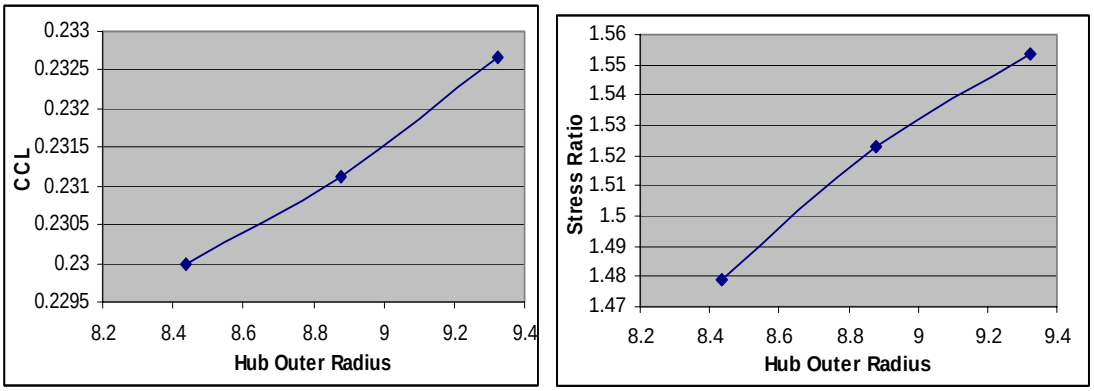

(a) (b)

Figure 6.6 Different Levels of Hub-Outer Radius against CCL and SR Values

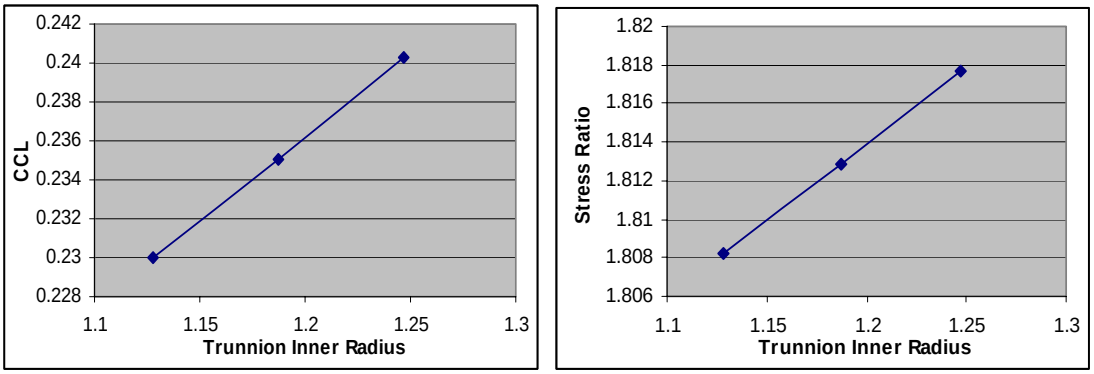

(a) (b)

Figure 6.7 Different Levels of Trunnion Inner Radius against CCL and SR Values

From the plots, we can clearly see that the data obtained are accurate since they form straight lines when plotted against different levels of each factor.

After the data obtained is verified to be accurate, statistical analysis can be done to study the effects of the factors on the stress ratio and the critical crack length. As explained in section 5.3, we use the 2^k factorial design for our statistical data analysis, where k is the number of factors. Since it involves *3* factors, it is called 2^3 Factorial Design and the total number of experiments required is $2^3 = 8$ experiments. The experiments required are the trials in which each of the factors is either at the low level or at the high level. Therefore, all the trials in which the factors have nominal values are eliminated. This leaves us with 8 trials; trial numbers 1, 3, 7, 9, 19, 21, 25, and 27. The values for critical crack length are as shown in Table 6.7. For the purpose of the analysis, the three factors are labeled as shown in the table.

Overall Minimum Critical Crack Length		**H_i (Hub Outer Radius) *B***			
		-5% (8.436)		**+5% (9.324)**	
		IN_i (Interference) *A*		**IN_i (Interference) *A***	
T_i (Trunnion Inner Radius) *C*	**Variations**	**Min (0.0021249)**	**Max (0.00386)**	**Min (0.0021249)**	**Max (0.00386)**
	-5% (1.1281)	(1) 0.22998	a 0.16011	b 0.23266	ab 0.19326
	+5% (1.2468)	c 0.24031	ac 0.16345	bc 0.24321	abc 0.19719

Table 6.7 Notations and Values for 2^3 Factorial Design Data Analysis for CCL

Using the values from Table 6.7, the calculations for the 2^3 Factorial Design are done as explained in section 5.4 to obtain the effects of the factors on the critical crack length. The effects are shown in Table 6.8. We can see that the interference between the trunnion and the hub has the most effect on the critical crack length (84%), followed by the hub radius (8%), and the interaction of the interference and the hub radius (5%). The trunnion inner radius has a very small effect (1%) when compared to the interference.

Factor	Effect Estimate	Sum of Squares	Percent Contribution	p-values
Interference, A	-0.058	6.736 x 10^{-3}	84.358	<0.00001
Hub Radius, B	0.018	6.566 x 10^{-4}	8.223	<0.00001
Trunnion Radius, C	7.041 x 10^{-3}	9.914 x 10^{-5}	1.242	<0.00001
AB	0.015	4.7 x 10^{-4}	5.886	<0.00001
AC	-3.402 x 10^{-3}	2.315 x 10^{-5}	0.29	<0.00001
BC	-1.236 x 10^{-4}	8.292 x 10^{-8}	1.038 x 10^{-3}	<0.00001
ABC	9.655 x 10^{-5}	2.061 x 10^{-6}	2.335 x 10^{-4}	<0.00001
Pure Error	--------	0	3.565 x 10^{-13}	--------
Total	--------	7.985 x 10^{-3}	--------	--------

Table 6.8 Percentage Contributions of the Factors for CCL

Similar analysis is done for the Stress Ratio. The notations and values used are shown in Table 6.9 and the effects of the factors are shown in Table 6.10. The interference between the trunnion and the hub has the most effect on the stress ratio (94%), followed by the interaction of the interference and the hub outer radius (5.64%).

Overall Minimum Stress Ratio		**H_i (Hub Outer Radius) *B***			
		-5% (8.436)		**+5% (9.324)**	
		IN_i (Interference) *A*		**IN_i (Interference) *A***	
T_i (Trunnion Inner Radius) *C*	**Variations**	**Min (0.0021249)**	**Max (0.00386)**	**Min (0.0021249)**	**Max (0.00386)**
	-5% (1.1281)	(1) 1.80818	a 1.47924	b 1.75506	ab 1.55340
	+5% (1.2468)	c 1.81769	ac 1.48916	bc 1.76230	abc 1.56511

Table 6.9 Notations and Values for 2^3 Factorial Design Data Analysis for SR

Factor	Effect Estimate	Sum of Squares	Percent Contribution	p-Values
Interference, *A*	-0.264	0.139	94.087	<0.00001
Hub Diameter, *B*	0.01	2.161 x 10^{-4}	0.146	<0.00001
Trunnion Diameter, *C*	9.599 x 10^{-3}	1.843 x 10^{-4}	0.124	<0.00001
AB	0.065	8.36 x 10^{-3}	5.64	<0.00001
AC	1.216 x 10^{-3}	2.956 x 10^{-6}	1.994 x 10^{-3}	<0.00001
BC	-1.23610^{-4}	3.057 x 10^{-8}	2.062 x 10^{-5}	<0.00001
ABC	1.015 x 10^{-3}	2.061 x 10^{-6}	1.39 x 10^{-3}	<0.00001
Pure Error	--------	1.425 x 10^{-15}	9.612 x 10^{-13}	--------
Total	--------	0.148	--------	--------

Table 6.10 Percentage Contributions of the Factors for SR

6.5 AASHTO Results

The American Association of State Highway and Transportation Officials (AASHTO) standards call for a hub radial thickness of 0.4 times the inner diameter, while currently a thickness of 0.1 to 0.2 times the inner diameter is used. Therefore, it is imperative to study how the critical crack length and the stress ratio change when the AASHTO standards are employed, and if it is better than the current practice. The low level of the hub diameter is chosen as 1.1 times the inner diameter, which is the current practice. The high level is chosen as the AASHTO recommended standard, which is 1.4 times the inner diameter. Hence,

$$\text{Low Level} = \frac{\text{Inner Diameter} + (0.1 \text{ x Inner Diameter})}{2}$$
$$= \frac{(6.472 \times 2) + (0.1 \times 6.472 \times 2)}{2}$$
$$= 7.1192$$

$$\text{High Level} = \frac{\text{Inner Diameter} + (0.4 \times \text{Inner Diameter})}{2}$$
$$= \frac{(6.472 \times 2) + (0.4 \times 6.472 \times 2)}{2}$$
$$= 9.0608$$

The interferences vary from maximum to minimum, and the trunnion inner diameter is varied by 10%. Since we need only *8* experiments for the 2^3 factorial design, only the high and low values are used. The values used are as shown in Table 6.11.

Variable Parameters		**1 (Low)**	**2 (High)**
Inner radius of the trunnion	T_i	1.06875	1.30625
Outer radius of the hub (minus flange)	H_i	7.1192	9.0608
Radial Interference (in)	IN_i	0.0021249 (min)	0.00386 (max)

Table 6.11 Values of the Different Levels of the Factors for the AASHTO Results

The experiments were conducted and the data obtained were post-processed as explained in section 6.3. The calculations for the statistical data analysis are done using the equations given in section 5.4. The results obtained for the Critical Crack Length are shown in Table 6.12 through Table 6.14.

Trial No	Treatment Combinations	*X* (in)	*Y* (Deg)	*Z* (in)	Time (sec)	*CCL* (in)
1	*T1-H1-IN1*	7.1192	-125	17	90	0.09735
2	*T1-H1-IN2*	7.1192	-125	17	96	0.06799
3	*T1-H2-IN1*	1.06875	-90	23	116	0.22689
4	*T1-H2-IN2*	6.472	-150	17	191	0.18302
5	*T2-H1-IN1*	7.1192	-125	17	85	0.09983
6	*T2-H1-IN2*	7.1192	-125	17	91	0.06954
7	*T2-H2-IN1*	1.30625	-90	23	106	0.24783
8	*T2-H2-IN2*	6.472	-150	17	188	0.19167

Table 6.12 Critical Crack Length Values for AASHTO Results

Overall Minimum Critical Crack Length		**H_i (Hub Outer Radius) *B***			
		Low (7.1192)		**High (9.0608)**	
		IN_i (Interference) *C*		**IN_i (Interference) *C***	
T_i (Trunnion Inner Radius) *A*	**Variations**	**Min (0.0021249)**	**Max (0.00386)**	**Min (0.0021249)**	**Max (0.00386)**
	Low (1.1281)	(1) 0.09735	c 0.06799	b 0.22689	bc 0.18302
	High (1.30625)	a 0.09983	ac 0.06954	ab 0.24783	abc 0.19167

Table 6.13 Notations and Values for 2^3 Factorial Design for CCL (AASHTO)

Factor	Effect Estimate	Sum of Squares	Percent Contribution	p-Values
Trunnion Diameter, A	8.404 x 10^{-3}	1.413 x 10^{-4}	0.384	<0.00001
Hub Diameter, B	0.129	0.033	90.067	<0.00001
Interference, C	-0.04	3.187 x 10^{-3}	8.669	<0.00001
AB	6.389 x 10^{-3}	8.163 x 10^{-5}	0.222	<0.00001
AC	-3.303x 10^{-3}	2.182 x 10^{-5}	0.059	<0.00001
BC	-0.01	2.039 x 10^{-4}	0.555	<0.00001
ABC	-2.84 x 10^{-3}	1.613 x 10^{-5}	0.044	<0.00001
Pure Error	--------	0	--------	--------
Total	--------	0.037	--------	--------

Table 6.14 Percentage Contributions of the Factors for CCL (AASHTO)

From the above results, the hub outer radius is observed to have the most effect on the critical crack length (90%), followed by the interference (8.67%).

The results obtained for the Stress Ratio are shown in Table 6.15 through Table 6.17.

Trial No	Treatment Combinations	*X* (in)	*Y* (Deg)	*Z* (in)	Time (sec)	*SR*
1	*T1-H1-IN1*	6.472	-115	17	60	1.36273
2	*T1-H1-IN2*	6.472	-115	17	45	1.10838
3	*T1-H2-IN1*	9.0608	-120	12.416	73	1.75767
4	*T1-H2-IN2*	6.472	-150	17	80	1.53136
5	*T2-H1-IN1*	6.472	-115	17	59	1.37644
6	*T2-H1-IN2*	6.472	-115	17	45	1.11621
7	*T2-H2-IN1*	9.0608	-120	12.416	72	1.77314
8	*T2-H2-IN2*	6.472	-150	17	78	1.55365

Table 6.15 Stress Ratio Values for AASHTO Results

Overall Minimum Stress Ratio		H_i (Hub Outer Radius) *B*			
		Low (7.1192)		High (9.0608)	
		IN_i (Interference) *C*		IN_i (Interference) *C*	
T_i (Trunnion Inner Radius) *A*	Variations	Min (0.0021249)	Max (0.00386)	Min (0.0021249)	Max (0.00386)
	Low (1.06875)	(1) 1.36273	c 1.10838	b 1.7567	bc 1.53136
	High (1.30625)	a 1.37644	ac 1.11621	ab 1.77314	abc 1.55365

Table 6.16 Notations and Values for 2^3 Factorial Design for SR (AASHTO)

Factor	Effect Estimate	Sum of Squares	Percent Contribution	p-Values
Trunnion Diameter, A	0.015	4.397×10^{-4}	0.096	<0.00001
Hub Diameter, B	0.413	0.341	74.3565	<0.00001
Interference, C	-0.24	0.115	25.198	<0.00001
AB	4.054×10^{-3}	3.287×10^{-5}	7.185×10^{-3}	<0.00001
AC	2.382×10^{-4}	1.135×10^{-7}	2.481×10^{-5}	<0.00001
BC	0.017	5.917×10^{-4}	0.129	<0.00001
ABC	3.174×10^{-3}	2.015×10^{-5}	4.405×10^{-3}	<0.00001
Pure Error	--------	2.705×10^{-15}	5.912×10^{-13}	--------
Total	--------	0.458	--------	--------

Table 6.17 Percentage Contributions of the Factors for the Stress Ratio (AASHTO)

From the above results, the hub outer radius is observed to have the most effect on the stress ratio (74%), followed by the interference (25%).

6.6 Explanation of the Results

From the results obtained for the 5% variation analyses, it is clearly seen that the interference between the trunnion and the hub is the factor that has the most effect on the critical crack length and the stress ratio. The values for critical crack length and stress ratio change the most when the interference value changes, whereas the change is very small when the trunnion inner diameter or the hub outer diameter is changed (Tables 6.7 and 6.9). This is in conjunction with one of the conclusions obtained from previous studies done at USF which consequently led to the recommendation that *AP2* is better than *AP1*, as the interference stresses between the trunnion and the hub are absent. However, the results obtained from the AASHTO analyses show that the hub outer diameter is the most significant factor followed by the interference. This behavior of the results can be attributed to two important reasons.

The first reason is that the percentage variations of the hub diameter in the AASHTO analyses are different from the percentage variations in the 5% analyses. While the variations are only 5% in the latter case, they are about 12% in the former. Since the variations are more in the AASHTO analyses, the percentage contribution is also more.

The second and the more important reason is due to the physics of the problem. The total stresses produced in the trunnion-hub assembly are a sum of the interference stresses and the thermal stresses. The interference stresses are influenced by the kind of fits used and the diameters of the trunnion and the hub. For the interference stresses to be minimum, the hub outer diameter needs to approach infinity (Ugural and Fenster 1995). In other words, the interference stresses decrease as the hub outer diameter increases.

Since the variation of the hub outer diameter is greater in the AASHTO analyses, the difference in the values obtained for *CCL* and *SR* between the two levels is also greater. Hence, the percentage contribution of the hub outer diameter is greater in the AASHTO analyses.

CHAPTER 7
CONCLUSIONS AND RECOMMENDATIONS

7.1 Conclusions

The main objective of this thesis is to study the effects of geometric parameters such as the hub outer diameter, the trunnion inner diameter, and the interference, on critical stresses and critical crack length during the assembly. The results obtained by varying the parameters by a value of ±5% revealed that the interference between the trunnion and the hub had the most effect on the critical crack length and the critical stresses developed during the assembly. For cases with low or minimum interference, the critical crack length and stress ratio were higher than in cases with maximum interference. Although this set of analyses revealed important and valid results, these values are not used in real life nor are they recommended by AASHTO.

The AASHTO standards call for a hub radial thickness of 0.4 times the diameter. However, in real life practice, the hub radial thickness used is 0.1 to 0.2 times the diameter. Hence, using the extremes as the hub thickness, ±10% variation in the trunnion inner diameter, and interferences ranging from minimum possible value to maximum possible value, it is found that the hub outer diameter is the most significant factor that affects the critical crack length and the critical stresses developed during the assembly, followed by the interference between the trunnion and the hub (Tables 6.14 and 6.17). The critical crack length values obtained for the AASHTO specifications were more than two times the critical crack length values obtained for the specifications used in real life practice (Table 6.12). The values for stress ratio were also higher (≈ 30% for low interference and ≈ 40% for high interference) for the AASHTO cases (Table 6.15).

Therefore, it can be concluded that the AASHTO standards are safer than the current practices used in the manufacturing of trunnion-hub-girder assemblies for bascule bridges. If employed, the AASHTO standards will yield higher critical crack length and

stress ratio. It can also prove out to be more economical during the manufacturing process by reducing the failures and hence, saving hundreds of thousands of dollars.

Comparing the two sets of analyses, that is, the 5% variations and the AASHTO cases, we see that while the interference affects the final results the most in the former, the hub outer diameter has the most significant effect in the latter. The variations in the interferences are same for both the analyses and they vary by approximately ±23%. The trunnion inner diameter and the hub outer diameter vary by ±5% in the first set of analyses; the trunnion inner diameter varies by ±10% and the hub outer diameter varies by approximately ±12% in the AASHTO cases. Therefore, the results obtained cannot be attributed entirely to the percentage variations in the factors and it cannot be concluded that the factor varying the most will have the most effect on the final results. As explained in section 6.5, the physics of the problem is a very important factor to be considered.

7.2 Recommendations for Future Work

Although this thesis evolved as a result of the recommendations made after completing the studies to understand the failures that occurred during the manufacturing of the trunnion-hub-girder assembly for bascule bridges, there is still scope for future work to completely optimize the geometry and the manufacturing process.

This thesis focused at the sensitivity of important parameters including the hub outer diameter, the trunnion inner diameter, and the interference, on the critical stresses and the critical crack length. It would be interesting to study and analyze the sensitivity of other parameters such as the hub length and the gusset thickness on the critical stresses and the critical crack length. Based on this, the entire geometry of the trunnion-hub assembly could be optimized and made available to the manufacturers to ensure safe manufacturing and effective use in the bridges that would be required to support more lanes of traffic in the years to come.

REFERENCES

Glen Besterfield, Autar Kaw & Roger Crane, 2001, *Parametric Finite Element Modeling and Full-Scale Testing Of Trunnion-Hub-Girder Assemblies for Bascule Bridges*, Mechanical Engineering Dept, USF, FL

Denninger, M.T., 2000, *Design Tools for Trunnion-Hub Assemblies for Bascule Bridges*, MS Thesis, Mechanical Engineering Dept, USF, FL

Ratnam, B., 2000, *Parametric Finite Element modeling of trunnion Hub Girder Assemblies for Bascule Bridges*, MS Thesis, Mechanical Engineering Dept, USF, FL

Nichani, S., 2001, *Full Scale Testing of Trunnion-Hub-Girder Assembly of a Bascule Bridge*, MS Thesis, Mechanical Engineering Dept, USF, FL

Ugural, A.C., and Fenster, S.K., 1995, *Advanced Strength and Applied Elasticity,* Prentice Hall PTR, New Jersey

ANSYS Inc., 2002, *ANSYS Release 7.0 Documentation*

Montgomery, D.C., 2001, *Design and Analysis of Experiments,* John Wiley & Sons, Inc., New York

Özişik, M. N., 1993, *Heat Conduction*, John Wiley & Sons, Inc., New York

Shigley, J.E., and Mischke, 1986, *Standard Handbook of Machine Design*, McGraw-Hill, New York

Timoshenko, S. P., and Goodier, J. N., 1951, *Theory of Elasticity*, McGraw-Hill Book Company, New York

Kreith, F., and Bohn, M., 1986, *Principles of Heat Transfer*, Harper & Row, New York

Logan, D. L., 1992, *A First Course in Finite Element Method*, PWS-KENT Publishing Company, Boston

Barron, R. F., (1999), *Cryogenic Heat Transfer*, Taylor and Francis Company, PA, pp. 161-172

Greenberg, H.D., and Clark, Jr. H.G., 1969, *A Fracture Mechanics Approach to the Development of Realistic Acceptance Standards for Heavy Walled Steel Castings*, Metals Engineering Quarterly, 9(3), 30-33

American Association of State Highway and Transportation Officials, ***1998,*** *Mobile Bridge Inspection, Evaluation, and Maintenance Manual*

Mechanical Engineering Dept, USF, FL, 2003, Scope of Work Proposal for *Optimization of Geometrical Parameters of Trunnion-Hub-Girder Assembly in Bascule Bridges*

APPENDICES

Appendix A: Program Flow and User Instructions

A.1 Program Flow

The flowchart of the programs is given in figures A.1 through A.3. It gives the flowchart of the ANSYS program, followed by the Excel program, and finally, the 2^k factorial design calculations, which is done using MathCAD.

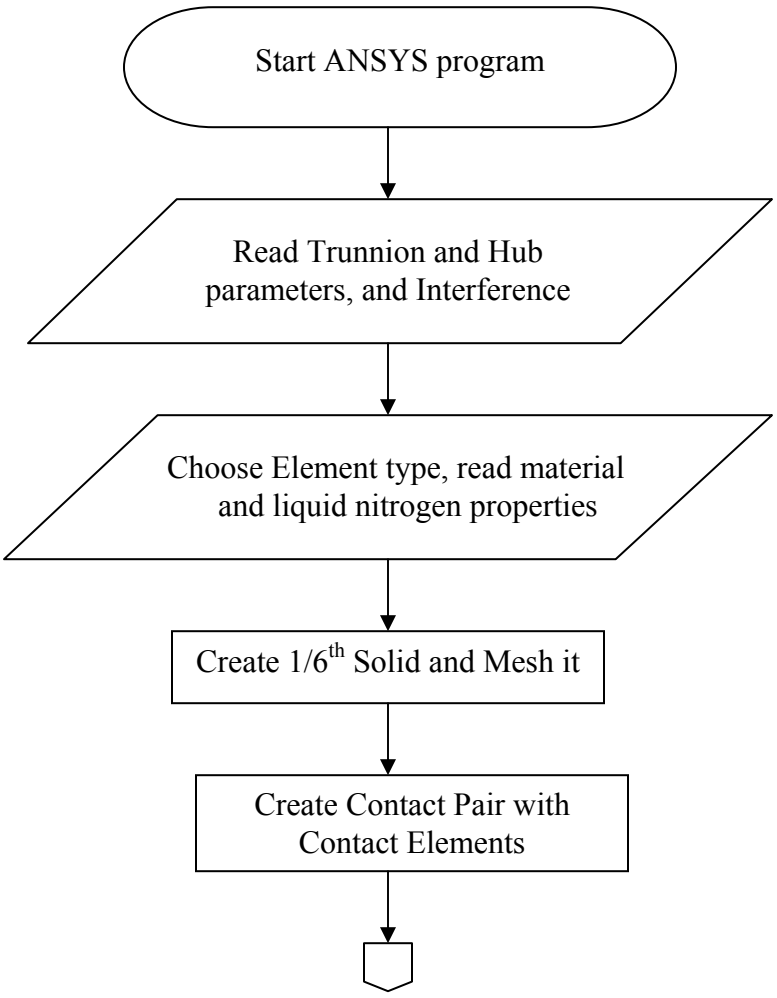

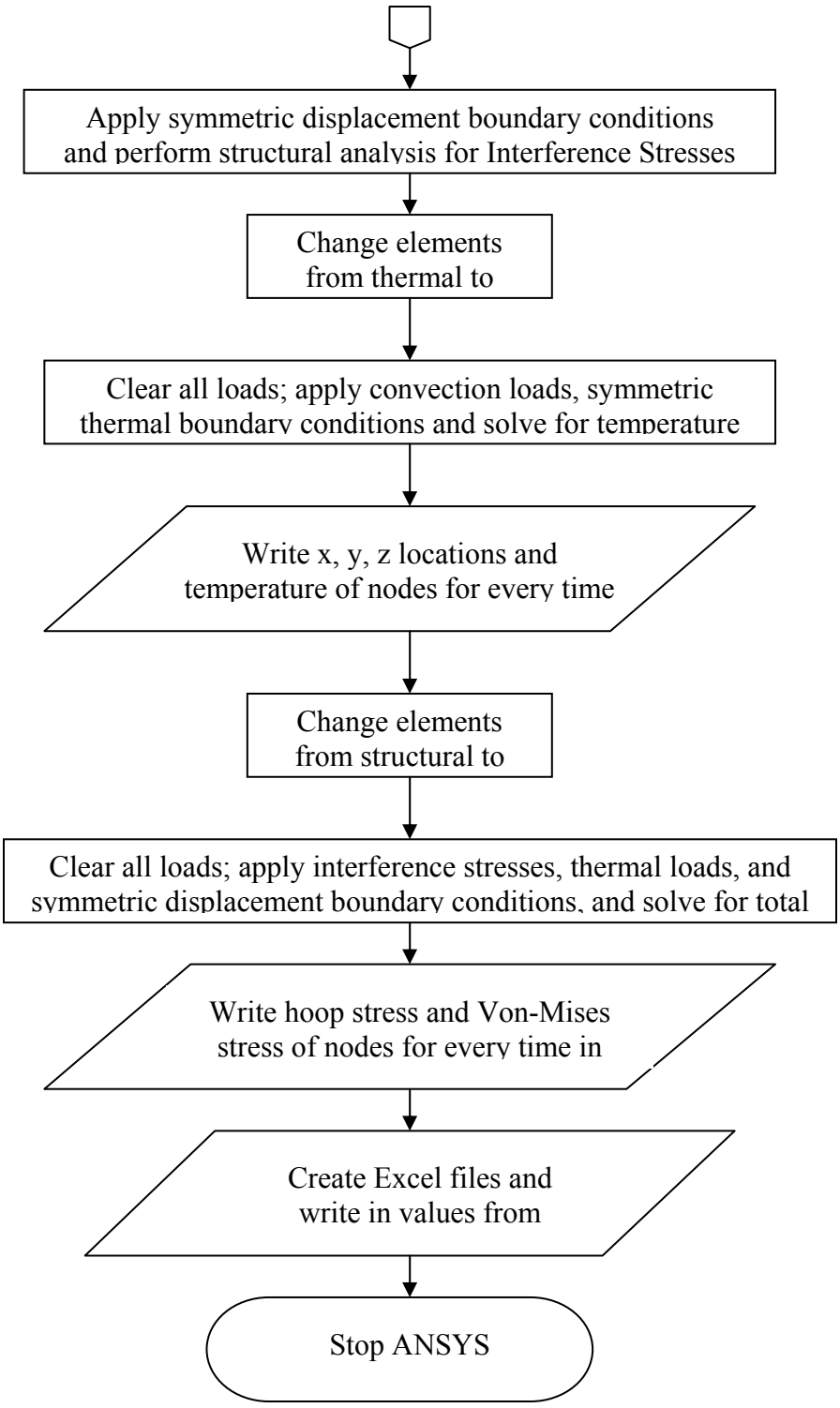

Figure A.1 Flowchart for the ANSYS Program

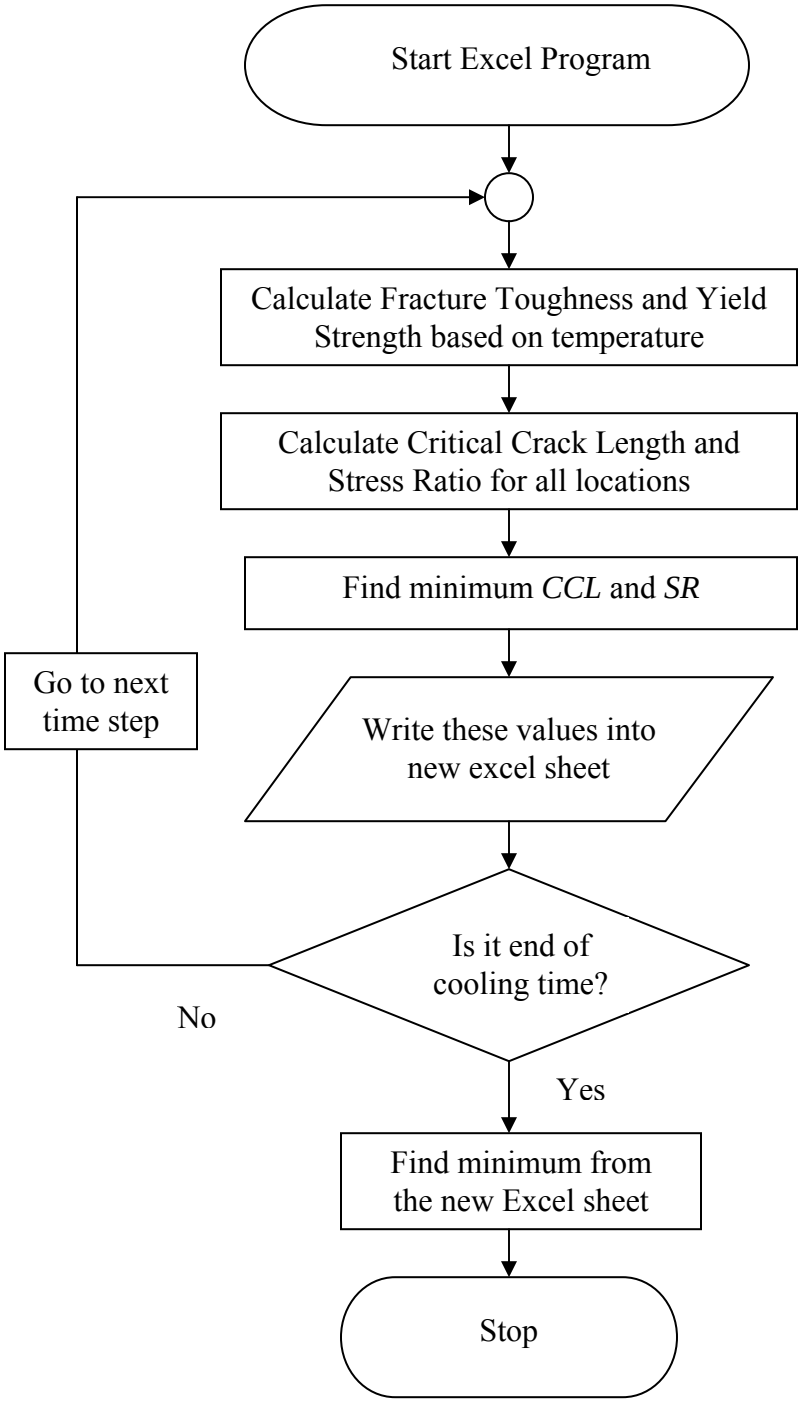

Figure A.2 Flowchart for the Excel Program

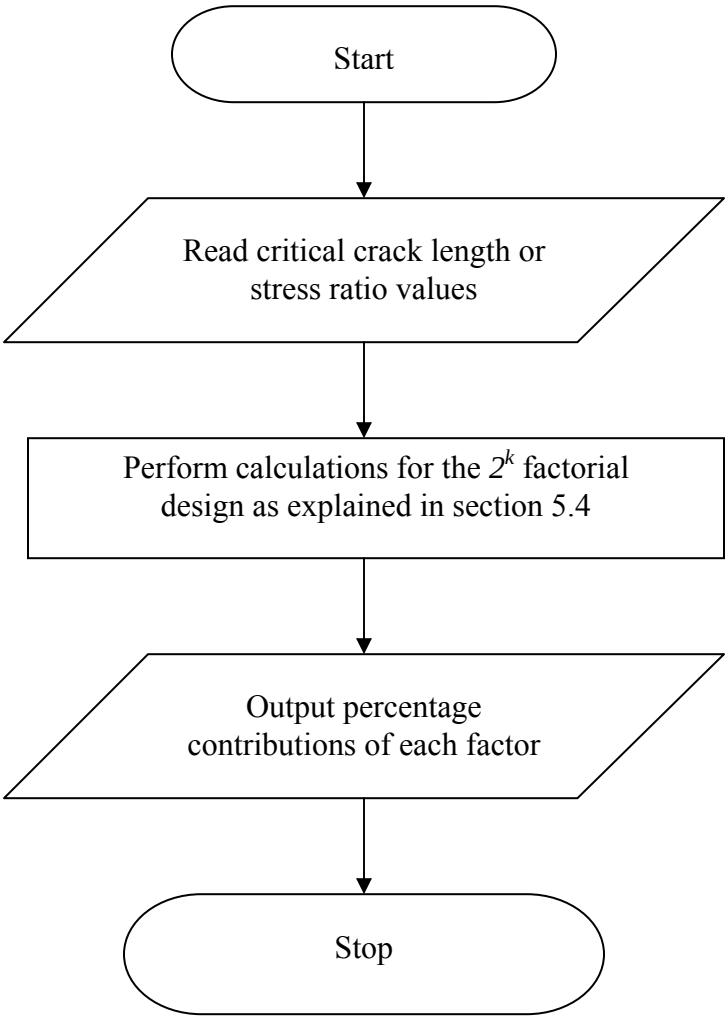

Figure A.3 Flowchart for the 2^k Factorial Design Data Analysis

A.2 Modeling the Experiment

The commands for the ANSYS program are stored in a file called 17th_Causeway_Complete. The first few lines in the command file read in the input parameters including the dimensions of the trunnion and the hub, interference, divisions for mesh, and the cooling time. They can be changed according to the need of the user and saved before starting the experiment. It is important to make sure that the command file for ANSYS, and the excel program, Data Analyzer, for calculating the *CCL* and *SR* using fracture toughness and yield strength are stored in the same directory. After starting

ANSYS, pull down the File menu and select Change Directory. When the window opens with all the directories, select the directory in which the command file is stored and click OK. Now, this directory is set as the working directory and all the files that result from the program will be stored in this directory, including the excel sheets with the results. The experiment can be started in two ways; pull down the File menu, click on Read Input From, select the command file and click OK, or click on the Open ANSYS file tab, from the drop down menu for file types in the window that opens, choose ANSYS Commands, select the command file and click OK. ANSYS starts reading the commands in the file and performs the appropriate functions. The total run time depends on the time for cooling, and the computer configurations used. For a cooling time of 300 seconds in the latest P4 processor with 512MB RAM, the run time is approximately 1.5 hrs. The number of the excel files created also depend on the cooling time, and are equal to the cooling time.

Once the ANSYS run is completed and the excel files are stored in the working directory, the excel program for calculating the *CCL* and *SR* can be started. The file, Data Analyzer, is an excel macro that calculates the Critical Crack Length and Stress Ratio. The first two rows of the file are for the input. The input is the number of files that the ANSYS program creates. Hence, the input will be that same number as the cooling time in the ANSYS program. After inputting the number of files, click the Analyze tab. The program starts calculating the fracture toughness, yield strength, *CCL* and *SR* for every location in each file, which represents each time-step for cooling. It then finds the minimum values for *CCL* and *SR* from each file and stores it in the Data Analyzer file along with its location and the time it occurs. From the values stored, it finds the minimum and outputs at the beginning of the worksheet.

The program for statistical data analysis, called per_con, is a MathCAD program that performs calculations as explained in section 5.4. The inputs are manually entered and the percentage contributions are shown in the same MathCAD sheet.

Appendix B: Verifications of Analyses

B.1 Introduction

To verify the various analyses and to check if the results are true, sample analyses were done for problems whose solutions were known. The solutions were first calculated with the help of analytical equations, and then simulated using ANSYS to obtain similar solutions. The final verification includes the application of the knowledge of thermal stresses – that a member will not experience any stresses due to temperature, if the temperature gradient in the member is equal to zero. Following are the various test analyses that were done.

B.2 Test 1 for Structural Analysis for Interference Stresses

At the end of step 2 of *AP1* (see section 1.2), the trunnion is fit into the hub to form an interference fit. This interference fit produces interference stresses in the trunnion-hub assembly. To verify the structural analysis to find the interference stresses, an interference fit between two cylinders was simulated and the stresses thus produced were found. The specifications of the 2 cylinders are:

Cylinder 1 - Inner Radius = 2" Outer Radius = 8.7"

Cylinder 2 - Inner Radius = 8.7" Outer Radius = 16.7"

It is assumed that both the cylinders are made of steel (E = 29 Msi, ν = 0.3), *FN2* fit is used at the interface, the radial displacement is of the form for axisymmetric problems, and that plane stress conditions apply.

The interference values on the cylinders for the *FN2* fit are calculated using the formula:

$$L = CD^{\frac{1}{3}}, \qquad \text{(B.1)}$$

where L is the limit in thousandths of an inch

C is the coefficient of the fit whose values are given in table B.1, and

D is the diameter.

Class of Fit	Hole Limits		Shaft Limits	
	Lower	Upper	Lower	Upper
FN2	0	+0.907	+2.717	+3.288

Table B.1 Coefficients for *FN2* fit

B.2.1 Exact Solution

The exact solution of the problem was obtained using Maple. The lower limit and the upper limit of the cylinders are first found, using equation B.1 and the coefficients from Table B.1. Hence,

Lower limit of cylinder 1: $l\lim 1 = 0.00704054$

Upper limit of cylinder 1: $u\lim 1 = 0.00852017$

Lower limit of cylinder 2: $l\lim 2 = 0$

Upper limit of cylinder 2: $u\lim 2 = 0.00235030$

The maximum diametrical interference in inches is:

$$\begin{aligned} del1 &= u\lim 1 - l\lim 2 \\ &= 0.00852017 - 0 \\ &= 0.00852017 \end{aligned}$$

The Radial Interference in inches is:

$$\delta 1 = \frac{del1}{2} = 0.00426008$$

The radial deflection in cylinder 1 is given by:

$$Ur1 = C_1.r + \frac{C_2}{r} \qquad \text{(B.2)}$$

The radial deflection in cylinder 2 is given by:

$$Ur2 = C_3 + \frac{C_4}{r} \qquad \text{(B.3)}$$

Radial stress on Cylinder 1: $\sigma_r^1 = \frac{E}{1-\nu^2}\left(C_1(1+\nu) - C_2\left(\frac{1-\nu}{r^2}\right)\right)$ (B.4)

Radial stress on Cylinder 2: $\sigma_r^2 = \frac{E}{1-\nu^2}\left(C_3(1+\nu) - C_4\left(\frac{1-\nu}{r^2}\right)\right)$ (B.5)

Hoop stress on cylinder 1: $\sigma_\theta^1 = \frac{E}{1-\nu^2}\left(C_1(1+\nu) + C_2\left(\frac{1-\nu}{r^2}\right)\right)$ (B.6)

Hoop stress on cylinder 2: $\sigma_\theta^2 = \frac{E}{1-\nu^2}\left(C_3(1+\nu) + C_4\left(\frac{1-\nu}{r^2}\right)\right)$ (B.7)

The boundary conditions for this problem are:

$$@\ \text{r} = 2\text{"};\ \sigma_r^1 = 0$$

$$@\ \text{r} = 16.7\text{"};\ \sigma_r^2 = 0$$

$$@\ \text{r} = 8.7\text{"};\ \sigma_r^1 - \sigma_r^2 = 0$$

$$@\ \text{r} = 8.7\text{"};\ \text{Ur2-Ur1} = \delta 1$$

The boundary conditions are substituted in equations B.2 through B.7 and solved for the constants C_1, C_2, C_3 and C_4. Hence,

$$C_1 = -0.0001266869$$
$$C_2 = -0.0009411028$$
$$C_3 = 0.00004469579$$
$$C_4 = 0.023149675$$

The constants C_1, C_2, C_3 and C_4 are used to calculate the stresses at the interface where r = 8.7, from the equations B.4 through B.7. Therefore, at interface,

$$\sigma_r^1 = -4971.09\,psi\ ,\quad \sigma_r^2 = -4971.09\,psi$$

$$\sigma_\theta^1 = -5525.82\,psi\ ,\quad \sigma_\theta^2 = 8674.45\,psi$$

The Von-Mises stress is found using the formula:

$$\sigma_e(1,2) = \sqrt{(\sigma_r^{1,2})^2 + (\sigma_\theta^{1,2})^2 - \sigma_r^{1,2} \cdot \sigma_\theta^{1,2}} \quad \text{(B.8)}$$

The Von Mises Stress for Cylinder 1 and 2 are:

$$\sigma_e(1) = 5270.39Psi \qquad \sigma_e(2) = 11961.58Psi$$

Hence, the actual Von-Mises stresses at the interface due to the interference fit are calculated to be 11.96 ksi for cylinder 2 and 5.27 ksi for cylinder 1.

B.2.2 ANSYS Solution

The same problem was solved in ANSYS. A structural analysis to determine the interference stresses was done by allowing the interference fit to take place. Contact elements as described in Chapter 4 are used at the interface. The problem is solved with no additional displacement constraints or external forces. Cylinder 1 is constrained within cylinder 2 due to its geometry. Stresses are generated due to the general misfit between the target (cylinder 2) and the contact (cylinder 1) surfaces. The Von-Mises stresses obtained due to the interference fit are shown. It can be seen that the maximum stresses occur at the interface. The interface can be seen as a thin white line.

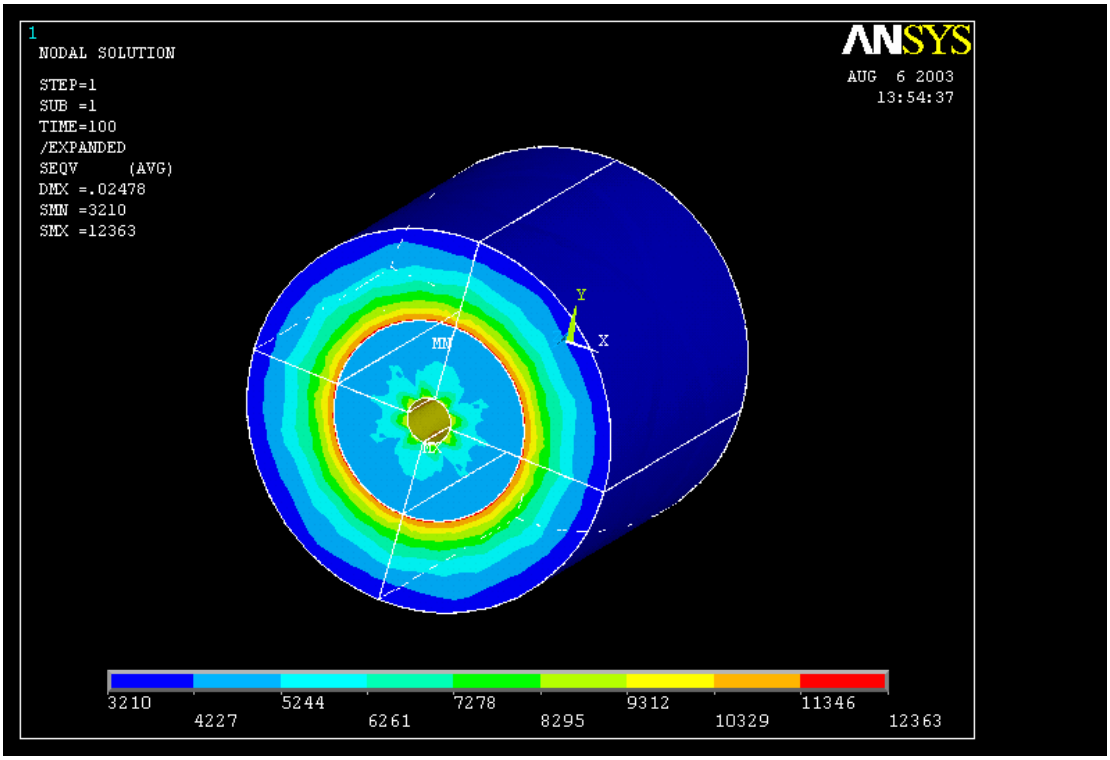

Figure B.1 Interference Stresses (Von-Mises) between 2 Cylinders (Isometric View)

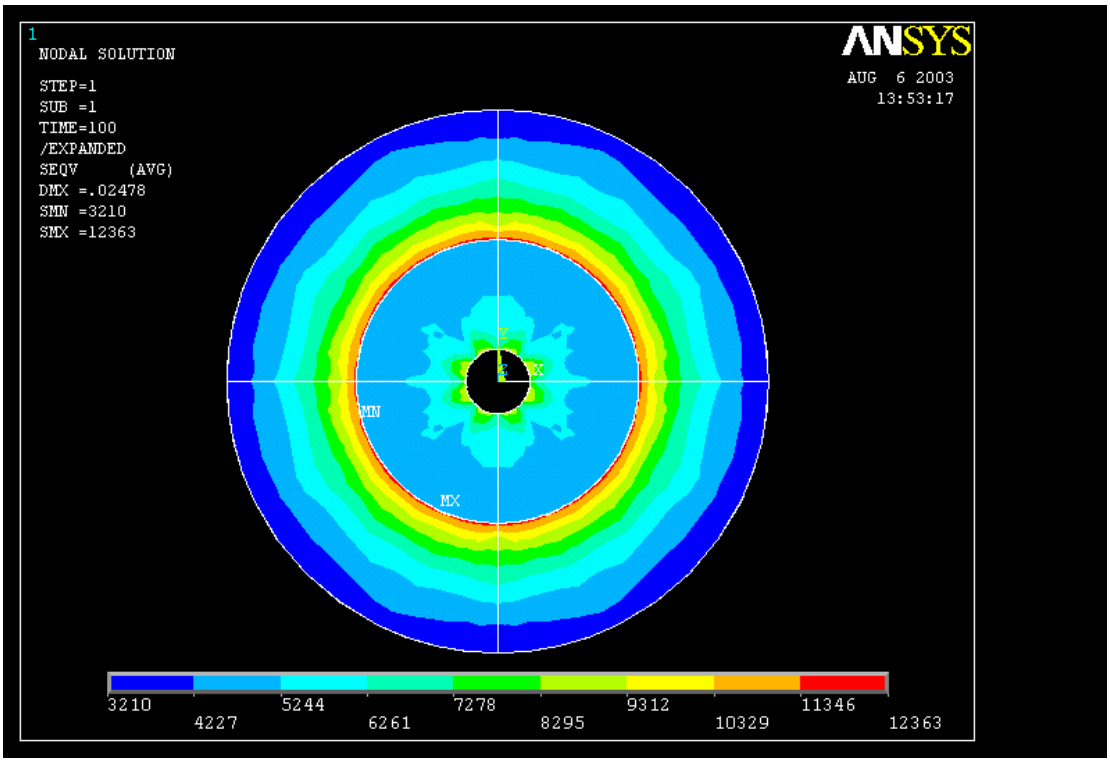

Figure B.2 Interference Stresses (Von-Mises) between 2 Cylinders (Front View)

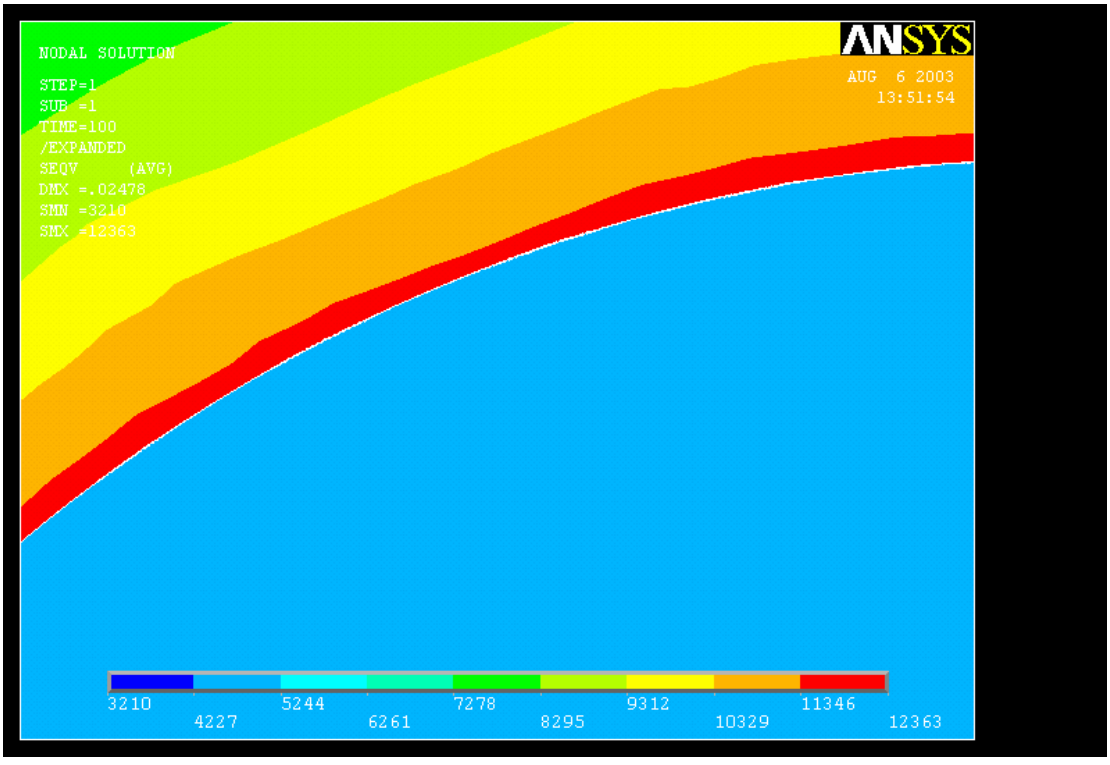

Figure B.3 Interference Stresses (Von-Mises) at the Interface

Hence, the Von-Mises stresses obtained from ANSYS at the interface due to the interference fit are found to be between 11.34 ksi and 12.36 ksi for cylinder 2, and between 4.22 ksi and 5.24 ksi for cylinder 1.

B.2.3 Comparison of Actual Solution vs. ANSYS Solution

To verify the accuracy of the result obtained from ANSYS, the percentage difference between the exact solution, obtained using Maple, and the solution obtained from ANSYS is calculated by making use of the formula,

$$\text{Percentage Difference} = \left| \frac{\text{Exact Solution - ANSYS Solution}}{\text{Exact Solution}} \right| \times 100 . \qquad \text{(B.9)}$$

The maximum value of the stress from ANSYS is used to find the percentage difference.

For cylinder 2,

$$\text{Percentage Difference} = \left| \frac{11961 - 12363}{11961} \right| \text{x } 100$$

$$= 3.36\%$$

For cylinder 1,

$$\text{Percentage Difference} = \left| \frac{5270 - 5244}{5270} \right| \text{x } 100$$

$$= 0.49\%$$

The percentage differences between the actual solution and the ANSYS solution for the stresses for the 2 cylinders are very small (3.36% and 0.49%) and hence, it can be concluded that the structural analysis to find the interference stresses is accurate.

B.3 Test 2 for Structural Analysis for Interference Stresses

This test was done using the trunnion-hub assembly as the model, with parameters and properties as explained in Chapter 3. The interference stress was compared with the interference stress that Ratnam (2000) obtained in his work. The value for the hoop stress that Ratnam (2000) obtained after interference was approximately 14121 psi while the Hoop stress obtained in this test is 13678 psi. The formula from equation B.9 was used and the percentage difference was found to be

$$\text{Percentage Difference} = \left|\frac{14121 - 13678}{14121}\right| \times 100 = 3.14\%$$

B.4 Test 1 for Thermal Analysis for Cooling in a Liquid Bath

Step 3 of *AP1* (see section 1.2) involves cooling the trunnion-hub assembly to shrink it so that it can be fit into the girder with an interference fit. This is done by immersing the assembly in a liquid nitrogen bath. The initial temperature of the trunnion-hub assembly is 80^0F and the temperature of liquid nitrogen is -321^0F, and its convection coefficient changes as a function of temperature. This is simulated in ANSYS to obtain the temperature distribution, which will then be used to find the stresses due to temperature gradients. This thermal analysis was verified using the following example.

A copper wire at 300 ^{0}F is cooled in a water bath maintained at 100 ^{0}F. The temperature distribution against time was obtained and plotted, and the temperature of the wire at specific times was found using ANSYS. These results were compared with the actual solutions, calculated using the analytical equations. The specifications of the problem are given below:

Diameter of the copper wire $d = (1/32)\,in$

Initial temperature of wire $T_0 = 300^0\,F$

Thermal conductivity of copper $k = 216\,Btu/hr\ \ ft\,F$

Specific heat of copper $C = 0.091\, Btu / lb\, F$

Density of copper $\rho = 558\, lb / cu\ ft$

Temperature of water bath $T_\infty = 100^0\, F$

Convection coefficient of water $h = 15\, Btu / hr\ ft^2\ F$

The formula to find the temperature distribution is given by,

$$T = T_\infty + (T_0 - T_\infty)e^{-\left(\frac{thA}{C\rho V}\right)} \tag{B.10}$$

where A and V are the surface area per unit inch and volume per unit inch, respectively.

The Biot number was calculated using the formula $Bi = \frac{hd}{4k}$. Hence,

$$Bi = \frac{15 \times \frac{1}{32} \times \frac{1}{12}}{4 \times 216} = 4.521 \times 10^{-5}$$

It was found to be much less than 0.1, implying that the internal resistance may be neglected.

B.4.1 Exact Solution

The exact solution of the problem is obtained using Maple, by substituting the variables in equation B.10. The units are kept consistent. The temperature distribution plot for time t = 0 to 0.012 hr is as shown in figure B.4.

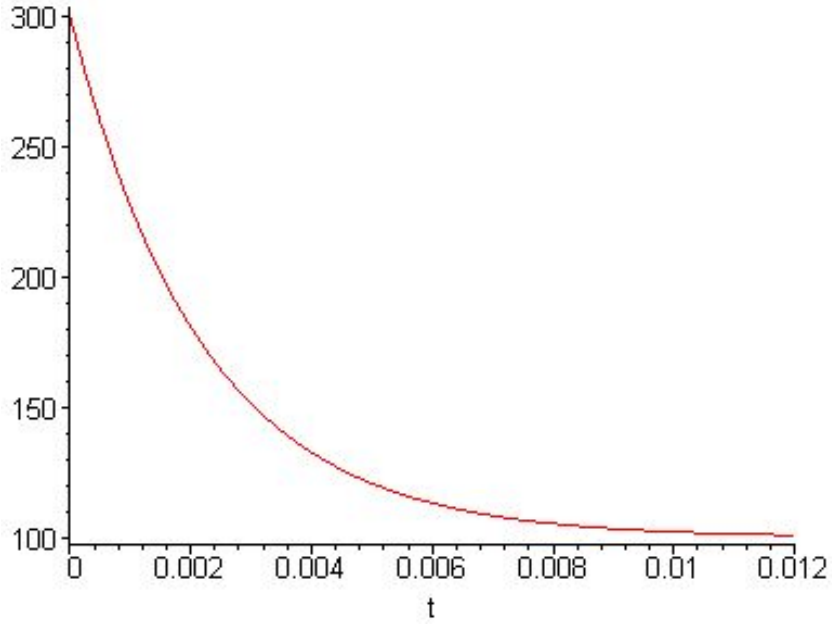

Figure B.4 Temperature Distribution of Copper Wire from Actual Solution

B.4.2 ANSYS Solution

The same problem was solved in ANSYS. A thermal analysis was done to find the temperature distribution, and the results were plotted against time. A long copper wire was first built with the given diameter. The properties, and the loads, that is, initial temperature and convection on areas, in this case, were specified. Temperatures at specific times were also obtained. The temperature against time plot from ANSYS for time t = 0 to 0.012 hr is shown below.

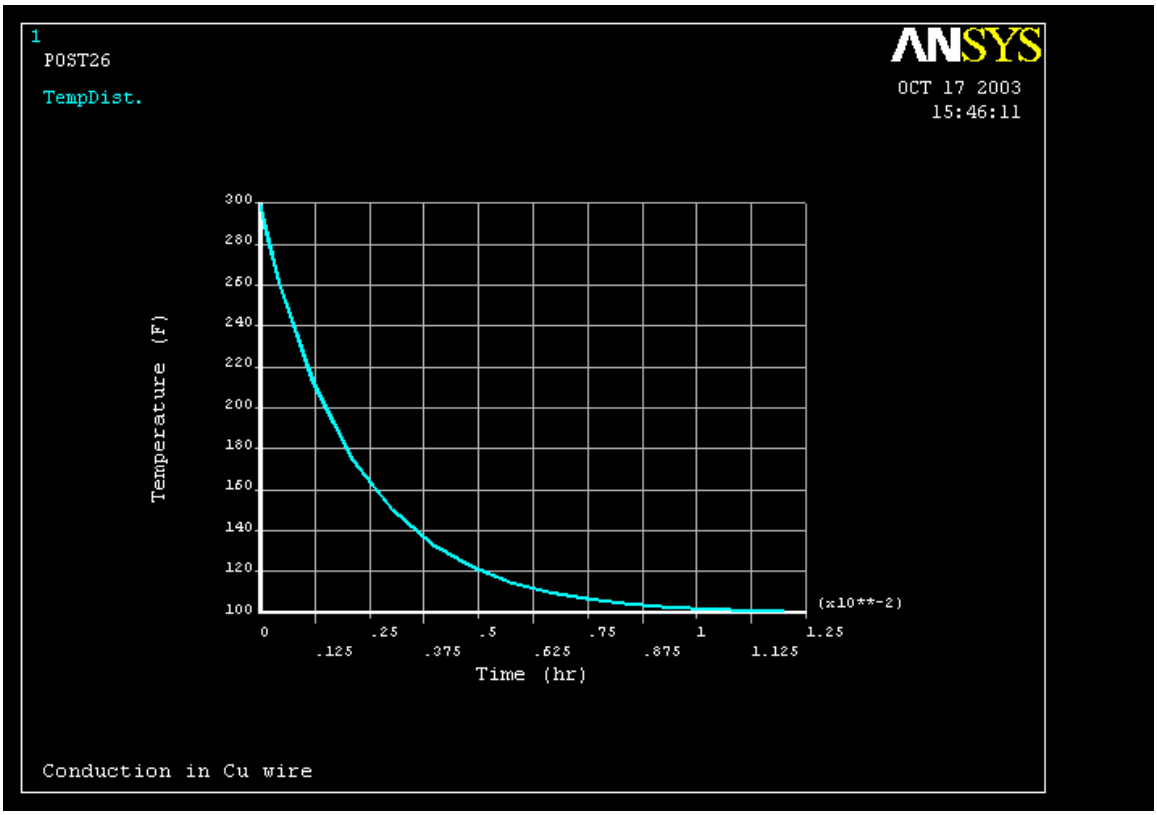

Figure B.5 Temperature Distribution of Copper Wire from ANSYS

B.4.3 Comparison of Actual Solution vs. ANSYS Solution

To verify the accuracy of the result obtained from ANSYS, the percentage difference between temperatures at specific times from the actual solution, obtained using Maple, and the temperatures at the same times from the solution obtained from ANSYS is calculated by making use of the formula given in equation B.9. The time, temperatures from Maple and ANSYS, and the percentage difference, are shown in Table B.2.

Figures B.4 and B.5, are very identical showing a similar temperature distribution solution in both Maple and ANSYS. In addition from Table B.2, we can see that the maximum percentage difference is only 1.722% (4.10×10^{-4} hr). Hence, it can be concluded that the thermal process to cool the trunnion-hub assembly is accurate.

Time (hr)	Temperature (F)		Difference	Percentage Difference
	ANSYS Solution	Maple Solution		
$1.00x10^{-5}$	298.929	299.095	0.165	0.055
$2.00x10^{-5}$	297.846	298.193	0.348	0.117
$5.00x10^{-5}$	294.634	295.514	0.879	0.298
$1.40x10^{-4}$	285.452	287.690	2.238	0.778
$4.10x10^{-4}$	261.468	266.049	4.582	1.722
$1.22x10^{-3}$	211.694	214.980	3.286	1.528
$2.13x10^{-3}$	174.463	176.085	1.622	0.921
$3.04x10^{-3}$	149.642	150.347	0.706	0.469
$3.95x10^{-3}$	133.095	133.316	0.222	0.166
$4.86x10^{-3}$	122.063	122.046	0.017	0.014
$5.76x10^{-3}$	114.709	114.655	0.054	0.047
$6.67x10^{-3}$	109.806	109.698	0.108	0.099
$7.58x10^{-3}$	106.537	106.417	0.120	0.113
$8.49x10^{-3}$	104.358	104.246	0.112	0.107
$9.40x10^{-3}$	102.905	102.810	0.095	0.093
$1.03x10^{-2}$	101.937	101.868	0.069	0.068
$1.12x10^{-2}$	101.291	101.242	0.050	0.049
$1.20x10^{-2}$	100.903	100.864	0.039	0.039

Table B.2 Comparison of Temperatures from Maple and ANSYS for Specific Times

B.5 Test 2 for Thermal Analysis for Cooling in a Liquid Bath

The properties of the material used (ASTM A203-A Steel), and that of liquid nitrogen vary as a function of temperature and are not constant as the temperature changes. These properties include thermal conductivity, specific heat, and thermal expansion of the material, and heat transfer coefficient of liquid nitrogen. This test was

done to compare the cooling of a cylinder with constant properties against the cooling with varying properties. Since, the properties of the material for different temperature values is known, the mean value was chosen as the constant property. The hypothesis for this test is that both the cooling procedures will be similar since the mean of the varying properties is chosen as the constant value. However, constant properties cannot be used for the trunnion-hub assembly process because the thermal expansion does not affect the cooling as significantly as it affects the thermal stresses.

The results are shown in figure B.6, and it can be clearly seen that both the cooling procedures are very similar, thus, proving the accuracy of the simulation of the cooling process with temperature dependent properties.

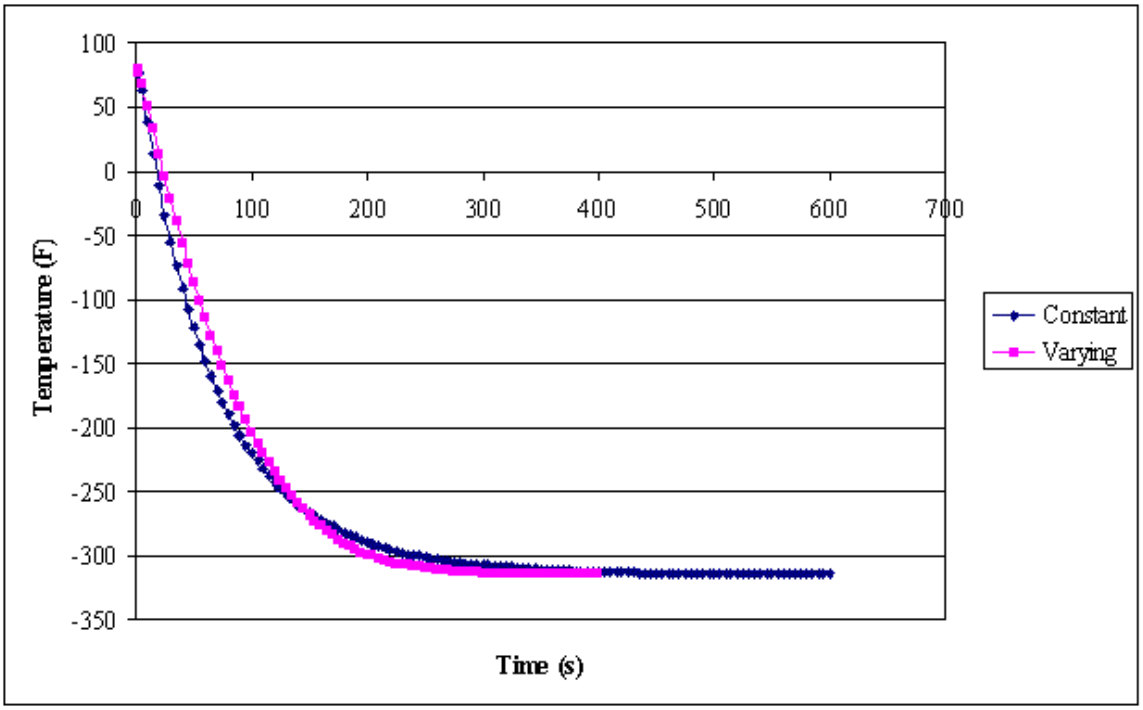

Figure B.6 Comparison of Cooling Processes with Constant and Varying Properties

B.6 Test 1 for Structural Analysis for Thermal Stresses

This test is done to verify the structural analysis for thermal stresses. The hypothesis for this test is that the body will not experience any stresses due to temperature when the temperature gradient in the body is close to or equal to zero. A copper cylinder was chosen for this test. A thermal analysis was done in ANSYS, where it was cooled in a liquid bath until it reached steady state. The stresses developed in the cylinder due to the temperature gradient while cooling was found. According to our hypothesis, as the cylinder reaches steady state, the stresses in the cylinder should also approach zero. The cooling of the cylinder and the thermal stresses developed are shown in figures B.7 and B.8, respectively.

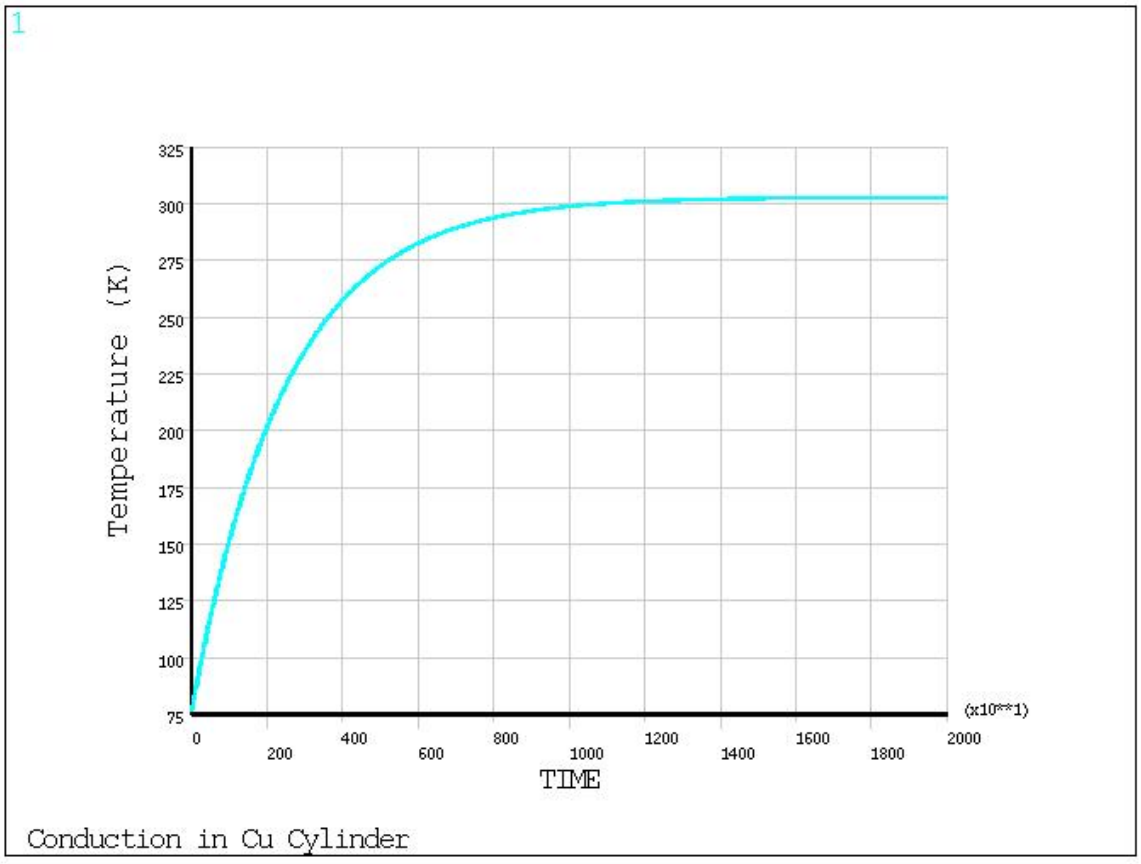

Figure B.7 Temperature Distribution for Cooling of the Copper Cylinder

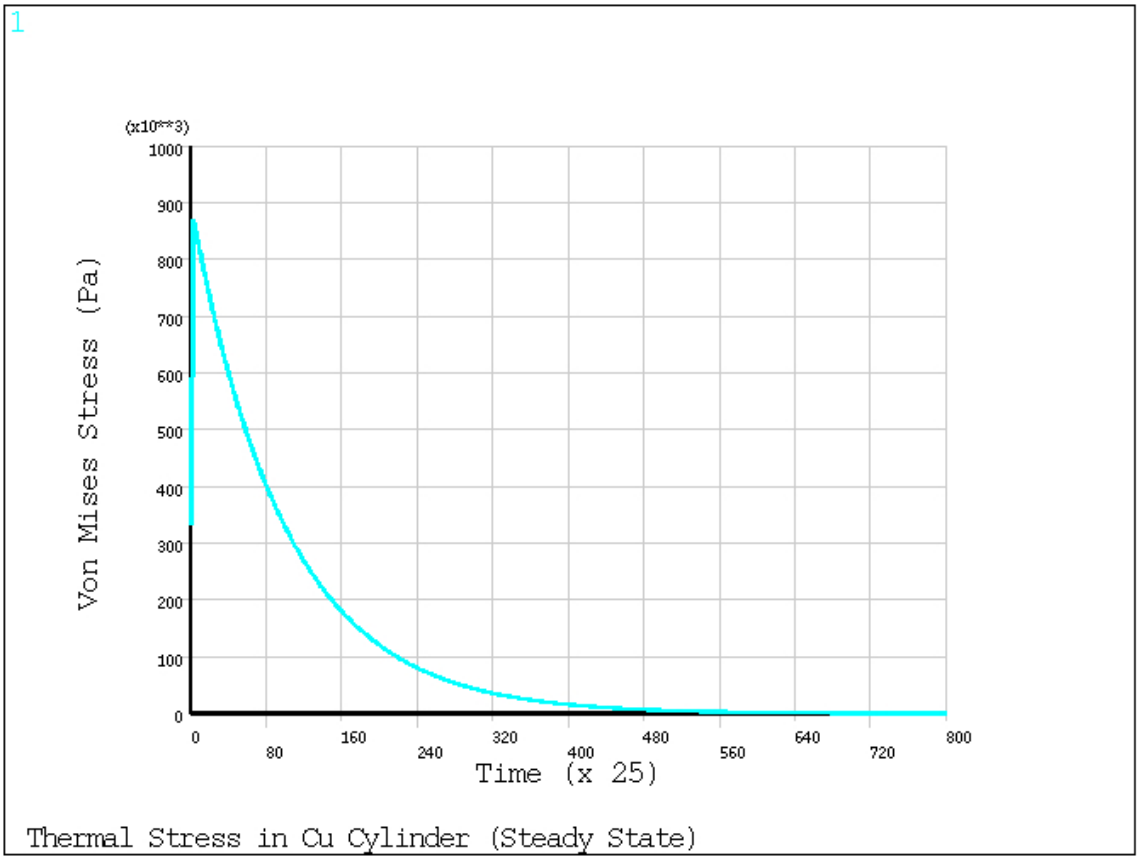

Figure B.8 Thermal Stresses during the Cooling of the Copper Cylinder

The cylinder reaches steady state of 300K after approximately 11,000 seconds. When comparing this with the thermal stress plot, the stresses rise sharply during the first few seconds of cooling but it decreases and it approaches zero, and is equal to zero after approximately 11,000 seconds. Thus, we can be sure that the thermal stress is accurate.

B.7 Test 2 for Structural Analysis for Thermal Stresses

For this test, the compound cylinder problem from section B.1 is made use of. The same hypothesis is used – that the stresses due to temperature gradient approach zero as the body approaches steady state. In this case, the compound cylinders are first shrink fitted with an interference fit, thus, producing interference stresses. This compound cylinder is then cooled in a liquid bath of -321 ^{0}F, till it reaches steady state. The stresses in the cylinders are then found. According to our hypothesis, the stresses should approach values close to the interference stresses as the cylinders approach steady state. This happens because the total stress increases during cooling because of the added stresses due to the temperature gradient. However, the temperature gradient approaches zero as the cylinder reaches steady, thus, nullifying the thermal stresses. Figure B.9 shows the Von-Mises stress in the cylinders, which is purely interference stresses; the maximum being 12363 psi and the minimum being 3210 psi.

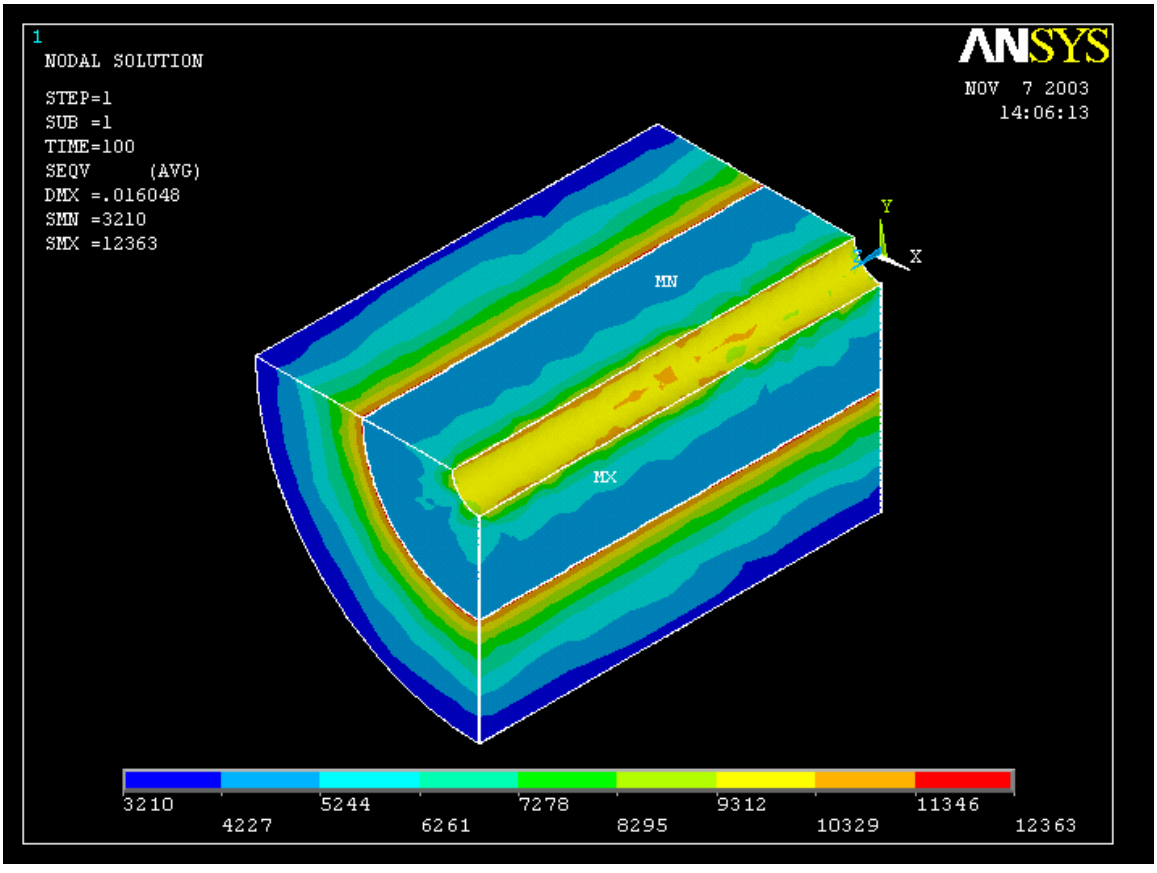

Figure B.9 Von-Mises Stresses in the Compound Cylinders after Interference

The cylinder is now cooled in a liquid bath of -321 ^{0}F till it reaches steady state. Figure B.10 shows the temperature distribution of the cylinders. The maximum temperature is -49.614 ^{0}F and the minimum temperature is -326.924 ^{0}F[5]. It can be seen that only parts of the cylinder attain the temperature of the liquid at this time-step and not the entire cylinder. Hence, there is some temperature gradient in certain parts of the cylinder and consequently, those parts of the cylinder will have stresses greater than the interference stresses.

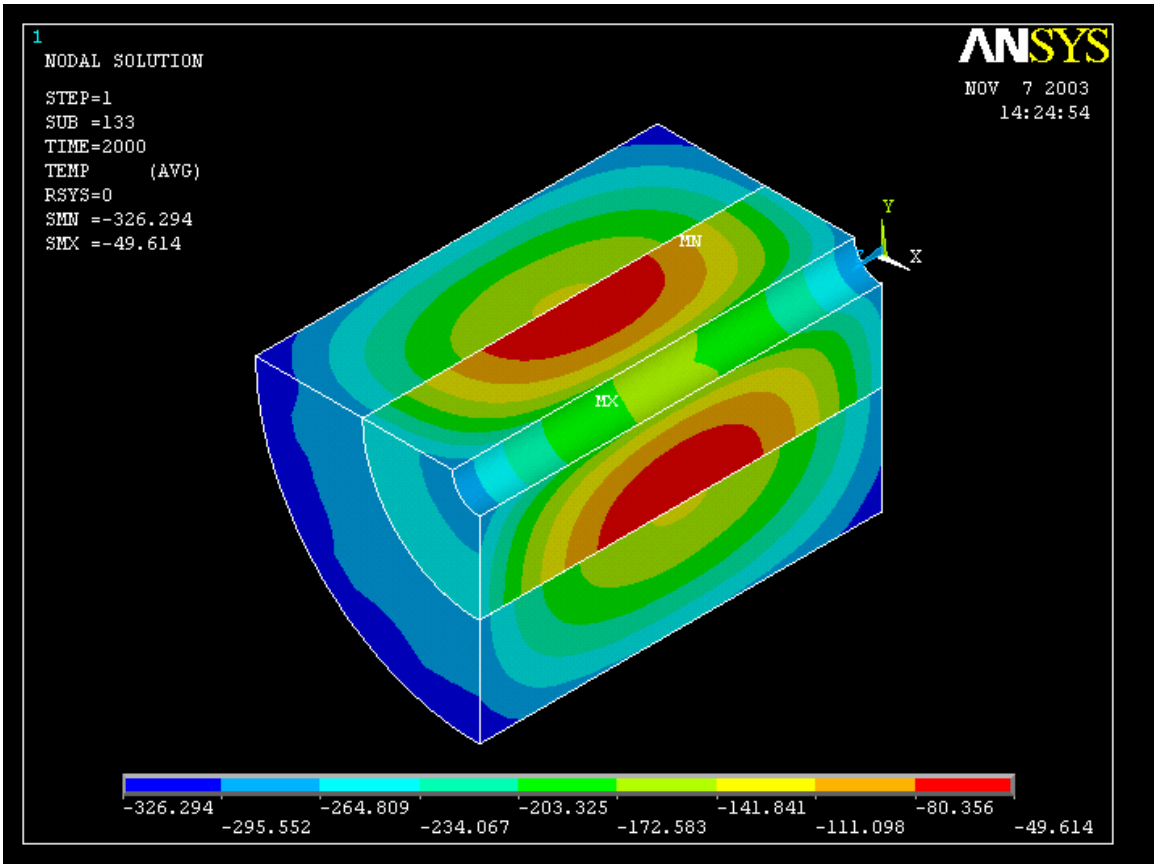

Figure B.10 Temperature Distribution in Compound Cylinders

[5] The temperature is less than -321 ^{0}F because ANSYS extrapolates to get values for nodes that do not have specific values.

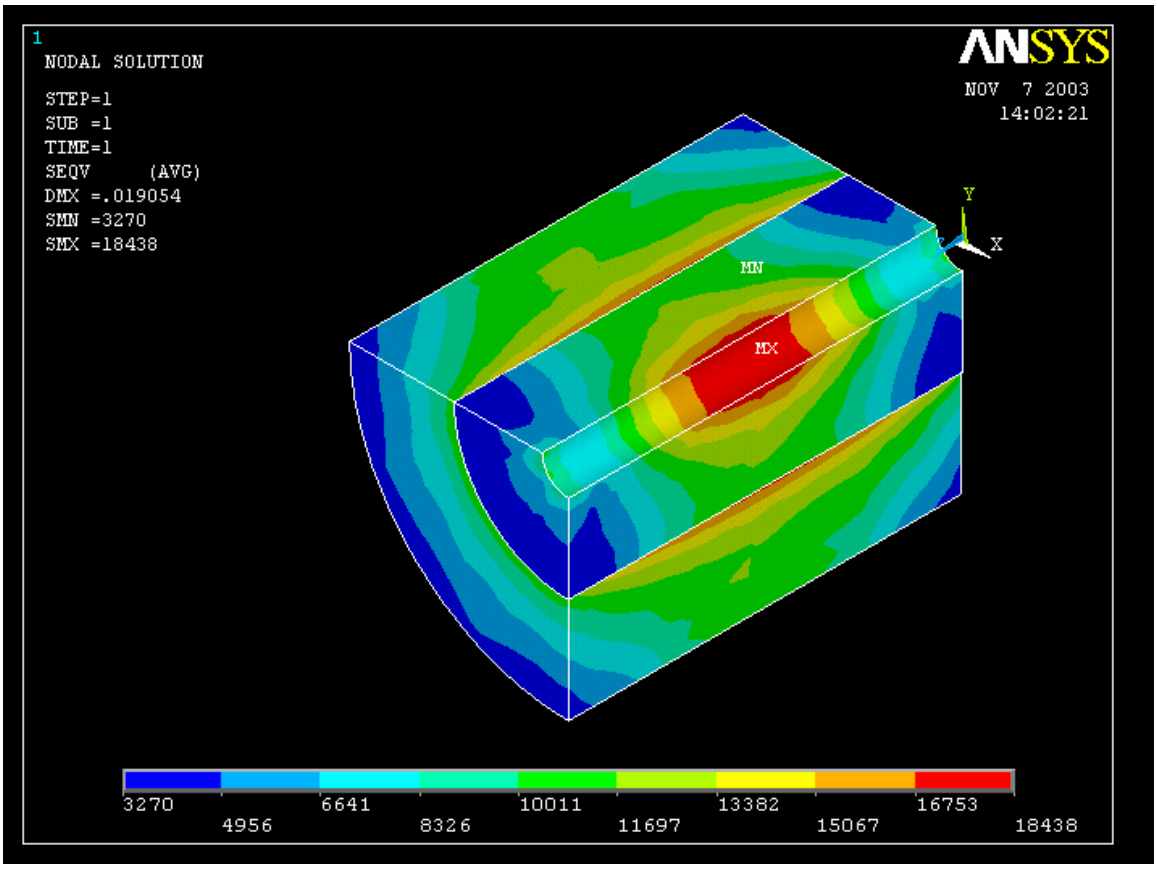

Figure B.11 Von-Mises Stresses in the Compound Cylinders after Cooling

The Von-Mises stress is again plotted for the compound cylinders after the cooling, as shown in figure B.11. According to our hypothesis, the stresses are expected to be close to the interference stresses. The minimum stress here is 3270 psi, which is very close to the minimum interference stress value, 3210 psi. The maximum stress here is 18438 psi, where as the maximum interference stress value was 12363 psi. The difference in the maximum stresses is due to the temperature gradient in parts of the cylinder that have not yet reached steady state. However, if the cylinders would be cooled till it totally reaches steady state, we could see the stresses going back to the interference stress values. This test analysis confirms the thermal stress analysis and also the entire simulation for the trunnion-hub assembly as the trunnion-hub assembly undergoes identical conditions.